TABLE OF CONTENTS

LIST OF TABLES

Page

LIST OF FIGURES

LIST OF ABREVIATIONS

AC	Alternating current
AFM	Atomic force microscopy
ASTM	American Society for Testing and Materials
BDS	Broadband dielectric spectroscopy
BM	Ball milling
BPR	Ball-to-powder weight ratio
DC	Direct current
DSC	Differential scanning calorimetry
E	Extrusion
EPR	Ethylene-propylene rubbers
ÉTS	École de Technologie Supérieure
FTIR	Fourier transform infrared spectroscopy
HV	High voltage
IoPOSS, IoPOS, IO	Isooctyl polyhedral oligomeric silsesquioxanes
IREQ	Institut de recherche d'Hydro-Québec
LDHMWPE	Low-density high molecular weight polyethylene
LDPE	Low-density polyethylene
MV	Medium voltage
MWS	Maxwell-Wagner-Sillars (theory)
NSERC	Natural Sciences and Engineering Research Council (of Canada)
OibPOSS, OibPOS, OIB	Octaisobutyl polyhedral oligomeric silsesquioxanes
OmPOSS, OmPOS, OM	Octamethyl polyhedral oligomeric silsesquioxanes
PE	Polyethylene
POSS, POS	Polyhedral oligomeric silsesquioxanes
PP	Polypropylene
PSB	Progressive-stress breakdown
R-C circuit	Resistor-capacitor circuit
SAOS	Small amplitude oscillatory shear
SEM	Scanning electron microscopy
TGA	Thermogravimetric analysis
TR-XLPE	Tree-retardant cross-linked polyethylene
UHMWPE	Ultra-high molecular weight polyethylene
XLPE	Cross-linked polyethylene
XSB	Xylene solution blending
ZnO	Zinc oxide

INTRODUCTION

Electrical insulation is a key component of underground power cables. To ensure electrical power's reliable and efficient transmission, insulation materials with good dielectric and thermal properties are required. Polyethylene (PE) is an excellent insulating material. It is widely used in alternating current (AC) power cables of a wide range of voltage levels, and is a potential candidate for high-voltage (HV) direct current (DC) power cables. However, PE is susceptible to electrical degradations caused by partial discharges and electrical trees for example, which detrimentally reduce its resistance to dielectric breakdown. Moreover, PE exhibits a low thermal conductivity, which makes it difficult to dissipate heat and it is therefore more prone to thermal aging. As operating voltages and power ratings grow higher, PE insulation is exposed to greater electrical stresses and heat. In order to ensure its reliable operation for long time periods, there is a compelling need to improve its dielectric and thermal performances (Dissado et Fothergill, 1992; Fothergill, 2013; Hanley et al., 2003).

In the past, addition of micrometric inorganic fillers, such as micro-silica, was attempted to this end. However, only limited successes were achieved. This is because micro-fillers usually introduce large interfacial void defects and local electric field enhancements. Moreover, microcomposites often have one property enhanced at the expense of another. For example, an improvement in resistance to electrical discharges can result in a decrease in short-time dielectric breakdown strength.

During the last decades, considerable attention has been given to a new class of dielectric material—nanodielectrics, i.e. dielectric composites containing nanometric fillers. They are frequently reported to have superior dielectric properties than neat polymers and microcomposites, probably due to the critical role of filler-matrix interphase, and thus have great potential to serve as the insulating material for HV power cables. Nonetheless, such property enhancements can only be achieved when nano-fillers have good size dispersions and spatial distributions within host dielectrics. However, due to nano-fillers' strong tendencies to agglomerate, and their generally poor compatibilities with polymers, their dispersions are often

compromised with aggregates of micrometric sizes. Furthermore, hydrophilic nano-fillers attract water to filler-matrix interfaces, not only impairing the crucial role of the interphase, but also causing property and material degradations (David et Fréchette, 2013; *Dielectric Polymer Nanocomposites*, 2010; Fréchette et al., 2001; Fréchette, 2013; Smith et al., 2008; Tanaka et Imai, 2013).

In order to facilitate homogeneous nanoscaled filler dispersions and prevent water absorption, inorganic nano-fillers are commonly treated with dispersants and coupling agents. Both take effect by surrounding the nano-filler with a layer of organic functionality, rendering it either polymer-compatible (as in the case of dispersants) or polymer-reactive (as in the case of coupling agents) (Bellucci et al., 2010). However, this adds extra work to material fabrication. Moreover, little is known about the long-term stability of these surface modifications under electro-thermal stresses (Wen et Ding, 2004). Furthermore, a thorough removal of hydrophilic groups may not be straightforward, and so is the complete prevention of filler aggregation and water absorption (Lau et al., 2013).

A. Research objective

In this context, the objective of this PhD research is to develop PE-based nanodielectrics with enhanced dielectric and thermal performances, as insulating materials for HV underground power cables. In order to avoid the aforementioned problems concerning surface modifications, polyhedral oligomeric silsesquioxanes (POSS), which are by nature nanoscaled molecules bearing built-in functionalities, are used.

B. Specific research objectives

Although POSS are nanoscaled molecules by nature, a vast majority of them exist in the form of crystalline solids at the micron scale. Consequently, besides proper selections of POSS, fabrication methods play a vital role in achieving POSS/PE nanodielectrics with enhanced performances. In this project, three fabrication methods are attempted.

The first method considered is *ball milling* (Suryanarayana, 2001; Zhang, 2004). Ball milling is widely used in mechanical alloying and milling. Moreover, it can be used to fabricate nano-powders and nanocomposite powders. In this work, with the goal of breaking micro-sized POSS crystals into nano sizes, high-energy ball milling, which involves high-energy impact and friction forces, is tested as a method for producing POSS/PE nanodielectrics. The results of this part are published in one journal article and several conference papers, as shown in Chapter 3 and APPENDIX I.

The second method involves *xylene solution blending* (Lau et al., 2013; Shaffer et Windle, 1999). It has potential for producing POSS/PE nanodielectrics, as both POSS and PE dissolve and are thus mixed at the molecular level in xylene solution. However, removal of xylene, by means of precipitation and evaporation, may lead to phase separation and changes in phase morphology. Moreover, residual xylene can affect composites' properties and disturb measurement results. In addition, xylene is comparatively expensive and environmentally unfriendly (George et Thomas, 2011). The findings of this part lead to the publication of one journal article and several conference papers, as shown in Chapter 4 and APPENDIX I.

The third method concerns *melt blending* (Loukus, Halonen et Gupta, 2004; Utracki, 2008). The key to obtaining homogeneous nanocomposites lies in the optimization of dispersive mixing and distributive mixing—the former involves reducing fillers to nanometric sizes and the latter involves spreading nano-fillers uniformly throughout the matrix (Bellucci et al., 2010). In this project, a twin-screw extruder is used. Low barrel zone temperatures are employed to increase shear and elongational stresses, and thus favor an effective dispersive mixing. Moreover, low temperatures also help prevent POSS evaporation and material degradation. The results found for this part are reported in one journal article and several conference papers, as shown in Chapter 5 and APPENDIX I.

C. Methodology

To evaluate the potential of the produced materials as electrical insulation materials for HV power cables, their thermal and dielectric properties, such as thermal conductivity, dielectric permittivity, short-time dielectric breakdown strength and resistance to prolonged AC stress under corona condition are respectively characterized by guarded heat flow thermal conductivity measurements, broadband dielectric spectroscopy (BDS), AC progressive-stress breakdown tests and surface erosion tests.

Microscopic features of the composites are observed, initially by laser scanning confocal microscopy, and more thoroughly by scanning electron microscopy (SEM) and atomic force microscopy (AFM), to study fillers' dispersions and distributions, and to help correlate molecular structure with macroscopic property changes.

In addition, thermal analyses such as differential scanning calorimetry (DSC), chemical analyses such as Fourier transform infrared spectroscopy (FTIR), and rheological measurements are conducted to study possible POSS-PE interactions at the molecular level, and to garner information for possible performance explanations.

CHAPTER 1

ELECTRICAL INSULATION FOR UNDERGROUND POWER CABLES

Electrical insulation, a type of dielectric material, is a key component of underground power cables. By physically enclosing and electrically insulating the conductor, it prevents electric current from flowing in unintended paths (e.g. to the earth ground) and ensures electric power's successful transmission to intended devices and locations. Due to advancements towards higher operating voltages and power ratings, electrical insulation materials with improved capabilities to withstand higher electrical field strengths and thermal loads are required. Consequently, it is of continuous interest to obtain insulating materials with enhanced performances, higher reliabilities, and longer lifetimes (Landinger, 2011).

1.1 A brief historical review

The first flexible insulating-fluid-impregnated paper-insulated cables were introduced in 1885. In the following years, there continued to be improvements in paper selections, insulating fluid selections, and general designs to control voids and increase dielectric strengths. Until the early-1980s, impregnated-paper-insulated lead-covered cables were the predominant power cables of underground transmission and distribution systems.

The use of synthetic polymers (e.g., elastomers, thermoplastics) as cable insulation was prompted by the industrial applications of these materials during and after World War II. Unlike impregnated-paper-insulated cables, synthetic-polymer-insulated cables can be extruded.

Butyl rubber was the material of interest for a period of time. Newer synthetic elastomers such as Neoprene (1931), chloroprene, and Hypalon (1951) were developed with improvements in processing and properties (e.g. enhanced resistances to flame and dielectric aging). Ethylene-propylene rubbers (EPR) were introduced in the 1960s. However, their uses in utility systems did not start to increase until the 1970s to 1980s, when easier extrusion was made possible to

reduce costs. Nowadays, EPR can be found in a large range of applications at various voltage levels. However, they are less popular than cross-linked polyethylene (XLPE) and tree-retardant XLPE (TR-XLPE) due to their relatively higher costs and dielectric losses.

Low-density high-molecular-weight polyethylene (LDHMWPE) was widely employed in underground power cables in the mid-1960s, thanks to its ease of processing (i.e. it can be readily extruded), low cost and good electrical properties. XLPE was commercially available since 1963. It has higher temperature withstands under normal and overload operations as compared to LDHMWPE, thanks to its thermoset network formed by PE molecules chemically joined together. However, in the early-1970s, premature failures of LDHMWPE-insulated and XLPE-insulated power cables as a result of water trees (medium-voltage cable applications) and contaminants (high-voltage cable applications) were frequently reported. To resolve these problems, several measures were introduced, such as the employment of a cable jacket to reduce moisture ingression and water penetration, the replacement of the steam-curing process with a dry-curing process, the adoption of TR-XLPE that hinders the growth of water trees, the application of smooth semi-conductive shields to dissipate ionic species, and the development of extra-clean insulating materials through extra-clean manufacturing processes, packaging and storage. Nowadays, LDHMWPE is commonly found in low voltage cables (less than 600 V), whereas XLPE and TR-XLPE are particularly popular for medium and high voltage power cables (Bernstein, 2011; Bernstein et Thue, 2011; Orton, 2013; Umeda et al., 2007; Underground Electric Transmission Lines, 2011).

1.2 Physical properties

To ensure electrical power's reliable and efficient transmission, insulating materials are required to have good physical properties. Needless to say, dielectric properties are the primary properties to be considered. In addition, electrical insulation materials are often exposed to stresses of a thermal, mechanical and ambient nature under service conditions. Consequently, thermal, mechanical and chemical properties also largely influence the performance and lifetime of insulating materials.

1.2.1 Dielectric properties

One basic parameter of an insulating material is its *electrical resistivity*. It represents the material's resistance to the passage of electric currents. Thanks to strong covalent bonds, polymeric dielectrics have virtually no free charges capable of leading to continuing conduction currents under normal conditions. Consequently, they have high electrical resistivities of generally 10^{16} Ω·m and above. The reciprocal of electrical resistivity, i.e., the *electrical conductivity*, is thus generally 10^{-16} S/m and lower.

The parameter of great interest in electrical engineering applications is the frequency-temperature-dependent *relative complex dielectric permittivity* ε_r^*. Its real and imaginary parts are commonly referred to as *dielectric constant* and *dielectric loss*, respectively. Relative values are used for the sake of practical convenience; they are obtained by having absolute complex dielectric permittivities divided by the vacuum dielectric permittivity ε_0 (ε_0 = 8.85×10^{-12} F/m). Materials with high dielectric constants have high capacities to store electric charges, and are thus widely used in capacitors to store electrical energy. In applications related to electrical insulation, however, materials with low dielectric constants are desired (ASTM Standard D150, 2011). Dielectric loss causes energy loss and decreases power-transmission efficiency, and is thus preferred to be as low as possible. More information on ε_r^* can be found in Chapter 2.

Another important aspect of electrical insulation is the *dielectric breakdown strength*. It represents the maximum electric field a dielectric can withstand without breaking down and thus failing to perform its insulating function. Dielectrics with high breakdown strengths contribute to not only increase the reliability of power-transmission systems, but also reduce the insulation thickness for cost reductions and better heat dissipation.

In service conditions, electrical degradation or aging, caused by electric fields orders of magnitude below the breakdown strength, has been found to be particularly detrimental for polymeric insulation materials. Consequently, *dielectric endurance* against such as partial

discharges, electrical trees, and water trees, is a parameter of great significance in describing insulating materials. Partial discharges arise from the breakdown of micro-voids defects. They cause material erosion and lead to micro-cracks and even electrical trees. Electrical trees are branched tree-like gas-filled connected channels. In addition to discharging voids, they can be initiated by conducting protrusions or contaminants due to local electric field intensifications. A short-circuit, and thus a breakdown, occurs when electrical trees completely traverse the insulation. Water trees are branched tree-like water-filled rarely-connected micro-cavities. They grow in moist conditions, from contaminants, boundary surfaces, and water-filled voids. Although they can traverse the insulation without causing failure, they can initiate electrical trees which eventually lead to dielectric breakdown.

Another criterion for evaluating insulating materials concerns *space charge dissipation*, i.e., the ability of insulation materials to dissipate space charges. Space charge accumulation can significantly distort the local electric field and accelerate the degradation process. It is also one of the major factors restricting the development of XLPE-insulated HVDC power cables.

1.2.2 Thermal properties

Temperature withstand is one of the main factors limiting the power a cable can transmit. HV cable conductors operate at about 80–90 °C with overload temperatures of about 130 °C (Bernstein, 2011; Underground Electric Transmission Lines, 2011). Consequently, it is vital that the insulations are capable of maintaining their insulating properties at those elevated temperatures. Cross-linking is a practical way to increase the temperature withstand of insulations; by chemically linking polymer chains into a giant molecular network, insulations are able to maintain their form stabilities and functions at elevated temperatures.

Thermal conductivity plays an important role in the performances and the lifetimes of polymeric insulations. This is because the heat generated by the conductor, Joule heating and dielectric losses can cause crystalline melting (in crystalline region), chain separations (in both crystalline and amorphous regions), and differential thermal expansions (in heterogeneous

systems). Such processes may introduce damaging structural defects (e.g., micro-voids), rendering insulations more susceptible to electrical degradations. High thermal conductivities allow the insulations to better dissipate heat, and thus reduce thermally-assisted agings and chances of thermal breakdown (Xiao et Du, 2016).

One of the crucial temperatures for polymeric materials is the *glass transition temperature* (T_g), the temperature at which polymers undergo a rubber-glass transformation. Below T_g, polymer chains are basically immobile except for some small subunits. Such severe restrictions of chain motions slow down the returns of mechanical strains and hinder the dissipations of mechanical impact energies. As a result, micro-voids, micro-cracks and discontinuities are susceptible to be generated under mechanical stresses, and the insulation is prone to brittle fracture during cable installation. Consequently, polymeric insulation materials generally have low T_g and are used above their T_g.

1.2.3 Other properties

As far as mechanical properties are concerned, insulations are preferred to have good flexibility and ability to withstand mechanical stresses, especially for those operated in cold northern regions. This is because mechanical stresses, such as pulling tensions and bending tensions, are often applied on cables during installation, when they go around bends and experience elevation changes along the route. As for chemical properties, it is desirable for insulating materials to have high resistance to reactive radicals that cause bond breaking and chain scission. Moreover, buried in underground constructions, insulation materials need to have excellent moisture resistance and solvent resistance. Furthermore, good flame resistance, ease of processing, environmental friendliness and recyclability are also favorable properties for polymeric insulations.

1.3 Nanodielectrics

Nanodielectrics are composite materials consisting of polymer matrices and nano-fillers, i.e. fillers for whom at least one dimension is at the nanoscale ranging from 10^{-9} to 10^{-7} m. They

have attracted widespread interest thanks to their superior dielectric properties as compared to neat polymers and microcomposites, to name a few, increased dielectric breakdown strengths, enhanced partial discharge resistances, elongated treeing lifetimes and reduced space charge accumulations (David et Fréchette, 2013; *Dielectric Polymer Nanocomposites*, 2010; Fréchette et al., 2001; Fréchette, 2013; Tanaka et Imai, 2013; Tiemblo et al., 2008).

Hypotheses dealing with the underling mechanisms of these property enhancements highlight the critical role of the filler-matrix interphase. Generally speaking, in the interphase region, polymer chains can experience changes in crystallinity, mobility, chain formations, and so on. These local morphological changes may increase the density and depth of charge-carrier trapping states, reduce the density, mobility and energy of charge carriers, and consequently help enhance polymers' dielectric properties (Fréchette, 2013; Lewis, 2004; Reed, 2010; Roy et al., 2007; Roy et al., 2005; Smith et al., 2008; Tanaka et al., 2005; Tian et al., 2012).

Fillers' homogeneous nanoscaled dispersion is considered to be an important prerequisite for achieving performance-enhanced nanodielectrics. However, due to nano-fillers' strong tendency to agglomerate, and their generally poor compatibilities with polymers, their dispersions are often compromised, showing aggregates of micrometric sizes. Furthermore, hydrophilic nano-fillers attract water to filler-matrix interfaces, not only impairing the crucial role of the interphase, but also causing property and material degradations.

Surface modifications of inorganic nano-fillers, with dispersants and coupling agents, are widely adopted to facilitate filler dispersion and avoid water absorption. As shown in Figure 1.1 (a), dispersants have one of their ends attached to nano-fillers, while the other ends protrude, stopping nano-fillers from approaching one another and preventing their agglomeration. In addition, the protruding ends are chosen to be compatible with the polymer matrix, and thus serve to enhance filler-matrix compatibility. As shown in Figure 1.1 (b), coupling agents have one of their ends attached to nano-fillers, as do dispersants, while the other ends chemically react with, and thus are chemically bonded to, the polymer matrix. In this way, coupling agents not only help with filler dispersion, but also increase filler-matrix adhesion.

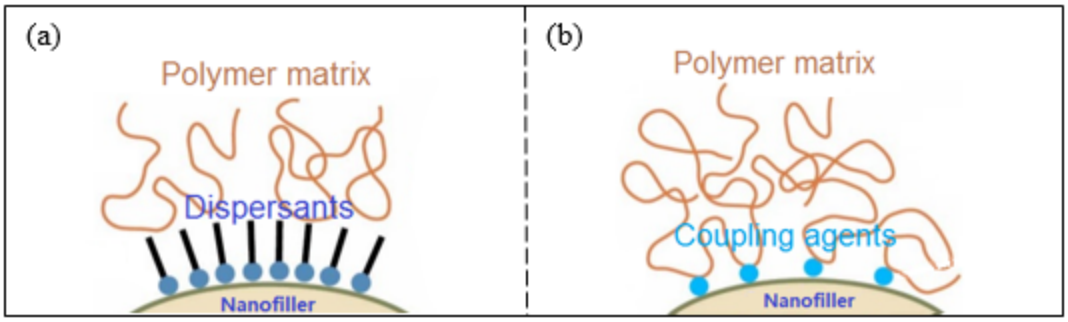

Figure 1.1 Surface modifications of inorganic nano-fillers
with (a) dispersants and (b) coupling agents. Modified from
(Dispersants & Coupling Agents: New Chemistry for a Mature Industry, 2013)

1.4 Materials review

1.4.1 Polyethylene (PE)

Polyethylene (PE) is a type of saturated hydrocarbon with a general formula $(\text{-}CH_2\text{–}CH_2\text{-})_n$, where n is the degree of polymerization, usually in the order of 10^4, but can be as low as 10^3 and as high as 10^6. It represents the number of ethylene monomers (CH_2=CH_2) that join together, during the polymerization process, to form the macromolecular chain of PE. The bigger the n, the longer the molecular chain, and the higher the molecular weight.

PE is nonpolar, due to the insignificant electronegativity difference (i.e., 0.35) between carbon atoms (i.e., 2.55) and hydrogen atoms (i.e. 2.20) (Electronegativity, 2017). Such a non-polarity renders PE low dielectric constant and dielectric loss, which is quite beneficial for its application as power cable insulation.

PE is a semi-crystalline material, which means that a portion of the molecules is in an orderly-aligned crystalline phase and the remaining portion is in a randomly-arranged rubbery amorphous phase. The crystalline fraction is high-modulus and stiff, whereas the amorphous fraction is low-modulus and flexible. 'Crystallinity' is the portion of PE that is crystalline. It plays an important role in PE's thermal, mechanical and electrical properties, as addressed in Chapters 4 and 5.

Detailed information on PE's physicochemical properties can be found in (Bernstein, 2011; McCrum, Buckley et Bucknall, 1997).

1.4.1.1 PE as power cable insulation

PE is an excellent insulating material for power cables, thanks to its high electrical resistivity (typically above 10^{16} Ω·m), low dielectric constant (i.e., 2.3), low dielectric loss (typically below 10^{-3}), high dielectric breakdown strength, low-temperature flexibility, resistance to moisture and corrosion, ease of processing, reasonably low cost, etc. Consequently, PE is the insulating material of choice for a large range of voltage applications throughout the history and in the present times, as introduced in section 1.1 (Dissado et Fothergill, 1992; Orton, 2013).

However, PE suffers from several drawbacks. First of all, its performances are inevitably degraded by aging processes of electrical, thermal, mechanical and chemical natures. Also, it is not tolerant of defects such as protrusions, contaminants and voids, the presence of which can initiate partial discharges and electrical trees. Moreover, it is susceptible to space charge accumulation, which can significantly distort the local electric field and accelerate aging processes. In addition, it requires a comparatively thick insulation wall to increase reliability, but this undermines economic benefits. Furthermore, it exhibits a low thermal conductivity, which results in difficult dissipation of heat and higher susceptibility to thermal aging. As operating voltages and power ratings grow higher, PE insulation is exposed to greater electrical stresses and heat. In order to ensure its reliable operation for long time periods, there is a compelling need to improve its dielectric and thermal performances (Dissado et Fothergill, 1992; Fothergill, 2013).

In the past, addition of micrometric inorganic fillers, such as micro-silica, was attempted to this end. However, only limited successes were achieved. This is because micro-fillers usually introduce large interfacial void defects and electric field enhancements. Moreover, microcomposites often have one property enhanced at the expense of another. For example, an

improvement in resistance to electrical discharges can result in a decrease in short-time dielectric breakdown strength.

During the last decades, considerable attention has been paid to nanodielectrics. Nano-silica/XLPE nanodielectrics, thanks to their improvements in several key dielectric properties, have been suggested as potential candidates for MV and HV power cables (Roy et al., 2007; Roy, 2005; Tanaka et al., 2011). However, silica nano-fillers usually suffer from the aforementioned agglomeration and water-affinity problems, and are thus commonly subjected to surface modifications. However, this adds extra work to material fabrication. Moreover, little is known about the long-term stability of these surface modifications under electro-thermal stresses (Wen et Ding, 2004). Furthermore, a thorough removal of hydrophilic groups may not be straightforward, and so is the complete prevention of filler aggregation and water absorption (Lau et al., 2013).

1.4.2 Polyhedral oligomeric silsesquioxanes (POSS or POS)

Polyhedral oligomeric silsesquioxanes (POSS or POS) are nanometric molecules typically measuring 1–5 nm. They are a family of compounds with a general formula $(RSiO_{1.5})_n$, where R is hydrogen or one of an extremely wide range of organic groups, and n is typically a small number such as six, eight or ten. Among the known structures of POSS, the cage structure is the most typical. As can be seen in Figure 1.2 (a), each of the eight silicon atoms locates at the vertex of the silicon-oxygen cage and carries an exo-cage functional group R coordinating around the silicon vertex tetrahedrally. The first POSS was synthesized by Scott in the 1940s (Scott, 1946). Although POSS are a class of compounds with extreme versatility, they did not attract commercial interests until the 1990s, when scale-up of POSS manufacture was made possible, and demands for developing hybrid materials rapidly increased. It should be noted that although POSS are nanoscaled molecules by nature, a vast majority of them exist in the form of crystalline solids at the micron scale. As can be seen in Figure 1.2 (b), as-received octaisobutyl-POSS (OibPOSS) are solids of 100–200 μm. Nanoscaled POSS molecules can only be obtained when POSS are well dispersed into matrices such as plastics, rubbers and

coatings (*Applications of Polyhedral Oligomeric Silsesquioxanes*, 2011; DeArmitt, 2010; Harrison, 1997).

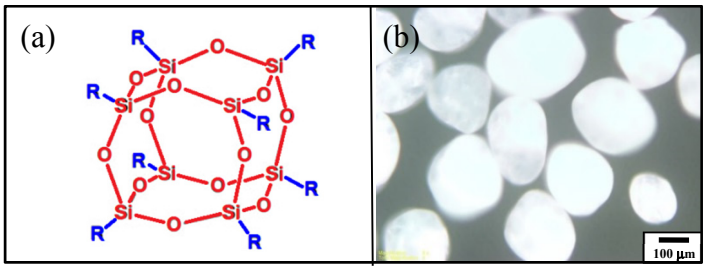

Figure 1.2 (a) A cage-structured POSS molecule
(modified from (Hybrid, 2014));
(b) as-received OibPOSS crystalline solids

1.4.2.1 POSS and nanodielectrics

POSS is a type of filler of great interest in the field of nanodielectrics. This is because they are (i) nanoscaled molecules by nature and (ii) hybrid consisting of both inorganic and organic components. While the chemically, thermally and mechanically robust inorganic Si-O core can play a similar role as traditional silica nano-fillers, the organic functional groups can help enhance filler-polymer compatibility and adhesion.

Depending on the reactivity of R, POSS can be incorporated into polymer matrices by either copolymerization/grafting reactions or physical blending.

POSS precursors bearing a number of polymerizable/graftable functionalities, such as alkenyl, methyl methacrylate and epoxy, are widely used to produce thermoplastic and thermoset nanodielectrics. In these synthesized nanodielectrics (Figure 1.3 (a)), inorganic POSS cages are covalently bonded to organic polymer chains, tailoring polymer properties at the molecular level. Many studies show that they can present increased glass transition temperature, increased thermal stability, reduced flammability, increased Young's modulus, and so on (Cordes, Lickiss et Rataboul, 2010; Schwab et Lichtenhan, 1998).

POSS whose functional groups are chemically inert species (e.g., saturated alkyl groups) are commonly used to produce thermoplastic nanodielectrics through physical blending. Needless to say, the higher the POSS-polymer compatibility, the greater the dispersion energy during composite fabrication, the better the resulting filler dispersion. In these composites (Figure 1.3 (b)), well-dispersed POSS exist in nanoscaled domains at thermodynamically stable states without any parts of them chemically bonded to any parts of polymer chains. Studies on polymer/unreactive-POSS composites concerning their crystallization behaviors, morphological and rheological characteristics, as well as thermal, mechanical and dielectric properties show that, in some cases, POSS are able to improve the thermal stability, the fire retardance, the modulus, the tensile strength, the AC breakdown strength and the corona endurance of polymers (Cordes, Lickiss et Rataboul, 2010; Horwath et Schweickart, 2002; Huang et al., 2009; Takala et al., 2008).

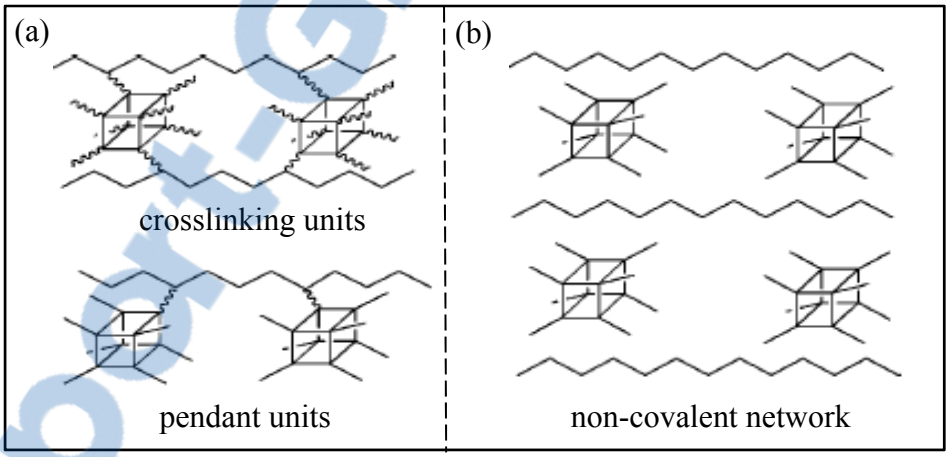

Figure 1.3 Schematic illustrations: nanodielectrics obtained by
(a) synthesis of reactive POSS and (b) addition of unreactive POSS.
Taken from (Cordes, Lickiss et Rataboul, 2010)

1.4.2.2 POSS-PE compatibility

POSS' dispersion within PE matrix largely depends on the compatibility between these two materials: the higher the POSS-PE compatibility, the greater the likelihood of a nanoscaled POSS dispersion. In this section, the compatibility between POSS and PE is explored by qualitative and quantitative evaluations. Three types of POSS are examined, namely,

octamethyl-POSS (OmPOSS), octaisobutyl-POSS (OibPOSS), and isooctyl-POSS (IoPOSS) (Figure 1.4). OmPOSS and OibPOSS are crystalline solids with densities of 1.5 g/cm^3 and 1.13 g/cm^3, molar masses of 537 g/mol and 873.6 g/mol, and average particle sizes of ~30 μm and ~200 μm, respectively. IoPOSS is a viscous liquid having a density of 1.01 g/cm^3 and a molar mass of 1322.5 g/mol (DeArmitt, 2010).

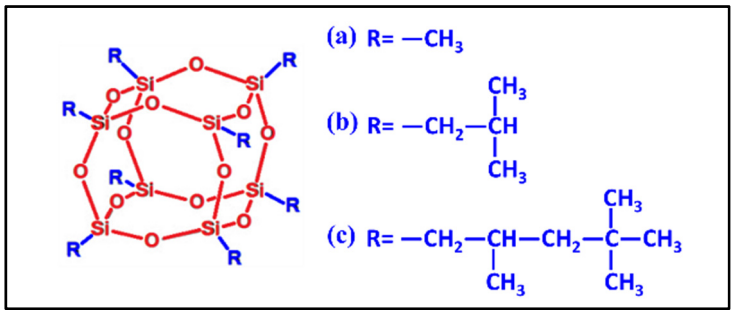

Figure 1.4 OmPOSS, OibPOSS, and IoPOSS with organic groups as (a) methyl group, (b) isobutyl group and (c) isooctyl group, respectively

The qualitative evaluation is performed based on an empirical "like dissolves like" rule. The functional groups of POSS, being nonpolar saturated hydrocarbons, have the same polarity as PE. Moreover, locating at the periphery of POSS molecule, they physically provide a nonpolar screening to POSS' polar silicon-oxygen core. Both characteristics render POSS appear to be "like" PE. Self-evidently, the longer and more oblate the nonpolar functional group, the more it is able to chemically dominate the polarity of POSS as well as to physically screen the polar Si-O cage. Considering the length and shape of POSS' alkyl group, OmPOSS is estimated to have the lowest compatibility with PE, OibPOSS, a medium, and IoPOSS, the highest.

The quantitative evaluation is carried out by calculating the Hildebrand solubility parameter of POSS with Hoy's group contribution method using equation (1.1) (Van Krevelen et Te Nijenhuis, 2009):

$$\delta = \frac{F\rho}{M_0} = \frac{\left(\sum F_i\right)\rho}{M_0} \tag{1.1}$$

where δ ((MPa)$^{1/2}$), F ((MPa)$^{1/2}$·cm^3/mol), ρ (g/cm^3), and M_0 (g/mol) are respectively the solubility parameter, the molar attraction constant, the density, and the molar mass of the substance in question. F_i (i=1, 2, 3...) are molar attraction constants of the chemical groups composing the substance.

The chemical groups consisting of POSS are Si-O, >C<, >CH–, –CH_2–, and –CH_3. Molar attraction constants of >C<, >CH–, –CH_2– and –CH_3 are found in Hoy's table, as 65.5, 176, 269, and 303.4 (MPa)$^{1/2}$·cm^3/mol, respectively (Van Krevelen et Te Nijenhuis, 2009, p. 194). Molar attraction constant of Si-O (not provided by Hoy's table) is calculated as 148.3–306.9 (MPa)$^{1/2}$·cm^3/mol, using poly(dimethylsiloxane), [-$Si(CH_3)_2O$-]$_n$ (ρ=0.98 g/cm^3, M_0=74 g/mol, δ=10–12.1 (MPa)$^{1/2}$ (Grulke, 1999; 2005, p. VII/690; Misra et al., 2009).

Substituting densities and molar masses of POSS, and molar attraction constants of POSS' chemical groups into equation (1.1), solubility parameters of OmPOSS, OibPOSS and IoPOSS are obtained, as 16.7–27.4 (MPa)$^{1/2}$, 15.5–20.4 (MPa)$^{1/2}$, and 14.9–17.8 (MPa)$^{1/2}$, respectively. They respectively worst, moderately, and best overlap with that reported for PE, i.e., 15.8–18.4 (MPa)$^{1/2}$ (Grulke, 1999; 2005, p. VII/704). Based on the proposition by Hildebrand that the solubility between two substances is high when their solubility parameters are close, OmPOSS is thus evaluated to have the lowest compatibility with PE, OibPOSS, a medium, and IoPOSS, the highest, in agreement with the qualitative evaluation presented earlier.

CHAPTER 2

DIELECTRIC POLARIZATION AND DIELECTRIC RELAXATION

As is briefly introduced in section 1.2.1, charges in polymeric dielectrics are not free to conduct electric currents under normal conditions. In this chapter, we shall see that they actually undergo delayed displacements or orientations.

2.1 Electrostatics of dielectrics

Consider a planar capacitor consisting of a pair of parallel electrodes. The surface area of each electrode is *A* and the distance between the two electrodes is *d*. Now, let the space between the two electrodes be *vacuum* (Figure 2.1 (a)). Attach the capacitor to a power source that supplies a constant direct voltage *U*. By the time the capacitor is fully charged, a charge density σ_0, i.e., the amount of electric charge per unit electrode area, appears on both electrodes. According to Gauss' law, a uniform electric field $\vec{E}$ is produced:

$$\sigma_0 = \vec{D}_0 \cdot \vec{n} \tag{2.1}$$

$$\vec{D}_0 = \varepsilon_0 \vec{E} \tag{2.2}$$

where $\vec{D}_0$ is the electric flux of the vacuum capacitor; $\vec{n}$ is the vector normal to the electrode; ε_0 is the vacuum permittivity, and is equal to 8.85×10^{-12} F/m. Let now the space between the two electrodes be filled with a *dielectric* bearing a dielectric constant of ε_r (Figure 2.1 (b)). Under the electric field $\vec{E}$, polarizing species get polarized whereby their positive-charge ends move towards and their negative-charge ends move against the direction of $\vec{E}$. This produces a dipole moment throughout the entire volume of the dielectric and gives rise to an internal electric field $\vec{E}_i$ opposing $\vec{E}$. To compensate for the decrease of $\vec{E}$, more charges are drawn from the power source to the capacitor's electrodes, resulting in an additional charge density of σ_p:

$$\sigma_p = \vec{P} \cdot \vec{n} \tag{2.3}$$

where $\vec{P}$ is the polarization of the dielectric. It is the dipole moment of the polarizing species per unit dielectric volume, and is equal to the additional charge density σ_p. This time, when the capacitor is fully charged, according to Gauss' law, the charge density σ and the electric flux $\vec{D}$ are:

$$\sigma = \vec{D} \cdot \vec{n} = \sigma_0 + \sigma_p \tag{2.4}$$

$$\vec{D} = \varepsilon_0 \varepsilon_r \vec{E} \tag{2.5}$$

Solve equations (2.1)–(2.5), $\vec{P}$ is obtained as:

$$\vec{P} = \varepsilon_0 (\varepsilon_r - 1) \vec{E} = \varepsilon_0 \chi_r \vec{E} \tag{2.6}$$

where χ_r is the dielectric susceptibility.

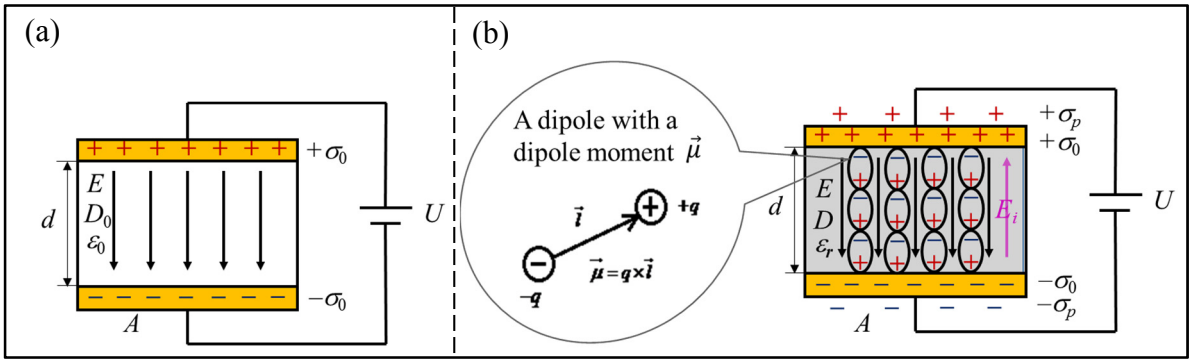

Figure 2.1 Electrostatics of a planar capacitor when its space is filled with (a) vacuum and (b) a dielectric medium

2.2 Polarization mechanisms in dielectrics

Based on different physical origins, polarization mechanisms in dielectrics can be classified as (Jonscher, 1983; Raju, 2003c; Steeman et van Turnhout, 2003):

- electronic polarization;
- atomic polarization;
- dipolar polarization;
- interfacial polarization.

2.2.1 Electronic polarization

Electronic polarization is induced by an external electric field. Upon the application of the field, outer electronic clouds slightly shift towards the opposite direction of the field, causing charge displacements with respect to inner atomic cores (i.e., nuclei), leading to electronic polarization (Figure 2.2 (a)). For nonpolar polymers bearing small densities such as polyethylene, their dielectric constants attributable to electronic polarization can be calculated by the Clausius-Mossotti equation, as shown in Chapter 5.

2.2.2 Atomic polarization

Like electronic polarization, atomic polarization is also induced by an external electric field. Upon the application of the field, atoms' nuclei connected by polar bonds are mutually displaced, leading to atomic polarization (Figure 2.2 (b)). The displacements are limited by the vibrational freedom of relevant atoms, and involve changes in bond lengths and bond angles.

2.2.3 Dipolar polarization

Dipolar polarization occurs in polar dielectrics. Due to the randomising influence of thermal agitation, polar molecules have random orientations and a zero net dipole moment. Upon the

application of an electric field, dipole orientations along the field line occur, giving rise to dipolar polarization (Figure 2.2 (c)).

2.2.4 Interfacial polarization

Interfacial polarization occurs in heterogeneous dielectrics, i.e., dielectrics composed of two or more dissimilar components that are immiscible with one another. Due to impurities that are often difficult to avoid and identify, there always exist some free charge carriers (mostly ions) capable of movements upon the application of an electric field. Due to different conductivities of different phases, charges are hindered in their motions by less-conductive phases and end up piling up at phases' boundaries/interfaces, giving rise to interfacial polarization (Figure 2.2 (d)).

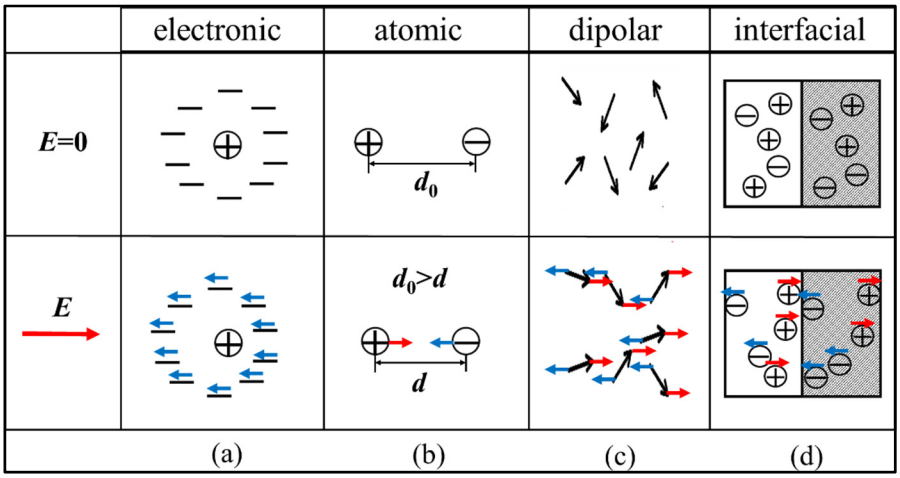

Figure 2.2 Polarization mechanisms in dielectrics

2.3 Dielectric relaxation

A certain time interval is required for polarization to build up and to decay. Take dipolar polarization as an example. Upon the application of an electric field, polarization starts to build up, whereby dipoles are gradually orientated, from their random distribution, along the electric field line under the ordering force of the electric field. Due to physical resistances brought

about by surrounding media, it takes a certain time interval before polarization reaches its maximum value. Similarly, when the electric field is suddenly removed, the decay of polarization to zero value where dipoles restore their random distribution from a field-imposed alignment also takes a certain time. This phenomenon is called *dielectric relaxation* (Raju, 2003a).

2.3.1 Dielectric relaxation in time domain

Upon the application of a time-dependent electric field $E(t)$, time-dependent dielectric polarization $P(t)$ is described as:

$$P(t) = \varepsilon_0 \int_0^{\infty} f(\tau) E(t-\tau) d\tau \tag{2.7}$$

where $f(\tau)$ is an arbitrary dielectric response function. The integral integrates all dielectric responses starting from an infinite backward time until the time of excitation, t. The physical sense of this is that the dielectric system retains "memory" of its past history as a result of dielectric relaxation (Jonscher, 1983, p. 39).

Under $E(t)$ the total current density $J(t)$ in a dielectric is the sum of displacement current and direct current (DC) characteristic of a conductivity σ_0:

$$J(t) = \sigma_0 E(t) + \frac{\partial D(t)}{\partial t} \tag{2.8}$$

The first term, direct current, comes from the contribution of charge carriers bearing non-zero mobility. The second term, displacement current, arises from delayed adjustments of polarising species in response to the exciting field, and for a constant electric field, it goes to zero at infinitely long times as polarizations attain their maximum values.

Taking into account the time factor, equations (2.5) and (2.6) become:

$$D(t) = \varepsilon_0 E(t) + P(t) \tag{2.9}$$

Combine equations (2.7)–(2.9), $J(t)$ is obtained as:

$$J(t) = \sigma_0 E(t) + \varepsilon_0 \frac{\partial}{\partial t}\left[E(t) + \int_0^\infty f(\tau) E(t-\tau)\, d\tau \right] \tag{2.10}$$

For a planar capacitor, as shown in Figure 2.1, it is more practical to express equation (2.10) in terms of the current $I(t)$ flowing through and the voltage $U(t)$ applied across the dielectric, as:

$$I(t) = \frac{C_0 \sigma_0 U(t)}{\varepsilon_0} + C_0 \frac{\partial}{\partial t}\left[U(t) + \int_0^\infty f(\tau) U(t-\tau)\, d\tau \right] \tag{2.11}$$

by taking into account the following relationships:

$$J(t) = \frac{I(t)}{A};\ E(t) = \frac{U(t)}{d};\ C_0 = \varepsilon_0 \frac{A}{d} \tag{2.12}$$

where C_0 is the vacuum capacitance, i.e., the capacitance of a vacuum capacitor.

2.3.2 Dielectric relaxation in frequency domain

Many aspects of dielectric response, especially those involving non-linear processes, are more easily understood in the time domain. However, most engineering applications deal with responses to sinusoidal signals. Moreover, there exist fairly-standard and commercially-available apparatuses that are able to measure sinusoidal signals with high accuracy. Therefore, analyzing dielectric response in the frequency domain provides considerable practical advantage. As a matter of fact, it provides considerable theoretical advantages as well, as demonstrated below (Jonscher, 1983, p. 42).

By defining the Fourier transform of dielectric response function, $f(t)$, as:

$$F^*(\omega) = \int_0^\infty f(t)\exp(-\mathrm{j}\omega t)dt \tag{2.13}$$

the Fourier transform of $I(t)$ (equation (2.11)) is obtained:

$$I^*(\omega) = \frac{C_0\sigma_0 U^*(\omega)}{\varepsilon_0} + \mathrm{j}\omega C_0 U^*(\omega)\left[1 + F^*(\omega)\right] \tag{2.14}$$

By taking the frequency-dependent relative complex susceptibility $\chi_r^*(\omega)$, and the frequency-dependent relative complex dielectric permittivity $\varepsilon_r^*(\omega)$, i.e.,

$$\chi_r^*(\omega) = \chi_r'(\omega) - \mathrm{j}\chi_r''(\omega) = F^*(\omega) \tag{2.15}$$

$$\varepsilon_r^*(\omega) = \varepsilon_r'(\omega) - \mathrm{j}\varepsilon_r''(\omega) = \chi_r^*(\omega) + 1 = \chi_r'(\omega) + 1 - \mathrm{j}\chi_r''(\omega) \tag{2.16}$$

into equation (2.14), $I^*(\omega)$ is further expressed as:

$$I^*(\omega) = \omega C_0\left[\left(\frac{\sigma_0}{\omega\varepsilon_0} + \varepsilon_r''(\omega)\right) + \mathrm{j}\varepsilon_r'(\omega)\right]U^*(\omega) \tag{2.17}$$

As can be seen, $I^*(\omega)$ consists of a real component, $I'(\omega) = \omega C_0 U^*(\omega)\left(\frac{\sigma_0}{\omega\varepsilon_0} + \varepsilon_r''(\omega)\right)$, and an imaginary component, $I''(\omega) = \omega C_0 U^*(\omega)\varepsilon_r'(\omega)$. $I'(\omega)$ is in-phase with voltage and gives rise to power losses. $I''(\omega)$ is the capacitor's charging current; it leads voltage by 90° and does not contribute to any power losses.

In frequency-domain dielectric spectroscopy measurements, the apparatus measures the current $I^*(\omega)$ flowing through and the voltage $U^*(\omega)$ applied across the dielectric as well as the phase angle, $90°-\delta$, between them (Figure 2.3). Based on the dimensions of the capacitor, the dielectric constant $\varepsilon_r'(\omega)$ and dielectric loss $\frac{\sigma_0}{\omega\varepsilon_0}+\varepsilon_r''(\omega)$ are calculated.

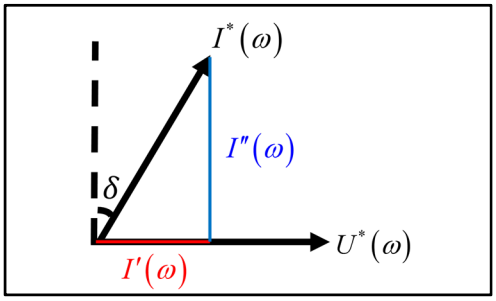

Figure 2.3 A phase diagram: the current flowing through and the voltage applied across a dielectric

2.3.3 Dielectric relaxation in polymers

Due to fast displacements of electronic clouds, electronic polarization occurs almost instantaneously, within times less than a half cycle of optical frequency (Figure 2.4). Electronic polarization is present in all dielectrics, and in nonpolar dielectrics such as polyethylene, it is the predominant form of polarization, contributing to the most significant part of dielectric constant over a broad frequency range from DC up to optical frequency. Since operating/utility frequencies are much lower, electronic polarization is not the source of dielectric loss in common electrical insulation applications (Dakin, 2006, pp. 17-19).

Due to involvement of heavier nuclei, atomic polarization is slower than electronic polarization and occurs at infrared frequency (Figure 2.4). Atomic polarization is present in most dielectrics. A particular case of this polarization, namely “ferroelectric”, gives rise to very high effective dielectric constants, in certain types of crystals and ceramics, at temperatures below the “Curie” temperature (Dakin, 2006, p. 16).

Due to delayed orientations of polarising species, dipolar polarization is slower than atomic polarization and occurs at microwave frequency, or lower frequencies in the case of large molecules such as polymeric chains (Figure 2.4). Dipolar polarization is commonly found in polymeric insulating materials, many of which contain polar groups or polar molecules that are sufficiently mobile to rotate, at least at elevated temperatures. Dipolar polarization usually causes dielectric loss in electrical insulation applications, as the frequency region where it occurs often coincides with the intended operating range (Dakin, 2006, pp. 20-21).

Due to long-range ion movements, interfacial polarization is typically the slowest to develop (Figure 2.4). Interfacial polarization is often observed in dielectric composites, polymer blends, and even semi-crystalline polymers, where at least two dissimilar phases exist. In electrical insulation applications, besides dipolar polarization, it is also of great interest to minimize interfacial polarization, as it is usually associated with conduction and dielectric loss at utility frequencies (Steeman et van Turnhout, 2003).

Both electronic polarization and atomic polarization are fairly independent of temperature. This is because forces opposing their displacements are not strongly temperature dependent. As temperature increases, dielectric constants attributable to these two polarizations slightly decrease, due to the decrease in material's density. In contrast, both dipolar polarization and interfacial polarization are sensitive to temperature. This is because both processes are largely influenced by material's internal viscosity, which is inversely correlated to temperature. As temperature increases, more dipoles are able to rotate more quickly, more ions are able to move more rapidly, giving rise to stronger dipolar polarization and interfacial polarization occurring at higher frequencies (Dakin, 2006, p. 18; Jonscher, 1983, p. 25).

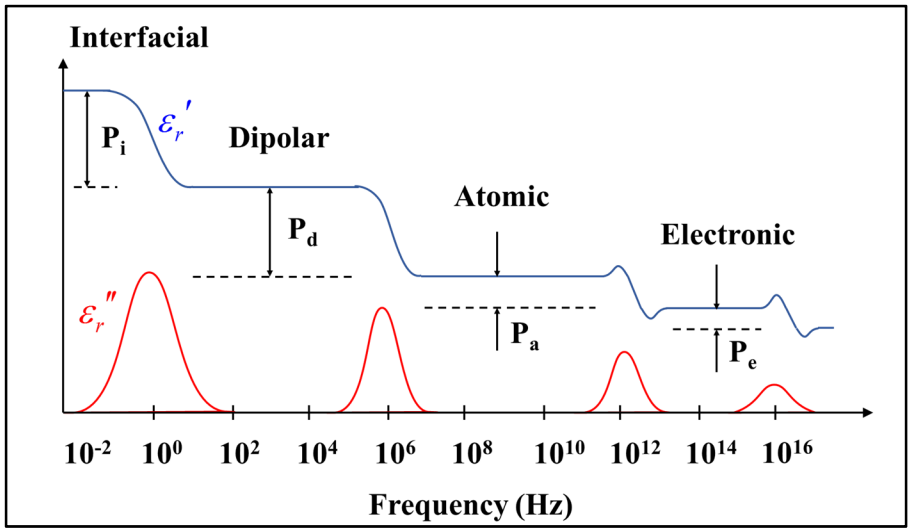

Figure 2.4 Dielectric relaxations in polymers.
Modified from (Raju, 2003b. Figure 4.13)

2.3.4 Equations to describe dielectric relaxation

The most basic equation to describe dielectric relaxation was established by Debye, through a Fourier transform of the exponentially declining displacement current. It was developed based on an ideal R-C circuit model that assumes a single relaxation time. However, more often than not, there is a distribution of relaxation times, particularly in polymers, where structural heterogeneities are commonly present. As improvements, equations based on Cole-Cole, Davidson-Cole and Havriliak-Negami theories were put forward (Dakin, 2006, pp. 22-24; Raju, 2003a).

Although Debye-based equations can reasonably well describe the relaxation process in polar dielectrics, they are not suitable for nonpolar dielectrics, which are generally characteristic of frequency-independent or "flat" dielectric responses. Practically speaking, the dielectric loss, from which some weak peaks can sometimes be discerned, may not be completely "flat". However, as long as a general flat trend with a variation "not more than a factor of 2 to 3 over five, six or more decades of frequency" is exhibited (Jonscher, 1996, p. 126), it is considered a "flat" loss. "Flat" loss is completely at variance with the Debye theory of ω^{-1} dependence.

Moreover, it is generally independent of temperature, which is incompatible with the Debye-like process that is proportional to 1/T (Raju, 2003b).

Based on overwhelming experimental evidence, Jonscher suggested a "Universal Law" of relaxation, where the empirical form of dielectric loss is approximated by the combination of two power-laws (Jonscher, 1981; 1983, p. 192):

$$\chi_r''(\omega) \propto \frac{1}{(\omega/\omega_p)^{-m} + (\omega/\omega_p)^{1-n}} \quad 0 < \begin{Bmatrix} m \\ 1-n \end{Bmatrix} < 1 \tag{2.18}$$

where ω_p is the peak frequency; m is the pre-peak exponent defining the frequency dependence of the power-law below ω_p; n is the post-peak exponent defining the frequency dependence of the power-law above ω_p. m and n are weakly dependent on temperature, remaining constant or decreasing slightly with increasing temperature (Raju, 2003b).

The post-peak dielectric response of the "Universal Law" becomes "flat" as n approaches unity, and thus can be used to describe the aforementioned relaxation behavior in non-polar dielectrics (Raju, 2003b). The post-peak dielectric response is obtained through a Fourier transform of post-peak time-domain response $f(t)$ (Jonscher, 1981):

$$f(t) \propto t^{-n} \xrightarrow{\textit{Fourier transform}} \chi_r^*(\omega) = B(\mathrm{j}\omega)^{n-1} \tag{2.19}$$

where B is a constant related to the movement of charge carriers. Taking into account the contributions of electronic polarization, ε_∞, and DC conductance, the dielectric permittivity of a non-polar dielectric can thus be described as:

$$\varepsilon_r^*(\omega) = \varepsilon_\infty + B(\mathrm{j}\omega)^{n-1} - \mathrm{j}\frac{\sigma_0}{\varepsilon_0 \omega} \tag{2.20}$$

2.3.5 Dielectric relaxation in heterogeneous dielectrics

Dielectric relaxation in heterogeneous dielectrics can be described by Maxwell-Wagner-Sillars (MWS) theory (Bánhegyi, 1986; Steeman et van Turnhout, 2003). MWS theory is based on a matrix-filler model (Figure 2.5), whereby a filler phase (denoted by f) is dispersed in a matrix phase (denoted by m), and both phases are embedded in an effective medium that possesses the property of the composite.

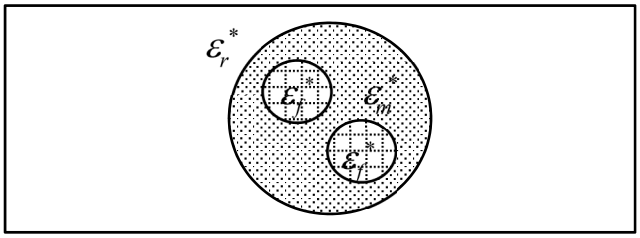

Figure 2.5 A schematic illustration:
the matrix-filler model used in MWS theory

The essence of MWS theory lies in that it expresses $\varepsilon_r^*(\omega)$ in terms of component properties and average fields:

$$\varepsilon_r^*(\omega) = \frac{\varphi_m \varepsilon_m^*(\omega)\langle E_m \rangle + \varphi_f \varepsilon_f^*(\omega)\langle E_f \rangle}{\langle E \rangle} \tag{2.21}$$

where φ_m and φ_f are volume fractions of the filler and the matrix, respectively; $\langle E_f \rangle$, $\langle E_m \rangle$, and $\langle E \rangle$ are electric fields averaged over the filler volume, the matrix volume and the composite volume, respectively. $\langle E \rangle$ is expressed as a weighted average of the component fields, as:

$$\langle E \rangle = \varphi_m \langle E_m \rangle + \varphi_f \langle E_f \rangle \tag{2.22}$$

In cases where the filler bears an ellipsoidal shape and has a low concentration, the ratio of the fields inside and outside the filler can be assumed as:

$$\frac{\langle E_f \rangle}{\langle E_m \rangle} = \sum_{k=1}^{3} \frac{\cos^2 \alpha_k}{1 + \left(\frac{\varepsilon_f^*(\omega)}{\varepsilon_m^*(\omega)} - 1 \right) A_k} \tag{2.23}$$

where k = 1, 2, 3 represent the three axes of the ellipsoid; α_k is the orientation factor of the ellipsoid, and is equal to the angle between the field and the ellipsoid's k-th axis; A_k is the depolarization factor of the ellipsoid, and is related only to the lengths of the ellipsoid's axes. For randomly oriented fillers, $\cos^2\alpha_1 = \cos^2\alpha_2 = \cos^2\alpha_3 = 1/3$, whereas for fillers fully oriented along the k-th axis, $\cos^2\alpha_k = 1$, $\cos^2\alpha_j = 0$ if $j \neq k$. For prolate ellipsoidal (rod-like) fillers, $0 \leq A_k \leq 1/3$, for oblate ellipsoidal (disc-like) fillers, $1/3 \leq A_k \leq 1$, and for spherical fillers, $A_1 = A_2 = A_3 = 1/3$ (Bánhegyi, 1986).

Combine equations (2.21)–(2.23), the equation to describe the dielectric relaxation in heterogeneous composites bearing randomly oriented fillers is derived as:

$$\varepsilon_r^*(\omega) = \frac{\varepsilon_m^*(\omega)\varphi_m + \frac{\varepsilon_f^*(\omega)\varphi_f}{3} \sum_{k=1}^{3} \frac{\varepsilon_m^*(\omega)}{\varepsilon_m^*(\omega) + \left[\varepsilon_f^*(\omega) - \varepsilon_m^*(\omega) \right] A_k}}{\varphi_m + \frac{\varphi_f}{3} \sum_{k=1}^{3} \frac{\varepsilon_m^*(\omega)}{\varepsilon_m^*(\omega) + \left[\varepsilon_f^*(\omega) - \varepsilon_m^*(\omega) \right] A_k}} \tag{2.24}$$

CHAPTER 3

POLYETHYLENE/POLYHEDRAL OLIGOMERIC SILSESQUIOXANES COMPOSITES OBTAINED BY BALL MILLING

Journal Article I

POLYETHYLENE-BASED DIELECTRIC COMPOSITES CONTAINING POLYHEDRAL OLIGOMERIC SILSESQUIOXANES OBTAINED BY BALL MILLING

Meng Guo[1, 2], Michel Fréchette[2], Éric David[1] and Nicole R. Demarquette[1]

[1]École de technologie supérieure (ÉTS),

1100 Notre-Dame Street West, Montreal, QC H3C 1K3, Canada

[2]Institut de recherche d'Hydro-Québec (IREQ),

1800 Boulevard Lionel Boulet, Varennes, QC J3X 1S1, Canada

This article has been published in:

Transactions on Electrical and Electronic Materials

Vol. 16, No. 02, 2015, pp. 53-61

http://dx.doi.org/10.4313/TEEM.2015.16.2.53

This article has been modified and edited for integration into the thesis.

Abstract

High-energy ball milling was tested as a method for producing ultra-high molecular weight polyethylene (UHMWPE)-based nanodielectrics containing 1 wt% and 5 wt% octaisobutyl-POSS (OibPOSS). The morphology, as well as the thermal and dielectric properties of the obtained samples were characterized by scanning electron microscopy (SEM), thermogravimetric analysis (TGA), broadband dielectric spectroscopy (BDS), and progressive-stress breakdown tests (PSB). The results showed that (i) ball milling was an effective method for producing UHMWPE/OibPOSS dielectric composites, but appeared ineffective in dispersing OibPOSS at the nanoscale, and (ii) the resulting UHMWPE/OibPOSS composites presented thermal and dielectric properties similar to those of neat UHMWPE.

3.1 Introduction

In a ball milling process, a vial containing sample and grinding balls is secured by a clamp and swung energetically in a '∞' pattern (i.e., a combination of back-and-forth and lateral movements). The sample gets milled and mixed with each swing, when balls impact the sample against the end of the vial. Thanks to the sufficient amplitude and speed of clamp motion, the balls' velocities are high, leading to impacts of high energy (Suryanarayana, 2001). In this work, high-energy ball milling was tested as a method for breaking micro-sized POSS crystals into nano sizes and thereby producing PE/POSS nanodielectrics.

Ultra-high molecular weight polyethylene (UHMWPE) powder and octaisobutyl-POSS (OibPOSS) powder were used, as introduced in section 3.2.1 "Materials". They were ball milled in desired mass fractions and the resulting powders were subsequently compression-molded into plate samples, as described under section 3.2.2 "Sample preparation". The obtained samples were characterized with thermogravimetric analysis (TGA), scanning electron microscopy (SEM), broadband dielectric spectroscopy (BDS), and progressive-stress breakdown tests (PSB), as addressed under section 3.2.3 "Characterization techniques". Finally, the results are presented and discussed in section 3.3 "Results and discussion".

3.2 Experimental

3.2.1 Materials

UHMWPE powder (nominal average particle size: ~150 μm, molecular weight: 3–6 million) was purchased from Alfa Aesar (Product No. 43951). OibPOSS powder (average particle size: ~200 μm) was purchased from Hybrid Plastics (Product No. MS0825).

3.2.2 Sample preparation

A high-energy shaker mill (SPEX CertPrep 8000) was used. As-received UHMWPE powder and as-received OibPOSS powder according to 100/0%, 99/1% and 95/5% mass fractions were

respectively ball milled in a zirconia vial with zirconia grinding balls for 30 minutes. The ball-to-powder weight ratio was ten. A combination of large and small balls was used: one 15 mm in diameter, two 10 mm in diameter, and five 5 mm in diameter.

Under a pressure of 6.3×10^6 Pa and an average temperature of 150 °C, the composite powders obtained from ball milling were compression molded into plate samples: UHMWPE, UHMWPE/OibPOSS (99/1), and UHMWPE/OibPOSS (95/5).

3.2.3 Characterization techniques

Thermogravimetric analysis was conducted on UHMWPE and UHMWPE/OibPOSS composites to (i) confirm whether the right amount of OibPOSS (i.e., 1 wt% and 5 wt%) had been incorporated into the relevant composites, and to (ii) study the thermal stability of the composites in comparison with that of UHMWPE. In order to better understand the thermogravimetric features of the materials in question, as-received OibPOSS powder was also tested. Tests were carried out using a TA Q50 instrument. Samples of ~12 mg were put in a platinum pan and heated from 30 °C to 600 °C at a rate of 10 °C/min in a nitrogen atmosphere (balance gas flux: 40 mL/min, sample gas flux: 60 mL/min). Thermogravimetric data were recorded with a sampling interval of 0.5 s/pt. In order to increase the reliability of results, two samples were tested for each type of material.

To evaluate the size dispersion and spatial distribution of OibPOSS within UHMWPE matrix, cross-sections of UHMWPE and UHMWPE/OibPOSS composites were observed with a Hitachi 3600N scanning electron microscope at an electron accelerating voltage of 5 kV. Cross-sections were obtained by cutting the samples (cooled to around -130 °C) with a diamond knife in a microtome (Leica RM2255). Furthermore, they were sputtered with a 2 nm platinum layer in a Quorum Q150T S machine prior to microscopy. In order to increase the reliability of observations, at least two cross-sections were prepared for each type of material, and several spots were observed on each cross-section.

Dielectric constants and dielectric losses of UHMWPE and UHMWPE/OibPOSS composites were measured using a Novocontrol broadband dielectric spectrometer. For each type of material, one sample with a thickness of ~0.5 mm and a diameter of 30 mm was tested. To ensure a good sample-electrode contact, the sample was first sandwiched between two soft and flexible silver foils (0.06 mm thickness, 30 mm diameter each). The silver foil-sample-silver foil structure was then placed between two round plate electrodes (2.35 mm thickness, 30 mm diameter each). To increase the accuracy of end results, an edge compensation (= 2.41 mm) on electrode thickness was used. During the measurement, an AC voltage of V_{rms}=3 V was applied to the sample in 10^{-2}–3×10^{6} Hz frequency range at 23 °C. The apparatus recorded the current and the current-voltage phase shift, and then calculated the complex dielectric permittivity of the sample based on sample geometry and edge-compensation value.

AC progressive-stress dielectric breakdown strengths of UHMWPE and UHMWPE/OibPOSS composites were tested according to (ASTM Standard D149, 2013) at 23 °C and 23%–26% relative humidity. For each progress-stress test, a sample with a ~0.23 mm thickness (standard deviation: 0.009–0.01) and a 20 mm diameter was placed between a pair of cylindrical rod electrodes (6.4 mm in diameter with edges rounded to 0.8 mm). Both sample and electrodes were immersed in an insulating fluid (Luminol TR-i, Type II Inhibée, Petro-Canada Lubricants Inc.). An AC voltage (60 Hz) with a 2 kV/s constant rate of rise was then applied on the sample from zero until breakdown occurred (in an average time of 10–20 s). This was repeated for a set of 10 samples for each type of material, and the breakdown voltage of each sample was recorded. The insulating fluid was refreshed after each 10-sample test series for each type of material. A statistical analysis of the breakdown data was performed in accordance with (IEEE Standard 930, 2005).

3.3 Results and discussion

3.3.1 Thermogravimetric analysis (TGA)

Thermogravimetric behaviors of OibPOSS, UHMWPE and UHMWPE/OibPOSS are shown in Figure 3.1 (a). A magnified view of Figure 3.1 (a) in a 150–450 °C temperature range is shown in Figure 3.1 (b). As can be seen, the weight loss of UHMWPE takes place in one step, with the maximum weight loss rate occurring at T_{max}=470 °C. Moreover, the weight loss of OibPOSS takes place in two steps. The major weight loss (92%, T_{max}=270 °C) is due to OibPOSS evaporation and the minor one (8%, T_{max}=311 °C) is possibly related to the degradation of a more stable phase formed during the heating throughout the first step (Fina et al., 2005a; Fina et al., 2005b). In the case of UHMWPE/OibPOSS composites, their weight losses take place in two steps. The first step (T_{max}=241 °C for 1 wt% and T_{max}=246 °C for 5 wt%) is corresponding to OibPOSS evaporation and the second step (T_{max}=470 °C for both 1 wt% and 5 wt%) is related to UHMWPE degradation. For all materials, negligible residues are left above 500 °C.

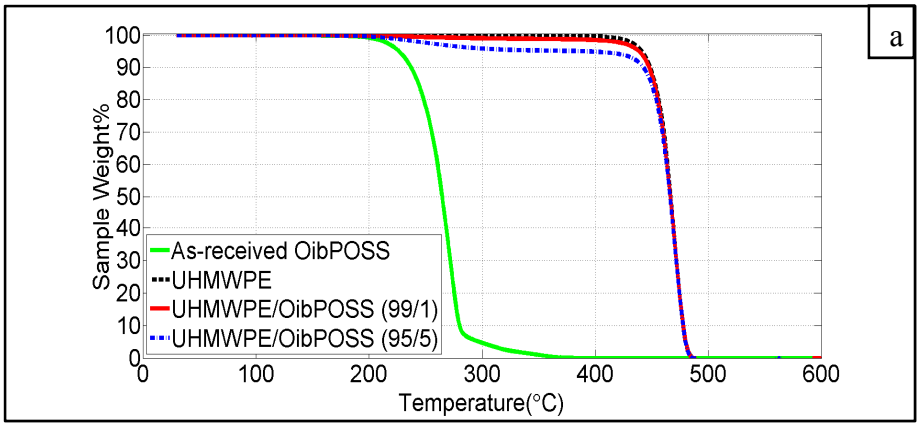

Figure 3.1 Thermogravimetric behaviors of OibPOSS, UHMWPE and UHMWPE/OibPOSS composites in (a) 0–600 °C temperature range and (b) 150–450 °C temperature range

Figure 3.1 (Continued)

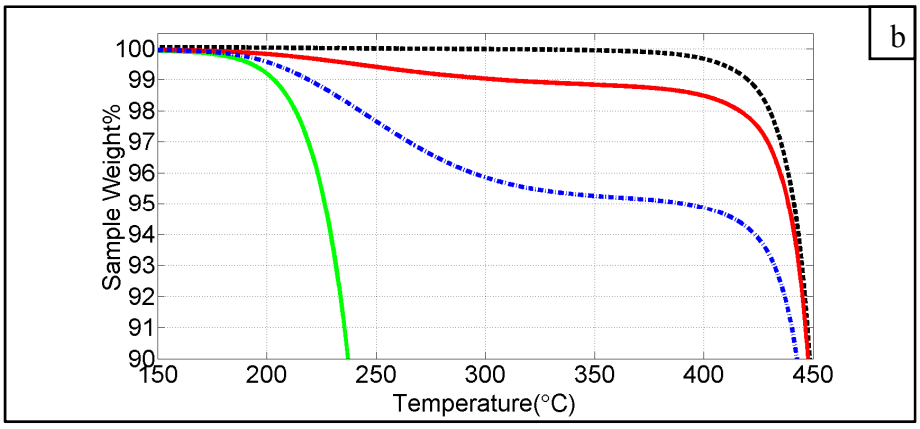

As shown in Figure 3.1 (b), near the end of the first step, a 99% weight loss plateau is found for UHMWPE/OibPOSS (99/1) and a 95% weight loss plateau is found for UHMWPE/OibPOSS (95/5). These confirm that right amounts of OibPOSS have been introduced into relevant composites.

The composites' thermogravimetric behaviors indicate that OibPOSS addition does not have any obvious effects on the thermal stability of UHMWPE in a nitrogen atmosphere. This is probably resulted from OibPOSS' evaporation, which occurs at a temperature lower than the degradation temperature of UHMWPE.

3.3.2 Scanning electron microscopy (SEM)

Figure 3.2 presents SEM images of (a) UHMWPE, (b) UHMWPE/OibPOSS (99/1) and (c) UHMWPE/OibPOSS (95/5). It can be seen from Figure 3.2 (a) that the cross-section of UHMWPE is reasonably clean, bearing a few cutting traces and impurities. As shown in Figure 3.2 (b), OibPOSS disperses in UHMWPE/OibPOSS (99/1) at micron scale (2–8 μm). They have a poor spatial distribution, and can seldom be found within the composite. As can be seen from Figure 3.2 (c), OibPOSS disperse in UHMWPE/OibPOSS (95/5) at submicron to micron scale, with a seemingly homogeneous spatial distribution. The observed morphology indicates that ball milling is an effective method for producing UHMWPE/OibPOSS composites, but appears ineffective in dispersing OibPOSS at the nanoscale.

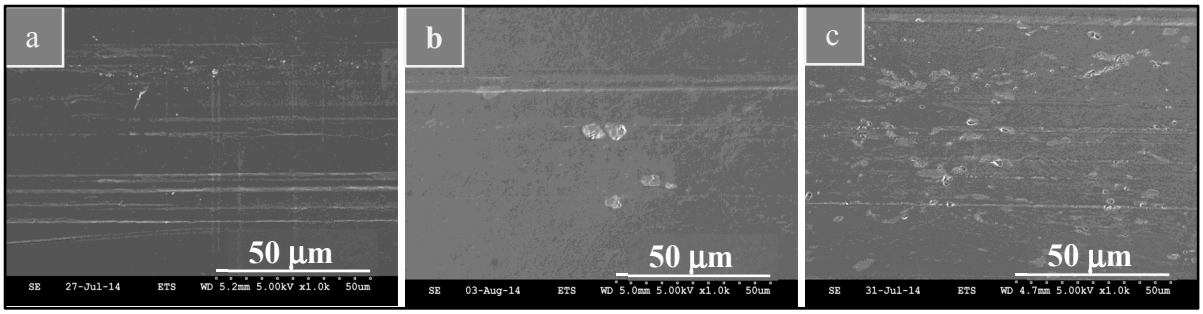

Figure 3.2 SEM images of (a) UHMWPE, (b) UHMWPE/OibPOSS (99/1) and (c) UHMWPE/OibPOSS (95/5)

3.3.3 Broadband dielectric spectroscopy (BDS)

Figure 3.3 presents relative real permittivities/dielectric constants (ε_r') and relative imaginary permittivities/dielectric losses (ε_r'') of UHMWPE and UHMWPE/OibPOSS composites as a function of frequency. As can be seen, the ε_r' of UHMWPE/OibPOSS composites are almost the same as that of UHMWPE, with a value of 2.3 over a wide frequency span of 10^{-2}–10^{6} Hz. Moreover, the ε_r'' of UHMWPE/OibPOSS composites are also almost the same as that of UHMWPE, which is too low (10^{-6}–10^{-4}) to be measured accurately. This indicates that OibPOSS addition has little effect on the dielectric response of UHMWPE.

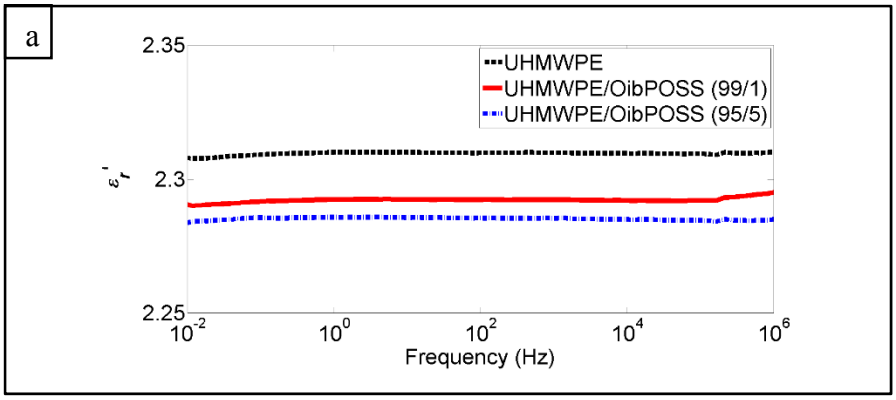

Figure 3.3 (a) Relative real permittivities and (b) relative imaginary permittivities of UHMWPE, UHMWPE/OibPOSS (99/1), and UHMWPE/OibPOSS (95/5)

Figure 3.3 (Continued)

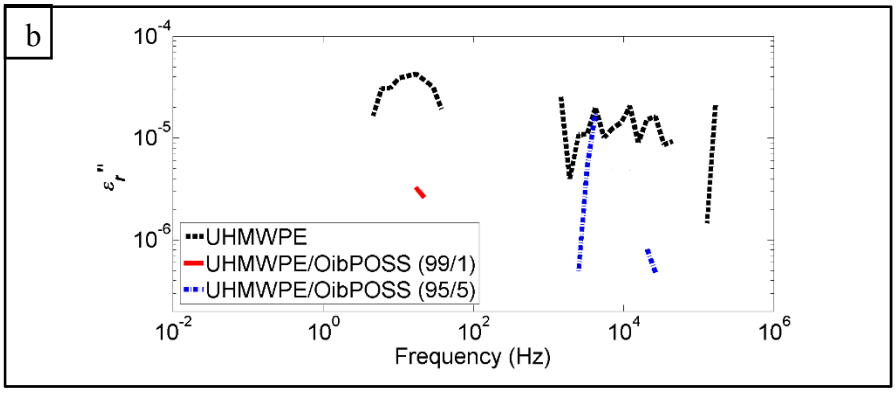

3.3.4 Progressive-stress breakdown tests (PSB)

Progressive-stress short-time dielectric breakdown is an electronic process caused by high-energy free electrons (Dissado, 2011; Ieda, 1980; Tian et al., 2012). Measures that can decrease the density and energy of free electrons contribute to enhance the dielectric breakdown strength.

POSS helps reduce the energy of free electrons by acting as electron-scattering sites. Moreover, changes in PE chains mobility, local PE structure, and local charge distribution may occur within the POSS-PE interphase, helping increase the density and depth of charge-carrier trapping states (Smith et al., 2008). Both aspects help enhance dielectric breakdown strength. However, micrometric POSS brings about microscopic void defects at the POSS-PE interface, affecting the breakdown strength negatively. The positive effects and the negative ones counteract one another, resulting in almost-unchanged dielectric breakdown strengths, as shown in Figure 3.4 and Table 3.1.

Table 3.1 Scale (α) and shape (β) parameters of the two-parameter Weibull distribution

Sample	Shape parameter β	Scale parameter α (kV/mm)
UHMWPE	33.8	136.5
UHMWPE/OibPOSS (99/1)	33.1	136.5
UHMWPE/OibPOSS (95/5)	28.4	135.6

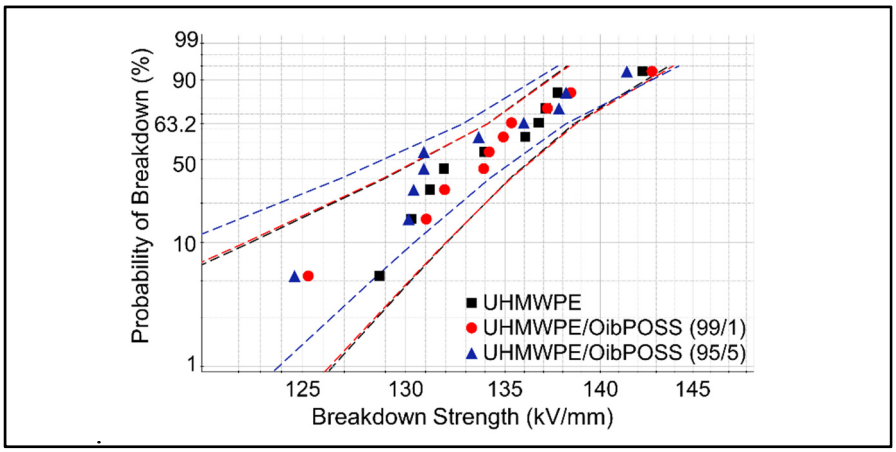

Figure 3.4 The two-parameter Weibulll distribution of UHMWPE and UHMWPE/OibPOSS composites (90% confidence interval)

3.4 Conclusion

High-energy ball milling was tested as a method for producing UHMWPE-based nanodielectrics containing 1 wt% and 5 wt% OibPOSS. Morphology, thermal and dielectric properties of the composites were characterized by scanning electron microscopy (SEM), thermogravimetric analysis (TGA), broadband dielectric spectroscopy (BDS), and progressive-stress breakdown tests (PSB). Microscopic observation showed that ball milling was an effective method for producing UHMWPE/OibPOSS composites, but appeared ineffective in dispersing OibPOSS at the nanoscale. Moreover, thermogravimetric behaviors, relative permittivities and short-time dielectric breakdown strengths of UHMWPE/OibPOSS composites were similar to that of UHMWPE.

3.5 Acknowledgements

Financial support from Hydro-Québec and the Natural Sciences and Engineering Research Council of Canada (NSERC) are highly appreciated. Helps and suggestions from Dr. Hugues Couderc are thankfully acknowledged.

CHAPTER 4

POLYETHYLENE/POLYHEDRAL OLIGOMERIC SILSESQUIOXANES COMPOSITES OBTAINED BY XYLENE SOLUTION BLENDING

Journal Article II

POLYETHYLENE/POLYHEDRAL OLIGOMERIC SILSESQUIOXANES COMPOSITES: ELECTRICAL INSULATION FOR HIGH VOLTAGE POWER CABLES

Meng Guo[1, 2], Michel Fréchette[2], Éric David[1],

Nicole R. Demarquette[1], and Jean-Christophe Daigle[2]

[1]École de technologie supérieure (ÉTS),

1100 Notre-Dame Street West, Montreal, QC H3C 1K3, Canada

[2]Institut de recherche d'Hydro-Québec (IREQ),

1800 Boulevard Lionel Boulet, Varennes, QC J3X 1S1, Canada

This article has been published in:

IEEE Transactions on Dielectrics and Electrical Insulation

Vol. 24, No. 02, 2017, pp. 798-807

http://dx.doi.org/10.1109/TDEI.2017.006144

This article has been modified and edited for integration into the thesis.

Abstract

Xylene solution blending was tested as a method for producing low-density polyethylene (LDPE)-based nanodielectrics containing 1 wt% and 5 wt% polyhedral oligomeric silsesquioxanes (POS) of different types—octamethyl-POS, octaisobutyl-POS, and isooctyl-POS. The chemical composition, the morphology, the thermal properties and the dielectric properties of the obtained samples were characterized by Fourier transform infrared spectroscopy (FTIR), scanning electron microscopy (SEM), thermogravimetric analysis (TGA), differential scanning calorimetry (DSC), thermal conductivity measurements, broadband dielectric spectroscopy (BDS), progressive-stress breakdown tests (PSB), and surface partial discharge tests. The results showed that although xylene solution blending was

an effective method for producing LDPE/POS dielectric composites, it appeared ineffective in dispersing POS at the nanoscale. Moreover, some of the composites presented an improved thermal conductivity, a maintained breakdown strength and an enhanced resistance to corona discharges.

4.1 Introduction

Xylene solution blending was attempted as a method for producing PE/POS nanodielectrics. The approach relies on a rationale that both POS and PE dissolve and are thus mixed at the molecular level in xylene solution. LDPE matrix and three types of POS were studied, as introduced in section 4.2.1 “Materials”. LDPE/POS composites were produced by xylene solution blending, and subsequently compression-molded into plate samples, as described under section 4.2.2 “Sample preparation”. The obtained samples were characterized concerning their chemical composition, morphology, thermal properties and dielectric properties, as addressed under section 4.2.3 “Characterization techniques”. Finally, the results are presented and discussed in section 4.3 “Results and discussion”.

4.2 Experimental

4.2.1 Materials

LDPE was purchased from Marplex Australia PTY. LTD. (Product No. ALKATEQ™ XDS34P). It is an unpigmented and additive-free powder with a density of 0.922 g/cm^3 and a typical particle size of 95% < 500 μm. The powder form (instead of the pellet form) was chosen as it can dissolve in xylene faster and more easily.

Three types of POS were used, namely, octamethyl-POS (OmPOS) (R=methyl group), octaisobutyl-POS (OibPOS) (R=isobutyl group), and isooctyl-POS (IoPOS) (R=isooctyl group) (Figure 1.4). They were purchased from Hybrid, product Nos. MS0830, MS0825 and MS0805, respectively (Hybrid, 2014). OmPOSS and OibPOSS are crystalline solids with densities of 1.5 g/cm^3 and 1.13 g/cm^3, and average particle sizes of ~30 μm and ~200 μm, respectively. IoPOS is a viscous liquid having a density of 1.01 g/cm^3 (DeArmitt, 2010). According to the

evaluation carried out in section 1.4.2.2 “POSS-PE compatibility”, OmPOS has the lowest compatibility with PE, OibPOS a medium, and IoPOS, the highest.

4.2.2 Sample preparation

OmPOS, OibPOS and IoPOS were respectively mixed with LDPE in 1/99% and 5/95% mass fractions. Xylene solution blending took place in a 250 mL round-bottom flask attached to a water-filled condenser. An 8 g LDPE+POS mixture, together with 150 mL xylene, were introduced into the flask at room temperature. Then, the LDPE/POS/xylene mixture was stirred with a magnetic stirring bar under continuous heating for 60 min. At this point, a boiling LDPE/POS/xylene mixture was obtained. Thanks to the condenser, the loss of xylene during the blending process was minimal. Moreover, as confirmed by visual observation, all mixtures obtained appeared to be clear solutions, except for that containing 5 wt% OmPOS, which appeared to be an opaque suspension. Subsequently, the boiling mixture was quickly poured into 750 mL, vigorously stirred, cold (~4 °C) methanol. Since xylene and methanol are miscible, whereas neither LDPE nor any of the three types of POS dissolve in methanol, the result of the last step was an immediate precipitation of LDPE/POS composites. The precipitations were filtered, and then thoroughly dried under fume hood and vacuum to a negligible weight loss. As a control, LDPE was prepared exactly the same way. Under an average temperature of 150 °C, a pressure of 6.3×10^6 Pa, and a duration of 15 min, the seven types of dried precipitations were respectively compression molded into two plates of different thicknesses: ~0.22 mm and ~0.5 mm.

Table 4.1 Mass (w) and volume (v) fractions of POS in each sample

Sample	**Mass fraction of POS w (wt%)**	**Volume fraction of POS v (vol%)**
LDPE/OmPOS (99/1)	1	0.6
LDPE/OibPOS (99/1)	1	0.8
LDPE/IoPOS (99/1)	1	0.9
LDPE/OmPOS (95/5)	5	3.1
LDPE/OibPOS (95/5)	5	4.1
LDPE/IoPOS (95/5)	5	4.6

Samples of LDPE, LDPE/OmPOS (99/1), LDPE/OibPOS (99/1), LDPE/IoPOS (99/1), LDPE/OmPOS (95/5), LDPE/OibPOS (95/5), and LDPE/IoPOS (95/5) were respectively cut off from relevant plates, and subjected to following characterizations (Table 4.1).

4.2.3 Characterization techniques

LDPE and LDPE/POS composites were characterized by Fourier transform infrared spectroscopy (FTIR) to verify if POS had been successfully incorporated into relevant composites. FTIR was performed with a Thermo Electron Corporation Nicolet Continuμm XL FTIR Imaging Microscope, in transmission mode, using thin samples of ~0.22 mm. In order to increase the reliability of results, at least two samples were tested for each type of material.

To evaluate the size dispersion and spatial distribution of POS within LDPE matrix, cross-sections of LDPE and LDPE/POS composites were observed with a Hitachi 3600N scanning electron microscope (SEM). Cross-sections were obtained by cutting samples cooled to around -135 °C with a diamond-knife-equipped microtome (Leica RM2255). To increase the reliability of observations, at least two cross-sections were prepared for each type of material, and several spots were observed on each cross-section.

LDPE, POS and their composites were studied by thermogravimetric analysis (TGA), to investigate composites' thermal stabilities and possible POS-LDPE interactions. Tests were carried out using a TA Q50 instrument. A single piece of sample of ~8 mg was heated from 30 °C to 600 °C at a rate of 10 °C/min in a nitrogen atmosphere. In order to increase the reliability of results, at least two samples were tested for each type of material.

To further evaluate possible POS-LDPE intermolecular interactions, melting temperatures and degrees of crystallinity of LDPE and LDPE/POS were characterized by differential scanning calorimetry (DSC). DSC tests were carried out using a TA Q20 apparatus in a nitrogen atmosphere. Two types of calibration were performed prior to measurements: baseline calibration and cell constant calibration. The former was conducted on an empty chamber from

-20 °C to 170 °C at a rate of 10 °C/min and the latter was done on an indium sample from 100 °C to 180 °C at the same rate. In each measurement, a single piece of sample of ~8 mg was firstly heated from 0 °C to 150 °C at a rate of 10 °C/min to erase previous thermal history, and then cooled from 150 °C to 0 °C at 10 °C/min, and once again heated from 0 °C to 150 °C at the same rate. Curves of the second heating were used to obtain melting temperatures and degrees of crystallinity of the materials. Two samples from each type of material were tested. Their results are presented in the form of averages ± variances in Table 4.2.

Thermal conductivities of LDPE and LDPE/POS composites were measured in accordance with (ASTM Standard E1530, 2011) using a thermal conductivity tester from TA Instruments (model QuickLine-10, DTC-25). A sample of interest was held, under a load of 15 psi, between an upper 45 °C metal surface and a lower 15 °C metal surface, for a sufficiently long time (from ~3 hrs to ~26 hrs) until the sample's thermal equilibrium was reached. One sample from each type of material was measured three times (except for LDPE, which was measured two times) to ensure the reliability of results.

Dielectric constants and dielectric losses of LDPE and LDPE/POS composites were obtained using a Novocontrol broadband dielectric spectrometer. Each sample of interest (30 mm diameter and ~0.5 mm thickness) was placed between two external round plate electrodes (30 mm diameter) to form a sandwich capacitor, before being mounted onto the measurement cell. An AC voltage of V_{rms}=3 V was applied to the sample in a 10^{-2}–10^{4} Hz frequency range at 23 °C. One sample from each type of material was measured three times to ensure the reliability of results.

Breakdown strengths of LDPE and LDPE/POS composites under AC progressive stress were tested in accordance with (ASTM Standard D149, 2013). To reveal breakdown strengths' statistical distribution, 11–12 samples were tested for each type of material. Each sample had a diameter of 20 mm and a thickness of ~0.22 mm (standard deviation: 0.008–0.011). In each test, a sample was fixed between a pair of cylindrical rod electrodes (6.4 mm in diameter with edges rounded to 0.8 mm) and immersed in an insulating fluid (Luminol TR-i, Type II Inhibée, Petro-

Canada Lubricants Inc.). An AC voltage of 60 Hz was applied on the sample, at a constant rate of rise of 2 kV/s, from zero until breakdown occurred. The voltage at which the sample was broken down was recorded, and the breakdown field was calculated based on sample thickness. All samples were broken down in 10–20 s, except for some from LDPE/OmPOS (95/5) and LDPE/OibPOS (95/5), which were broken down at 8 s or 9 s. All tests were performed at 21–23 °C. After each test series, i.e., 11–12 tests on 11–12 samples of one type of material, insulating fluid was refreshed and electrodes were cleaned to get rid of black residues.

Surface partial discharge tests were conducted on LDPE and LDPE/POS to evaluate their resistances to prolonged AC stress under electrical discharge conditions. One to four samples from each type of material were tested. In each test, a sample was fixed on a round plate electrode with the tip of a rod electrode facing to it from a 100 μm air gap. A sinusoidal AC voltage of V_{peak}=10 kV and 300 Hz was applied on the rod electrode, whereas the round plate electrode was connected to the ground (i.e., zero voltage). Corona discharges were produced between the sample and the tip, causing erosion to the sample. Each sample was eroded for 35 hours. After each erosion test, electrodes were gently polished to remove erosion residues. To evaluate eroded volumes, the samples eroded were firstly cleaned in a methanol ultrasonic bath for 5 min to get rid of erosion debris and then subjected to surface profilometry in a mechanical profilometer (Dektak 150).

4.3 Results and discussion

4.3.1 Fourier transform infrared spectroscopy (FTIR)

FTIR spectra of LDPE, POS, and their composites are shown in Figure 4.1. The intense absorption band at ~1115 cm^{-1} wavenumber arises from the vibration of Si–O bond in POS' silicon-oxygen backbone. Absorption bands at 1270 cm^{-1}, 1230 cm^{-1}, and 1227 cm^{-1} correspond to Si–C stretching vibrations, whereas those at 773 cm^{-1}, 837 cm^{-1} and 910 cm^{-1} are brought about by Si–C bending or deformation vibrations. Absorption bands at 2825 cm^{-1} and ~2965 cm^{-1} are attributable to C–H stretching vibrations in methanediyl and methyl groups, and

can be related to the joint contribution of POS and PE (Coates, 2006; Krimm, Liang et Sutherland, 1956; Launer, 2013). The above observations indicate that POS have been successfully incorporated into relevant composites.

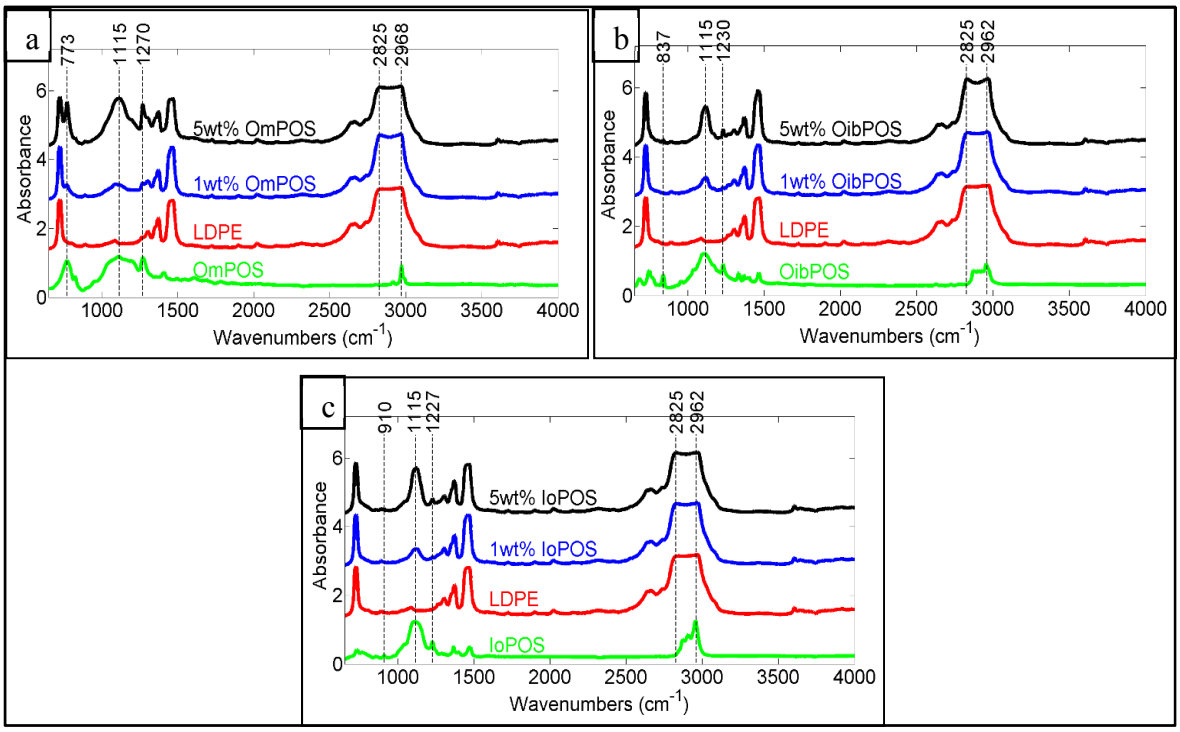

Figure 4.1 FTIR spectra of (a) LDPE, OmPOS and LDPE/OmPOS composites, (b) LDPE, OibPOS and LDPE/OibPOS composites and (c) LDPE, IoPOS and LDPE/IoPOS composites

4.3.2 Scanning electron microscopy (SEM)

Typical images of LDPE and LDPE/POS composites are presented in Figure 4.2. It can be seen in Figure 4.2 (a) that LDPE is reasonably clean, bearing few holes, impurities, and cutting traces. As shown in Figure 4.2 (b), OmPOS generally assume quasi-rectangular shapes and are distributed sparsely, yet acceptably evenly in LDPE/OmPOS (99/1). OmPOS are averaged at 5–10 μm, although they can be as small as ~1.5 μm and as big as ~20 μm. As OmPOS loading increases to 5 wt%, as shown in Figure 4.2 (c), OmPOS' distribution is denser, and the quantity and size of bigger OmPOS crystals increases. As can be seen in Figure 4.2 (d), OibPOS are

present mostly in triangular shapes and are distributed homogeneously in LDPE/OibPOS (99/1). The size of OibPOS ranges from several hundred nanometers up to ~5 μm, averaging at ~2 μm. In LDPE/OibPOS (95/5), OibPOS are dispersed in basically two patterns: (i) sparsely distributed crystals of comparatively large sizes (Figure 4.2 (e)), and (ii) small crystals and their clusters (Figure 4.2 (f)). Dispersion and distribution features of IoPOS in its 1 wt% and 5 wt% composites can be found in Figure 4.2 (g) and Figure 4.2 (h). As can be seen, in both cases, IoPOS are present as spherical or quasi-spherical droplets. However, the distribution pattern they adopt is quite different. In the 1 wt% composite, IoPOS are generally distributed as inclined strips, being filled with small droplets of mostly 1–3 μm. In the 5 wt% composite, bigger (5–10 μm) and smaller droplets (2–5 μm) appear to have a homogeneous distribution.

In brief, for composites containing solid OmPOS and OibPOS, it would seem that at 1 wt% loading, OibPOS can be more easily dispersed at small sizes than OmPOS. This may be due to higher compatibility of OibPOS with PE. Moreover, for both OmPOS and OibPOS, 5 wt% loading seems to be a too large amount to have POS homogeneously dispersed into small sizes. As for viscous-liquid IoPOS, notwithstanding its higher PE compatibility, its 1 wt% composite does not seem to accomplish a better dispersion than does LDPE/OibPOS (99/1). However, its 5 wt% composite, which bears an average droplet size of ~5 μm, and the biggest only as big as ~10 μm, achieves a better dispersion than the other two 5 wt%-POS-containing composites.

Xylene solution blending is ineffective in producing PE/POS nanodielectrics, although POS of several hundred nanometers can be achieved. This may be because, despite the compatibility between POS and PE, interactions among POS molecules are stronger than those between POS and PE. As a result, POS crystallizes (in the case of OmPOS and OibPOS) or forms droplets (in the case of IoPOS) upon precipitation.

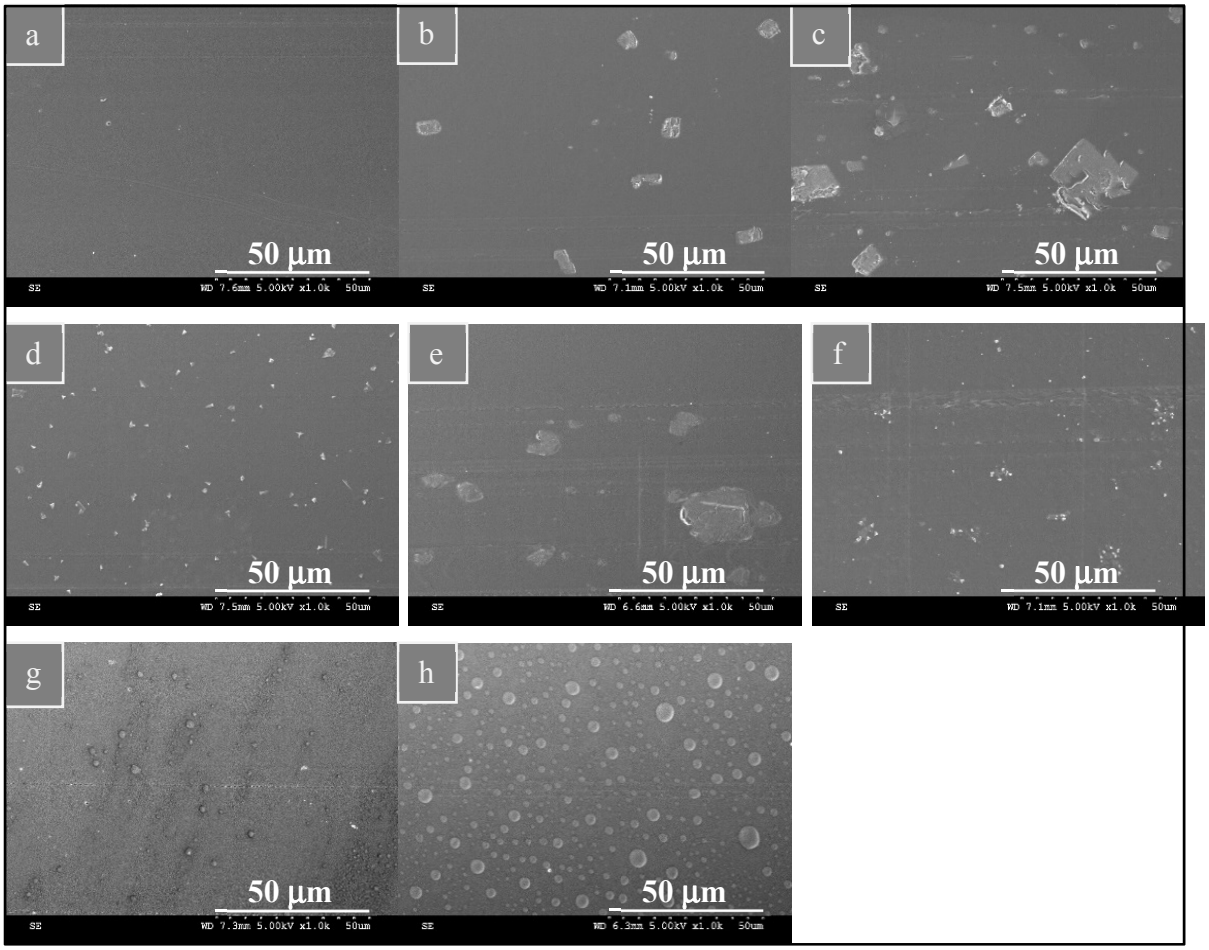

Figure 4.2 SEM images of (a) LDPE, (b) LDPE/OmPOS (99/1), (c) LDPE/OmPOS (95/5), (d) LDPE/OibPOS (99/1), (e) LDPE/OibPOS (95/5), (f) LDPE/OibPOS (95/5), (g) LDPE/IoPOS (99/1) and (h) LDPE/IoPOS (95/5)

4.3.3 Thermogravimetric analysis (TGA)

Thermogravimetric behaviors of LDPE, POS and their composites are shown in Figure 4.3 (a). Magnified views of Figure 4.3 (a) in 150–500 °C range are shown in Figure 4.3 (b, c). As can be seen, LDPE degradation takes place in a single step. The temperature at which LDPE experiences its maximum weight loss rate is T_{max}=510 °C. Weight losses in OmPOS and OibPOS take place in two steps, whereas in IoPOS, it is in a single step. The major weight losses observed (OmPOS: 93%, T_{max}=262 °C; OibPOS: 92%, T_{max}=270 °C; IoPOS: 100%, T_{max}=372 °C) are probably due to POS evaporation, whereas the minor ones (OmPOS: 4%,

T_{max}=335 °C; OibPOS: 8%, T_{max}=311 °C) are possibly related to the degradation of more stable phases formed during the heating throughout the first step (Fina et al., 2005a; Fina et al., 2005b). At 600 °C, negligible amounts of residues are left for OibPOS and IoPOS, whereas for OmPOS, it is 3%. All POS-containing composites degrade at temperatures very similar to that of LDPE. This indicates that POS do not have any significant effect on the thermal stability of LDPE in a nitrogen atmosphere.

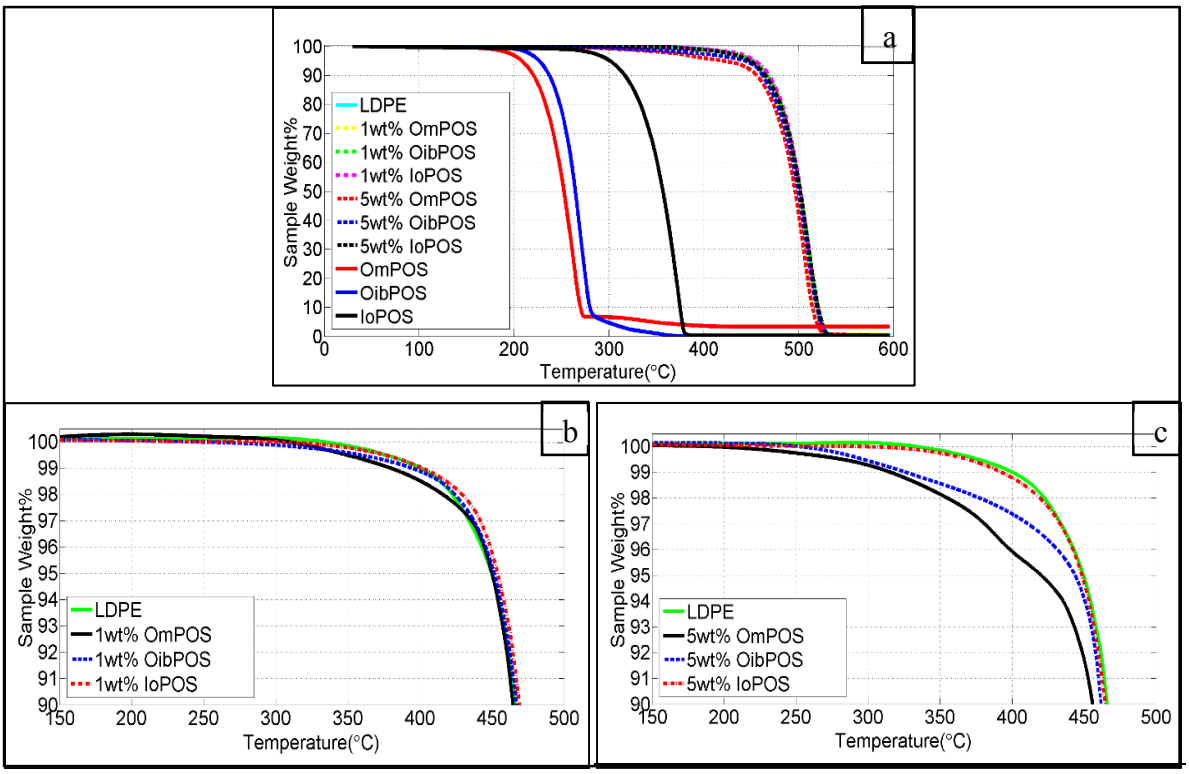

Figure 4.3 TGA curves of (a) LDPE, OmPOS, OibPOS, IoPOS, and their composites in 30–600 °C temperature range, (b) LDPE and LDPE/1 wt% POS in 150–500 °C temperature range and (c) LDPE and LDPE/5 wt% POS in 150–500 °C temperature range

The composites' thermal behaviors are quite interesting. If POS had maintained their own specific thermal behaviors, then (i) LDPE/OibPOS and LDPE/IoPOS composites should have experienced a complete loss of POS by 400 °C, and had a degradation of mere LDPE afterwards; (ii) LDPE/OmPOS composites should have lost most of their OmPOS by 300 °C, and had degradation temperatures slightly higher than that of LDPE due to stable OmPOS

residue. However, as can be seen in Figure 4.3, these are not the cases: composites containing 1 wt% OibPOS, 1 wt% IoPOS and 5 wt% IoPOS follow the thermal behavior of LDPE closely, presenting little characteristics of the incorporated POS; composites containing 1 wt% OmPOS, 5 wt% OmPOS and 5 wt% OibPOS experience POS losses (respectively of 0.5%, 3% and 1.5%) at around 400 °C upon degradation.

Some tentative explanations are given for the above thermal behaviors. Thanks to relatively high PE compatibility and small sizes, IoPOS is well intertwined with PE and can no longer be thermally distinguished from PE. Due to comparatively low PE compatibility and large sizes, only 0.5 wt% (in LDPE/1 wt% OmPOS) and 2 wt% (in LDPE/5 wt% OmPOS) OmPOS behave as PE whereas the remaining amounts experience weight losses delayed to higher temperatures. Bearing a medium PE compatibility, small sizes at 1 wt% loading, and large sizes at 5 wt% loading, OibPOS seems to follow the trend of IoPOS in LDPE/1 wt% OibPOS while that of OmPOS in LDPE/5 wt% OibPOS.

4.3.4 Differential scanning calorimetry (DSC)

DSC curves of the second heating runs were analyzed by Universal Analysis software. The typical result obtained is shown in Figure 4.4. As can be seen, while melting temperature can be directly read from the graph, degree of crystallinity needs to be calculated by having heat of melting of the PE portion of sample divided by 293.6 J/g, the heat of melting of PE when it was 100% crystalline (Sichina, 2000). In the case shown in Figure 4.4, a LDPE/5 wt% OibPOS sample, degree of crystallinity would be: $130.6 \div 0.95 \div 293.6 \times 100\% = 46.8\%$. Using the same method illustrated above, melting temperatures and degrees of crystallinity of LDPE and LDPE/POS composites were obtained, as listed in Table 4.2.

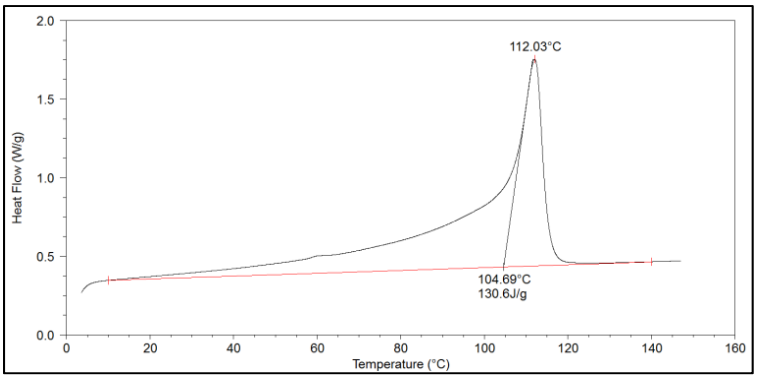

Figure 4.4 The second heating curve of a LDPE/5 wt% OibPOS sample, analyzed by Universal Analysis

As can be seen, melting temperatures of composites are almost the same as that of PE. This indicates that despite physical hindrances induced by POS, macromolecule chains of PE are reasonably free to move at elevated temperatures. In addition, POS does not seem to have any effect on the degree of crystallinity of PE. This indicates that POS causes little disruption to PE chains' orderly arrangements necessary for crystallization.

Table 4.2 Samples' melting temperatures and degrees of crystallinity

Sample	Melting temperature (°C)	Degree of crystallinity (%)
LDPE	111.8 ± 0.0	45.0 ± 0.2
LDPE/1wt% OmPOS	111.9 ± 0.2	45.7 ± 0.2
LDPE/1wt% OibPOS	111.9 ± 0.2	45.4 ± 0.3
LDPE/1wt% IoPOS	112.0 ± 0.1	45.2 ± 0.3
LDPE/5wt% OmPOS	111.8 ± 0.2	45.9 ± 0.4
LDPE/5wt% OibPOS	111.8 ± 0.2	46.6 ± 0.3
LDPE/5wt% IoPOS	111.8 ± 0.0	47.1 ± 0.2

4.3.5 Thermal conductivity

Thermal conductivities of LDPE and LDPE/POS are displayed in Figure 4.5. As can be seen, LDPE has a low thermal conductivity of 0.277 W/m·K. This is because LDPE has only a small volume of crystal lattice to transport thermal energy phonons (i.e., elastic vibration waves in

crystal lattices). Moreover, phonons are susceptible to scattering in amorphous regions, where many free volumes, defects and boundaries exist (Huang, Jiang et Tanaka, 2011; Tsekmes et al., 2013).

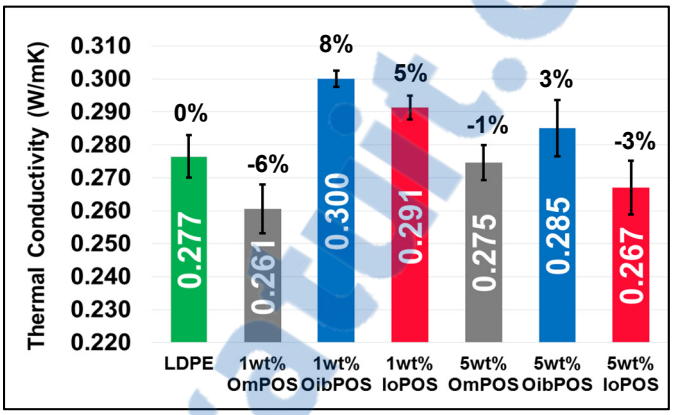

Figure 4.5 Thermal conductivities of LDPE and LDPE/POS composites (error bars stand for standard deviations)

The thermal conductivity of LDPE/OmPOS (99/1) is decreased by 6%. This is because OmPOS has a relatively low PE compatibility, a relatively low volume occupation (Table 4.1), and is dispersed in comparatively large sizes (Figure 4.2 (b)). These factors result not only in a relatively small number of filler to transport phonons, but also make the filler-matrix interphase more susceptible to large defects. As a consequence, in LDPE/OmPOS (99/1), phonon scattering dominates over phonon transport, leading to a reduced thermal conductivity. As the content of OmPOS increases to 5 wt%, the volume occupation of OmPOS increases (Table 4.1), largely multiplying the number of crystal lattice. As a result, positive effects get enhanced and somehow neutralize the negative ones, resulting in LDPE/OmPOS (95/5) with an almost unchanged thermal conductivity as compared to LDPE.

Compared to OmPOS, OibPOS has a higher PE compatibility, a larger volume occupation (Table 4.1), and a much better dispersion (Figure 4.2 (d)). These features advantageously increase the number of phonon-transporting site and reduce phonon-scattering interfacial defects. Subsequently, LDPE/OibPOS (99/1) undergoes an 8% improved thermal conductivity.

However, size and number of interfacial defects increase with OibPOS loading (Figure 4.2 (e, f)), negatively influencing the thermal conductivity.

For viscous-liquid IoPOS, instead of phonon transport, heat convection may be the main heat transfer mechanism (Figure 4.2 (g. h)). Furthermore, the seemingly-aligned pattern presented in LDPE/IoPOS (99/1) may be the main reason for LDPE/IoPOS (99/1)'s enhanced thermal conductivity over its 5 wt% counterpart.

4.3.6 Broadband dielectric spectroscopy (BDS)

Relative permittivities of LDPE and LDPE/POS are presented in Figure 4.6. As shown in Figure 4.6 (a), LDPE has a real permittivity ε_r' as low as ~2.32 over a wide frequency span from 10^{-2} to 10^4 Hz. Figure 4.6 (b) for its part shows its imaginary permittivity ε_r'' to be very low, around 10^{-4}. Curve irregularities are probably resulted from apparatus errors, as the losses present are too low to be measured accurately. Moreover, losses at frequencies below 10^2 Hz are highly affected by noise and thus not presented here.

As can be seen in Figure 4.6 (a), LDPE/POS composites have ε_r' similar to that of LDPE, except for LDPE/OmPOS (95/5), whose ε_r' is slightly higher, at 2.35. This is probably attributable to POS' intrinsic PE-similar ε_r'. The results here are somewhat different from those in (Takala et al., 2008), which reported a 0.15–0.2 ε_r' increase in PP/1 wt% OmPOS and PP/5 wt% OmPOS and a 0.14 ε_r' decrease in PP/5 wt% IoPOS.

As can be seen in Figure 4.6 (b), LDPE/POS composites have ε_r'' similar to that of LDPE, except for LDPE/OmPOS (95/5), whose ε_r'' is slightly higher. This indicates negligible loss increases due to POS addition. Similarly, (Takala et al., 2008) found that the dielectric loss of PP/5wt% OmPOS was higher than that of neat PP, and that dielectric losses of PP/1wt% OmPOS, PP/1wt% IoPOS and PP/5wt% IoPOS were similar to that of neat PP.

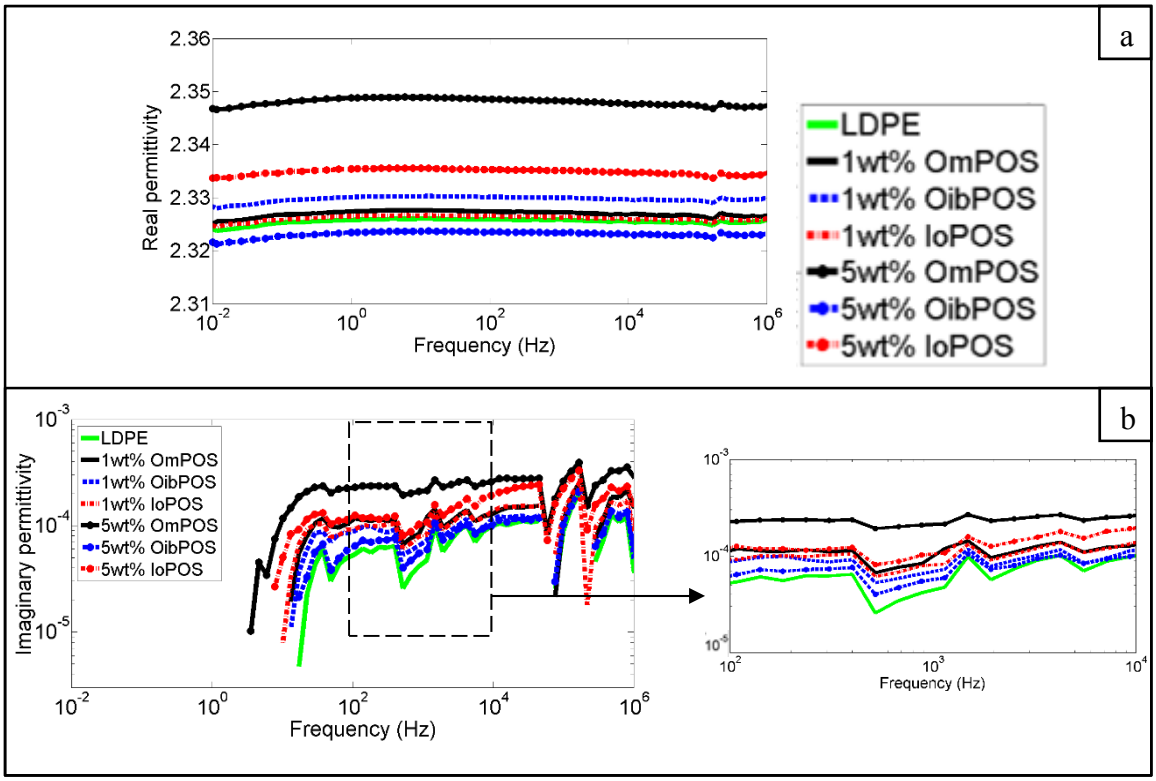

Figure 4.6 (a) Relative real permittivities and (b) relative imaginary permittivities of LDPE and LDPE/POS composites

4.3.7 Progressive-stress breakdown tests (PSB)

Breakdown strengths obtained are fitted with the two-parameter Weibull distribution, as shown in Figure 4.7. Shape (β) and scale (α) parameters are calculated from the Weibull distribution, as listed in Table 4.3. β reflects the scattering of breakdown strengths; α is the breakdown strength at which the cumulative breakdown probability is 63.2%, and it is commonly used to represent the material's breakdown strength. Obviously, the bigger the β and α, the narrower the data scattering, and the greater the material's breakdown strength.

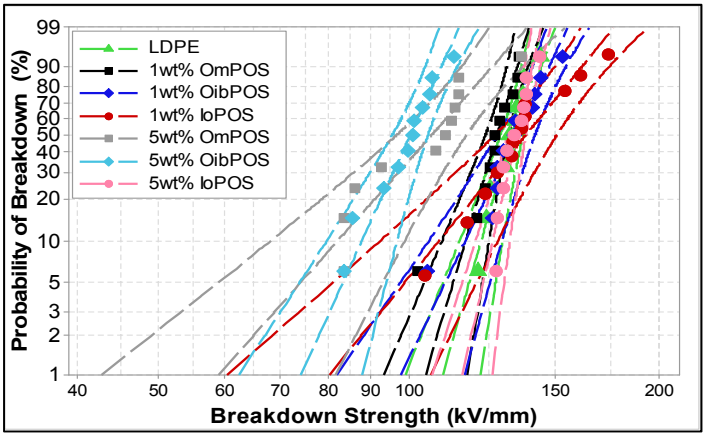

Figure 4.7 The two-parameter Weibull distribution
of LDPE and LDPE/POS composites
(95% confidence interval)

Table 4.3 Scale (α) and shape (β) parameters of the two-parameter Weibull distribution

Sample	Shape parameter β	Scale parameter α (kV/mm)
LDPE	22.2	135.0 ± 3.8
LDPE/1 wt% OmPOS	21.5	129.7 ± 3.7
LDPE/1 wt% OibPOS	13.3	138.2 ± 6.5
LDPE/1 wt% IoPOS	7.8	144.8 ± 11.2
LDPE/5 wt% OmPOS	7.2	112.0 ± 9.8
LDPE/5 wt% OibPOS	14.0	102.9 ± 4.5
LDPE/5 wt% IoPOS	28.0	136.5 ± 3.0

Effects of POS on LDPE's breakdown strength are two-sided. On the one hand, POS act as electron-scattering sites, contributing to increase breakdown strength. On the other hand, POS bring interfacial defects, contributing to decrease breakdown strength (Takala et al., 2008; Tian et al., 2012). These two counteracting effects seem to reach a sort of balance in LDPE/OmPOS (99/1)—the dielectric breakdown strength of LDPE/OmPOS (99/1) is similar to that of LDPE. As for LDPE/OibPOS (99/1) and LDPE/IoPOS (99/1), it is hard to say if they have higher breakdown strengths than LDPE does. This is because, although their α values are higher than that of LDPE, their β values are much lower than that of LDPE, indicating wider scatterings of breakdown strengths.

As POS content increases to 5 wt%, breakdown strengths of LDPE/OmPOS (95/5) and LDPE/OibPOS (95/5) decrease greatly, mainly due to the increase in big crystals, which multiplies large interfacial defects. Most interestingly, the breakdown strength of LDPE/IoPOS (95/5) remains almost the same, if any, slightly higher than that of LDPE. This may be attributable to high IoPOS-PE compatibility and favorable IoPOS dispersion, which result in an only moderate increase of interfacial defects. As a comparison to the results presented here, (Takala et al., 2008) showed that AC breakdown strengths of PP/3wt% OmPOS and PP/5wt% IoPOS were obviously higher than that of neat PP.

4.3.8 Surface partial discharge tests

Surface partial discharge (erosion) tests rate materials with respect to their resistances to prolonged AC stress under corona-discharge conditions. They are an important complement of progressive stress breakdown tests, which exclude the harmful effects of long-term aging processes. The eroded volumes obtained (in inversed references to erosion resistances) are presented in Figure 4.8.

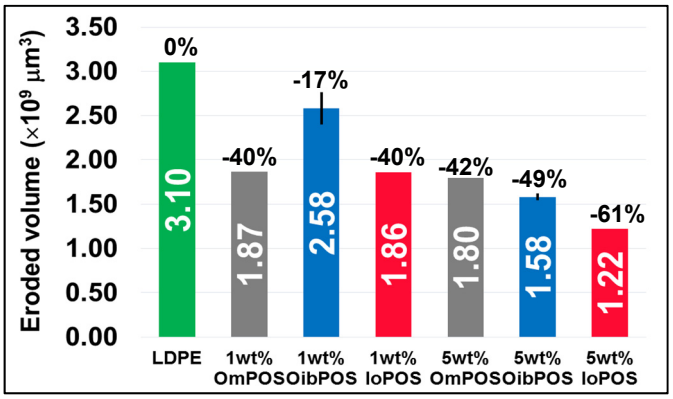

Figure 4.8 Eroded volumes of LDPE and LDPE/POS composites
(error bars stand for standard deviations)

As can be seen, all LDPE/POS composites have reduced eroded volumes, and thus enhanced resistances to corona discharges. This may be attributable to the inorganic silicon-oxygen core of POS, which is more erosion-resistant than organic PE. Moreover, POS is reported to have a

superior erosion resistance against atomic oxygen radicals that are often involved in corona-induced degradations. Furthermore, a Si-O rich passivating layer is said to be found on the sample surface near high electric field regions, protecting the material from corona damages (Horwath et Schweickart, 2002; Phillips et al., 2000).

With POS loading increasing from 1 wt% to 5 wt%, erosion resistances of LDPE/OibPOS and LDPE/IoPOS increase from 17% to 49% and 40% to 61%, respectively. This may be brought about by the increase in POS' volume and number, which multiplies the size and number of erosion-resistant sites. Almost no enhancement is observed for LDPE/OmPOS when OmPOS increases from 1 wt% to 5 wt%. This may be ascribed to the increase in the size and number of interfacial defects, which enhances local electric fields and makes the material more susceptible to partial discharges.

Erosion resistances of LDPE/5 wt% POS appear to follow an ascending trend from OmPOS to OibPOS to IoPOS. Reasons for LDPE/IoPOS (95/5) greatest improvement may lie in IoPOS' highest PE compatibility, largest volume occupation, and favorable dispersion, all of which make the benefits of erosion-resistant sites exercise the strongest domination over the drawbacks of erosion-susceptible interfacial defects.

4.4 Conclusion

Xylene solution blending was shown to be an effective method for producing PE/POS composites. Although POS and PE were mixed at the molecular level in solution blending, only microcomposites were obtained. POS had little effects on the thermal stability, the melting temperature and the degree of crystallinity of PE. The thermal conductivity of LDPE/OibPOS (99/1) saw the biggest improvement (8%), followed by LDPE/IoPOS (99/1) (5%) and LDPE/OibPOS (95/5) (3%). Except for LDPE/OmPOS (95/5), which had a dielectric permittivity slightly higher than that of LDPE, the rest of the composites all had dielectric permittivities similar to that of LDPE. Compared to PE, LDPE/OmPOS (99/1), LDPE/OibPOS (99/1), LDPE/IoPOS (99/1) and LDPE/IoPOS (95/5) saw improvements in

corona resistance of 40%, 17%, 40% and 61%, respectively. Moreover, all these four composites maintained breakdown strengths similar to that of PE. The other two composites containing 5 wt% POS, however, were able to improve their corona resistances (42%–49%), but at a cost of reduced breakdown strengths. Breakdown strength tends to decrease whereas corona resistance tends to increase with POS loading. It would seem that LDPE/5 wt% IoPOS was capable of providing the best balance between these two effects, thus enhancing dielectric performance most clearly. Moreover, LDPE/OibPOS (99/1) and LDPE/IoPOS (99/1) showed multi-functional improvements in terms of improved thermal conductivities, enhanced corona resistances and maintained breakdown strengths.

4.5 Acknowledgements

Financial support from the Natural Sciences and Engineering Research Council of Canada and Hydro-Québec are greatly appreciated. The authors also highly appreciate the consultations generously offered by Dr. K.Y. Lau and Prof. A. S. Vaughan.

CHAPTER 5

POLYETHYLENE/POLYHEDRAL OLIGOMERIC SILSESQUIOXANES COMPOSITES OBTAINED BY EXTRUSION

Journal Article III

POLYETHYLENE/POLYHEDRAL OLIGOMERIC SILSESQUIOXANES COMPOSITES: DIELECTRIC, THERMAL AND RHEOLOGICAL PROPERTIES

Meng Guo[1, 2], Éric David[1], Michel Fréchette[2], and Nicole R. Demarquette[1]

[1]École de technologie supérieure (ÉTS),

1100 Notre-Dame Street West, Montreal, QC H3C 1K3, Canada

[2]Institut de recherche d'Hydro-Québec (IREQ),

1800 Boulevard Lionel Boulet, Varennes, QC J3X 1S1, Canada

This article has been published in:

Polymer

Vol. 115, 2017, pp. 60-69

https://doi.org/10.1016/j.polymer.2017.03.015

This article has been modified and edited for integration into the thesis.

Abstract

Composites of low-density polyethylene (LDPE) containing 1 wt% and 5 wt% polyhedral oligomeric silsesquioxanes (POSS) of different substituents (methyl, isobutyl, isooctyl) were obtained by extrusion. The composites' potential application in HV power cable insulation was investigated by broadband dielectric spectroscopy (BDS), progressive-stress breakdown tests (PSB), and surface partial discharge tests. Thermal conductivity and viscoelastic characteristic were also examined as they play an important role in both material property and manufacture. Additional measurements using scanning electron microscopy (SEM) and differential scanning calorimetry (DSC) were carried out to obtain information for possible performance explanations. The results showed that POSS could enhance the erosion resistance and slightly improve the thermal conductivity of LDPE without compromising its dielectric breakdown strength or unfavorably increasing its dielectric permittivity or viscosity.

5.1 Introduction

Melt blending with a twin-screw extruder was tested as a method for producing LDPE-based nanocomposites containing various alkyl substituted POSS of different loadings. The potential application of LDPE/POSS composites in HV power cable insulation was evaluated by examining their electrical properties. Thermal conductivity and viscoelastic characteristic were also investigated, as they influence not only the electrical properties, but also the manufacture of insulating materials. Additional measurements using scanning electron microscopy and differential scanning calorimetry were carried out to obtain information for possible performance explanations.

5.2 Experimental

5.2.1 Materials

The same raw materials as those described in Chapter 4 were used. Specifically, low-density polyethylene (LDPE) and three types of POSS were employed: octamethyl-POSS (OmPOSS), octaisobutyl-POSS (OibPOSS) and isooctyl-POSS (IoPOSS). More detailed descriptions can be found in section 4.2.1 “Materials”.

5.2.2 Sample preparation

As-received LDPE powder and as-received POSS powder/viscous liquid in mass fractions of 99/1% and 95/5% were premixed and then introduced into a twin-screw extruder. Low barrel zone temperatures of 110–130 °C were employed to increase shear and elongational stresses, thus favoring an effective dispersive mixing during extrusion. Moreover, low temperatures also helped prevent POSS from evaporation in the extrusion process. A 50 rpm rotation speed, which favored a longer residence time, was used to fabricate LDPE/1 wt% POSS composites, whereas a 200 rpm rotation speed, which favored higher stresses, was used to fabricate LDPE/5 wt% POSS composites. Composites were extruded using a rod die, quickly air-cooled, and subsequently introduced into a pelletizer. The obtained pellets were compression molded

into plate samples under an average temperature of 150 °C and a pressure of 6.3×10^6 Pa. Reference LDPE samples were also produced under the same conditions for comparison (Table 5.1).

Table 5.1 Samples' denotations, mass (*w*) and volume (*v*) fractions of POSS in each sample

Material	Sample	*w* (wt%)	*v* (vol%)
LDPE extruded at 50 rpm	LDPE50	0	0
99 wt% LDPE+1 wt% OmPOSS	LDPE/OM1	1	0.6
99 wt% LDPE+1 wt% OibPOSS	LDPE/OIB1	1	0.8
99 wt% LDPE+1 wt% IoPOSS	LDPE/IO1	1	0.9
LDPE extruded at 200 rpm	LDPE200	0	0
95 wt% LDPE+5 wt% OmPOSS	LDPE/OM5	5	3.1
95 wt% LDPE+5 wt% OibPOSS	LDPE/OIB5	5	4.1
95 wt% LDPE+5 wt% IoPOSS	LDPE/IO5	5	4.6

5.2.3 Characterization techniques

POSS size dispersion and spatial distribution within LDPE matrix were evaluated with a Hitachi 3600N and a Hitachi SU8230 scanning electron microscope (SEM). Prior to SEM observation, cross-sections were obtained using a microtome and coated with a thin layer of gold to prevent charge accumulation. To increase the reliability of observation, several cross-sections were prepared for each composite, and many spots were observed on each cross-section.

Thermal behaviors of LDPE and LDPE/POSS composites were studied by differential scanning calorimetry (DSC) using a TA Q20 instrument on samples of 8–10 mg in a nitrogen atmosphere. Prior to DSC measurements, baseline calibration and cell constant calibration were performed on an empty chamber and with an indium standard, respectively. For the measurements, samples were first heated from 0 °C to 150 °C at 10 °C/min to erase previous thermal history, and then cooled from 150 °C to 0 °C at 10 °C/min, and once again heated from 0 °C to 150 °C at 10 °C/min. Measurements were repeated at least two times with fresh samples to increase the reliability of results.

Thermal conductivity values of LDPE and LDPE/POSS composites were measured following ASTM E1530 (ASTM Standard E1530, 2011), using a DTC-25 thermal conductivity tester from TA Instruments. Samples were held, under a load of 15 psi, between two smooth metal surfaces of 45 °C (upper) and 15 °C (lower), long enough to reach thermal equilibrium. At least one sample from each type of material was measured at least two times to ensure the reliability of results.

Viscoelastic characteristics of LDPE and LDPE/POSS composites were characterized by small amplitude oscillatory shear (SAOS) measurements using a modular compact rheometer MCR 501 (Anton Paar GmbH). Prior to SAOS measurements, strain sweep tests were carried out in 0.01%–20% strain range with angular frequencies of 1 rad/s, 10 rad/s and 100 rad/s, to determine the linear viscoelastic regime of the materials. SAOS measurements were done on samples of ~1 mm using a parallel plate geometry of 25 mm diameter under an isothermal condition of 150 °C, a fixed strain of 0.3%, and an angular frequency of 0.01–300 rad/s. To increase the reliability of results, two measurements were carried out for each type of material.

Relative complex permittivities of LDPE and LDPE/POSS composites were obtained using a Novocontrol broadband dielectric spectrometer. Samples of 40 mm in diameter and ~0.5 mm in thickness were measured with an AC voltage of V_{rms}=3 V in a 10^{-2}–5×10^{5} Hz frequency range at 23 °C. One sample from each type of material was measured twice to ensure the reliability of results.

AC progressive-stress breakdown tests were performed in accordance with ASTM D149 (ASTM Standard D149, 2013) at ambient temperature. As presented in Figure 5.1, samples bearing a diameter D=20 mm and a thickness d=0.23 mm (standard deviation: 0.008–0.011) were fixed between a pair of cylindrical rod electrodes (6.4 mm in diameter with edges rounded to 0.8 mm) and immersed in a Luminol TR-i insulating fluid. An AC voltage of 60 Hz was applied on the samples, at a 2 kV/s constant rate of rise, going from zero until breakdown occurred. Breakdown voltages U were recorded and breakdown strengths E were calculated from $E=U\div d$. 24–25 samples were broken down for each type of material for statistical analysis.

Surface partial discharge tests were conducted to evaluate composites' resistances to prolonged AC stress under an electrical discharge condition. One to three samples from each type of material were tested. As demonstrated in Figure 5.2, samples were fixed in a point-to-plane geometry (air gap=100 μm), where the rod electrode was connected to a sinusoidal AC voltage (V_{peak}=10 kV, 300 Hz) and the plate electrode was connected to the ground. An erosion time of 35 hours was used. Eroded samples were subjected to surface profilometry in a mechanical profilometer (Dektak 150) for evaluation of their eroded volumes.

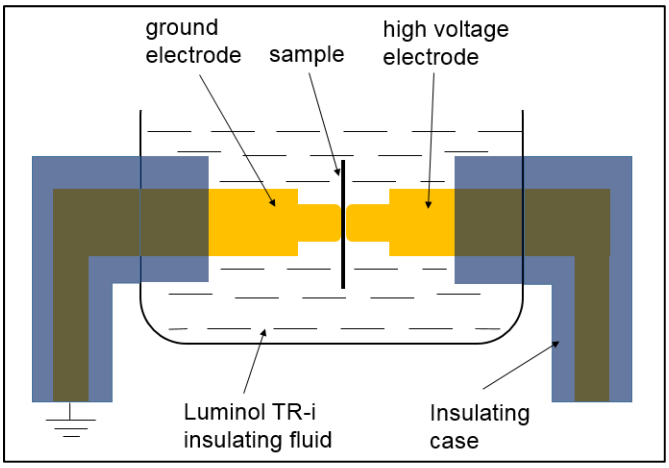

Figure 5.1 A schematic representation of the setup used for dielectric breakdown tests

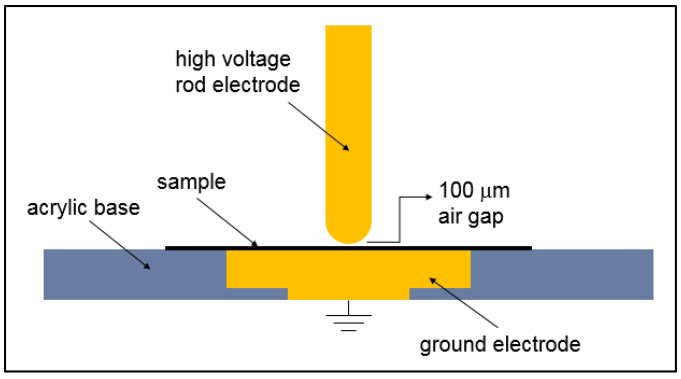

Figure 5.2 A schematic representation of the setup used for surface erosion tests

5.3 Results and discussion

5.3.1 Scanning electron microscopy (SEM)

POSS dispersion within LDPE matrix was previously shown to be influenced by the chain length of POSS' alkyl groups (Guo et al., 2016). Similar findings were reported in studies dealing with PP/POSS composites (Fina et al., 2005b; Pracella et al., 2006). As can be seen, the compatibility between OmPOSS and LDPE is low, leading to micron-sized crystalline aggregates for both 1 wt% and 5 wt% filler contents (Figure 5.3 (a, b)). OibPOSS has a better compatibility with LDPE, and thus a finer dispersion at ~2 µm for the 1 wt% filler content (Figure 5.3 (c)). Increased OibPOSS concentration, however, ends up with big aggregates (Figure 5.3 (d)). IoPOSS has the highest compatibility with LDPE. Consequently, IoPOSS in LDPE/IO1 display a very fine dispersion with no microscopic evidence of phase separation (Figure 5.3 (e)), and those in LDPE/IO5 are generally presented in submicron to one micron sizes (Figure 5.3 (f)).

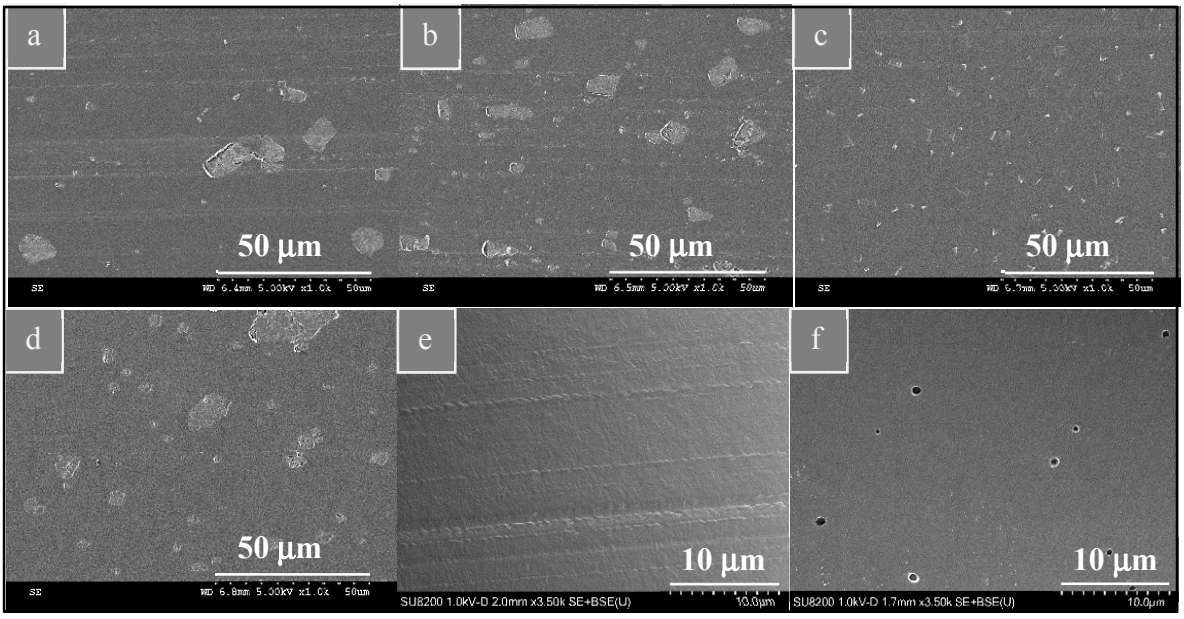

Figure 5.3 SEM images of (a) LDPE/OM1, (b) LDPE/OM5, (c) LDPE/OIB1, (d) LDPE/OIB5, (e) LDPE/IO1 and (f) LDPE/IO5

5.3.2 Differential scanning calorimetry (DSC)

With Universal Analysis software, crystallization onset temperatures T_{ons} and peak temperatures T_c were respectively determined from the onsets and the maxima of exothermal peaks after a linear extrapolation from 10 °C to 140 °C on the cooling curve. Melting temperatures T_m and enthalpies ΔH_m were respectively determined from the maxima and the areas of endothermal peaks after a linear extrapolation from 10 °C to 140 °C on the second heating curve, as illustrated in Figure 5.4. The degree of crystallinity X_c was calculated from $\Delta H_m \div \Delta H_m^\circ \div (1\text{-}w)$ where w are mass fractions of POSS and ΔH_m°=293.6 J/g for PE (Sichina, 2000).

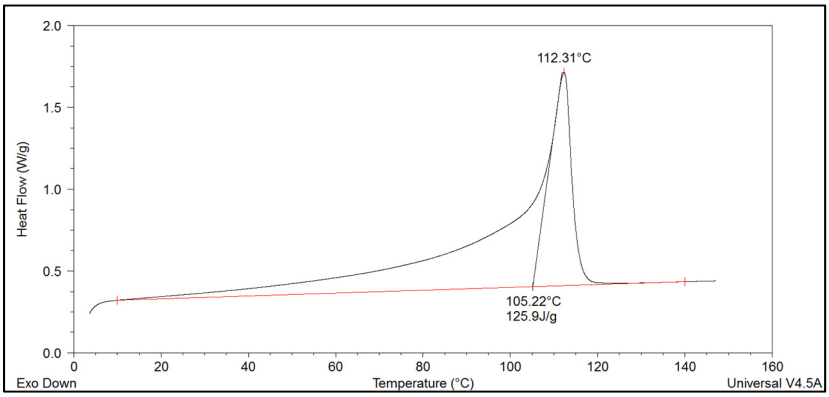

Figure 5.4 DSC analysis on the second heating curve of a LDPE/OM5 sample. As can be read from the graph, T_m = 112.3 °C and ΔH_m = 125.9 J/g. The degree of crystallinity is calculated by X_c = 125.9 ÷ 293.6 ÷ (1-0.05) × 100% = 45%

DSC analysis results are shown in Figure 5.5. As can be seen, POSS does not have any significant influence on the melting behavior, the crystallization behavior, or the degree of crystallinity of LDPE; T_{ons}, T_c, T_m and X_c of the composites are quite similar to those of LDPE, with values of around 102 °C, 99 °C, 112 °C and 45%, respectively. This indicates that despite physical hindrances induced by POSS, macromolecule chains of LDPE are reasonably free to move at elevated temperatures, and their orderly packings necessary for crystallization are not disrupted.

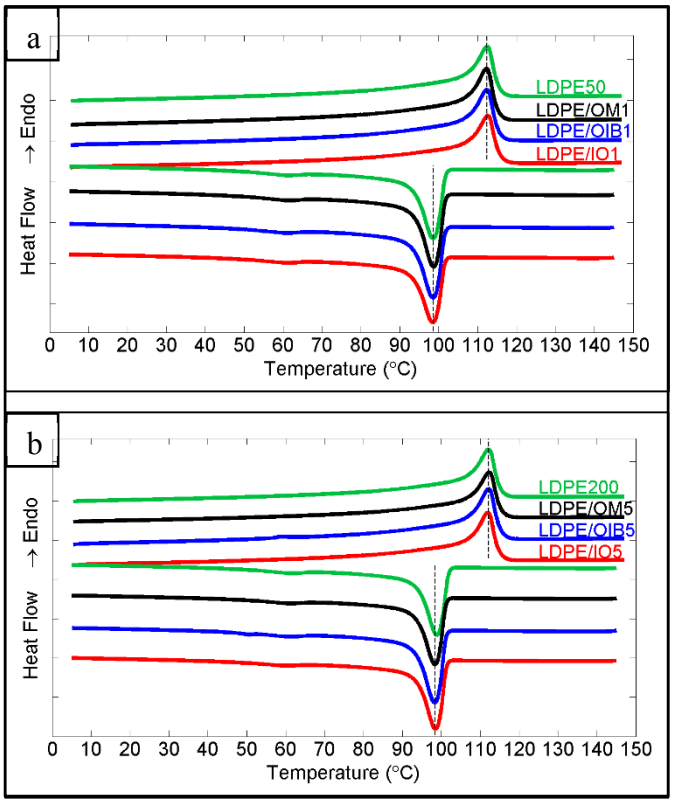

Figure 5.5 Cooling curves and the second heating curves of (a) LDPE50 and LDPE/1 wt% POSS and (b) LDPE200 and LDPE/5 wt% POSS

Similar results were found in LDPE-based systems containing 0.5–6 wt% octavinyl-POSS (Huang et al., 2009) and HDPE-based systems containing 1–5 wt% OmPOSS (Joshi et Butola, 2004). When the content of OmPOSS increased to 10 wt%, however, increased T_{ons} and T_c values were observed, indicating a nucleating effect (Joshi et Butola, 2004). In PP-based systems, increased T_{ons} and T_c values and accelerated crystallization resulted from the addition of 3–30 wt% OmPOSS. On the other hand, decreased T_{ons} and T_c values and retarded crystallization were found with the addition of 3–6 wt% OibPOSS and 3–10 wt% IoPOSS (Fu et al., 2001; Pracella et al., 2006). These results show that the influence of POSS on the crystallization behavior of polymers depends, at least to a certain degree, on the type of polymer concerned, as well as on the type and concentration of POSS.

The melting temperature and the degree of crystallinity have significant influence on polymers' electrical properties. An increase in melting temperature can enhance breakdown strengths, when thermal breakdown is the dominating breakdown mechanism. An increase in crystallinity can lengthen electron mean free path and result in decreased breakdown strengths in electron avalanche-dominated failures (Tanaka et al., 1991). On the other hand, it can boost polymer modulus and lead to improved breakdown strengths in electromechanical-dominated failures (Claude et al., 2008). However, since the POSS-containing systems studied in this paper experience changes neither in the melting temperature nor in the degree of crystallinity, changes in their electrical properties cannot be explained from these two aspects.

5.3.3 Thermal conductivity

Thermal conductivities of LDPE and LDPE/POSS composites are displayed in Figure 5.6. It is found that POSS has only a minor influence on the thermal conductivity of LDPE, probably due to the intrinsic low thermal conductivity of POSS (Huang et al., 2012). This is different from findings concerning fillers such as silica (El-Tonsy et al., 2016), alumina (Zhang et al., 2011) and boron nitride (Zhou et al., 2007), which generally report relatively large thermal conductivity increase.

Thermal conductivities of LDPE/IoPOSS composites increase with POSS loading. This is mainly attributable to increase in POSS' volume occupation, which shortens mean inter-POSS distance, and thus results in more efficient heat transfer. Thermal conductivities of LDPE/OibPOSS composites decrease with POSS loading, despite the boost in volume occupation and phonon-transporting sites. This is probably owing to increase in large aggregates, which multiplies phonon-scattering defects at the filler-matrix interphase. Thermal conductivities of LDPE/OmPOSS composites are lower than that of LDPE, likely as a result of fairly severe interfacial phonon-scattering due to poor OmPOSS-LDPE compatibility and OmPOSS dispersion (Huang et al., 2012; Huang, Jiang et Tanaka, 2011; Tsekmes et al., 2013).

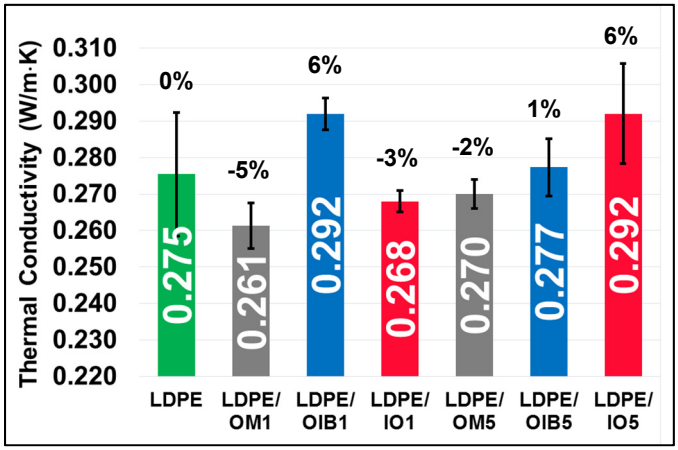

Figure 5.6 Thermal conductivities of LDPE
and LDPE/POSS composites
(error bars stand for standard deviations)

High thermal conductivities are desirable for power cable insulation. They allow insulation to better dissipate heat generated by conductor, Joule heating and dielectric loss, and thus reduce thermally-assisted aging and the chance of thermal breakdown (Xiao et Du, 2016). Moreover, they help shorten manufacturing process, and thus bring economic benefits (Ebadi-Dehaghani et Nazempour, 2012).

5.3.4 Rheological measurements

The linear Cole-Cole plot of loss viscosity (η'') versus storage viscosity (η') and the log-log Han-Chuang plot of storage modulus (G') versus loss modulus (G'') for all composites and for neat LDPE are shown in Figure 5.7 (a) and Figure 5.7 (b), respectively. All curves have a smooth semicircular shape in the Cole-Cole plot, and a same gradient in the Han-Chuang plot. These give a rough indication of the rheological compatibility of LDPE/POSS systems (Cho et al., 1998; Han et Chuang, 1985; Zhou et al., 2008), as reported in LDPE-based systems containing 0.5–6 wt% octavinyl-POSS (measured at 140 °C) (Huang et al., 2009), as well as in HDPE-based systems containing 1–5 wt% OmPOSS (measured at 180 °C) (Joshi et al., 2006).

Figure 5.7 (c-e) show that POSS has little influences on the G', G''or complex viscosity ($|\eta^*|$) of LDPE in a wide frequency range, with the exception of LDPE/OM5 and LDPE/IO5, which respectively exhibit slightly higher and somewhat lower values than those of neat LDPE. Further examinations of $|\eta^*|$ versus POSS loading at low (1 rad/s) and high (300 rad/s) frequencies (Figure 5.7 (f, g)) show that $|\eta^*|$ decreases at 1 wt% POSS loading and thereafter (i) increases all the way to a value higher than that of neat LDPE with the increase in OmPOSS loading; (ii) increases to a value similar to that of neat LDPE with the increase in OibPOSS loading; and (iii) further decreases with the increase in IoPOSS loading. For OmPOSS and OibPOSS, at 1 wt% concentration, they may act as weak lubricants, resulting in slightly decreased $|\eta^*|$. At 5 wt% concentration, they may act as steric barriers hindering flow, although POSS aggregates are relatively large as compared to the dimension of PE chains, and are thus hardly capable of inducing any effective resistance to the motion of PE chains (Huang et al., 2009; Joshi et al., 2006). As for IoPOSS, lubricating effect is dominant, probably as a consequence of its viscous-liquid characteristic.

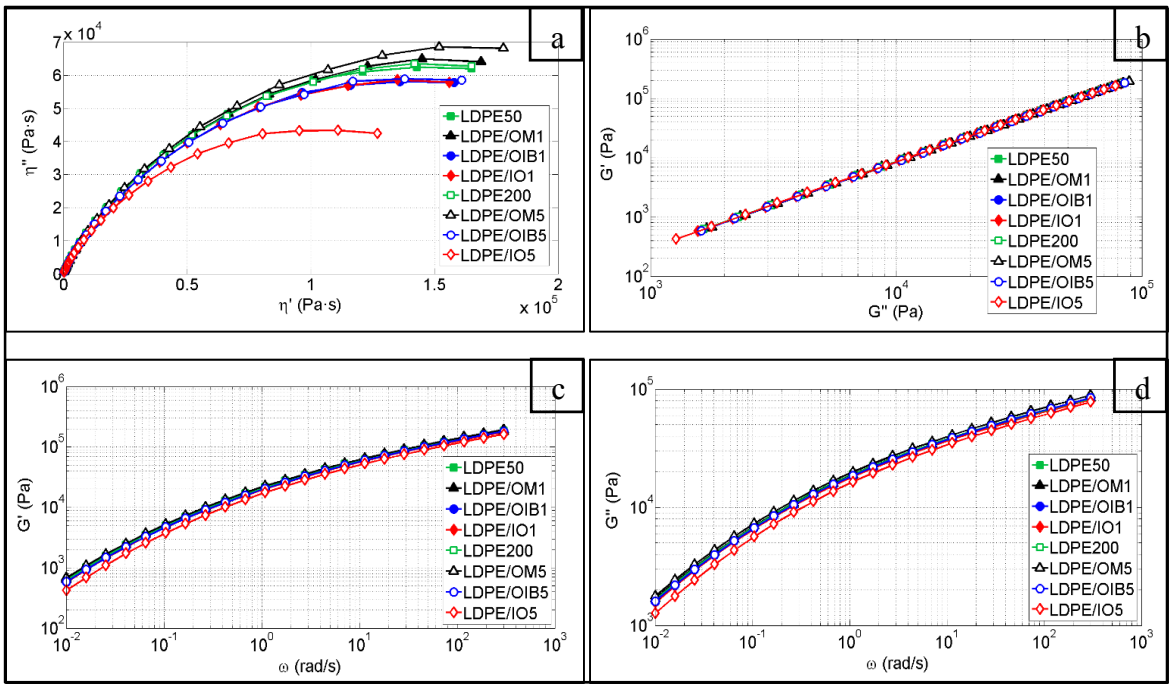

Figure 5.7 LDPE and LDPE/POSS composites: (a) Cole-Cole plot, (b) Han-Chuang plot, (c) G'versus ω, (d) G''versus ω, (e) $|\eta^*|$ versus ω, (f) $|\eta^*|$ versus POSS loading at ω=1 rad/s and (g) $|\eta^*|$ versus POSS loading at ω=300 rad/s

Figure 5.7 (Continued)

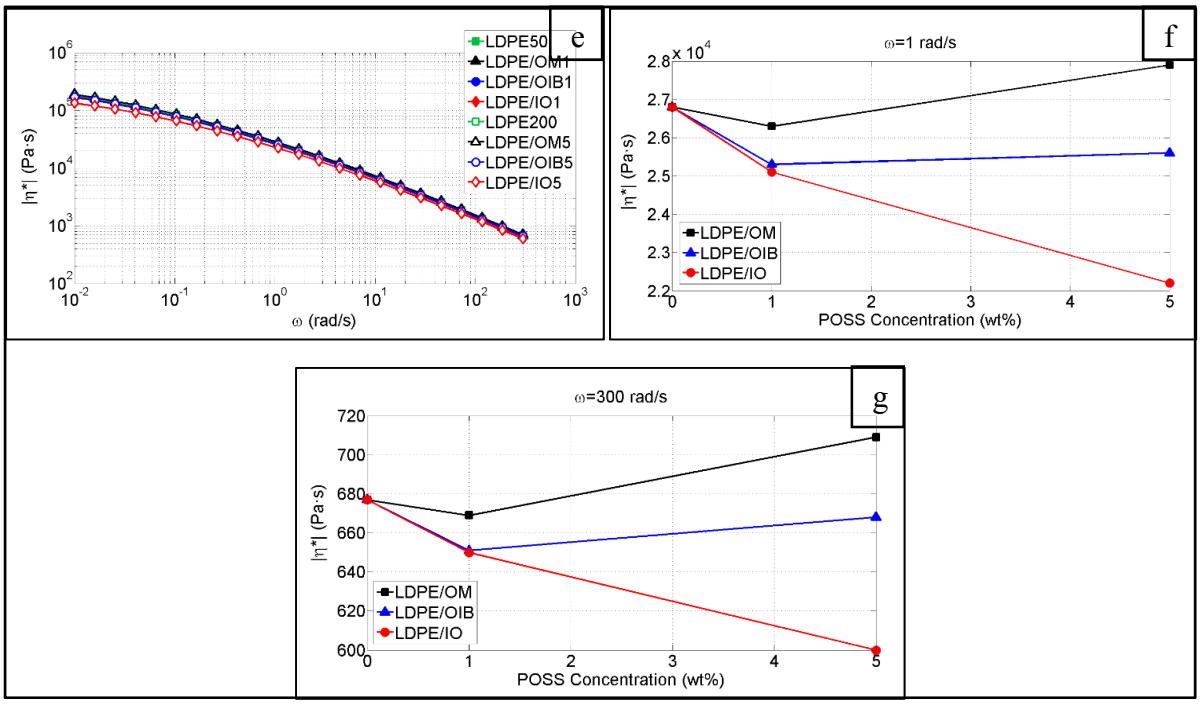

Viscoelastic behaviors reveal the compatibility and the microscopic interaction of a composite system. Moreover, they can influence the system's electrical properties, such as conductivity (Dakin, 2006) and dielectric breakdown strength (Huang et al., 2009). Melt viscosity is also an important consideration in manufacturing. While filler incorporation usually leads to an unfavorable viscosity increase obstructing material processing, POSS is shown to largely retain or even reduce the viscosity of LDPE.

Table 5.2 Dielectric constants calculated by Clausius-Mossotti equation

Material	***M* (g/mol)**	**α_e (Fm^2)**	**Calculated ε_r'**
LDPE	$(14.03)_n$	$(2.03\times10^{-40})_n$	2.30
OmPOSS	536.96	6.52×10^{-39}	3.11
OibPOSS	873.68	1.14×10^{-38}	2.51
IoPOSS	$(165.33)_m$	$(2.24\times10^{-39})_m$	2.35

n typically ranges from 1000 to 40000; m=8, 10, 12

5.3.5 Broadband dielectric spectroscopy (BDS)

Assuming that POSS is nonpolar thanks to its symmetric molecular structure, its dielectric constant (ε_r') can be calculated using Clausius-Mossotti equation, which is accurate to ~1% when used for small-density nonpolar materials (Raju, 2003c):

$$\frac{\varepsilon_r' - 1}{\varepsilon_r' + 2} = \rho \cdot \frac{N_A}{3\varepsilon_0} \cdot \frac{\alpha_e}{M} \tag{5.1}$$

where ρ is the density of POSS in the kg/m^3 unit; N_A is the Avogadro constant, and is equal to 6.02×10^{23} mol^{-1}; ε_0 is the vacuum permittivity, and is equal to 8.85×10^{-12} F/m; M is the molecular weight of POSS in the kg/mol unit; α_e is the molecular electronic polarizability of POSS in the Fm^2 unit, and is equal to the sum of electronic polarizabilities of all atoms constituting the POSS molecule. By taking the density values given in section 4.2.1 and the electronic polarizability values listed in (Raju, 2003c), ε_r' values of OmPOSS, OibPOSS and IoPOSS were calculated, as shown in Table 5.2. As a reference, ε_r' value of LDPE was also calculated in the same way.

Relative complex dielectric permittivities (ε_r^*) of LDPE and LDPE/POSS composites measured at V_{rms}=3 V and 23 °C are presented in Figure 5.8. As shown in Figure 5.8 (a), LDPE/POSS composites have ε_r' values quite close to those of LDPE, possibly attributable to the ε_r' values of POSS, which are intrinsically similar to that of LDPE, as shown in Table 5.2. However, bigger ε_r' differences between neat polymers and composites were reported for OmPOSS-loaded and IoPOSS-loaded PP systems (Takala et al., 2008) and LDPE systems containing octavinyl-POSS (Huang et al., 2009). Variation of ε_r' and ε_r'' in LDPE/IO5 at frequencies below ~1 Hz arises from charge diffusion in the region of electrode. However, the result here is affected by noise and shall be seen more clearly at elevated temperatures, as will be addressed

in Chapter 6. It should be noted that the ε_r' decrease below 1 Hz is a measurement artifact that gets magnified in a narrow plotting range.

As can be seen in Figure 5.8 (b), except for LDPE/OM5 and LDPE/IO5, LDPE/POSS composites have low ε_r'' similar to those of LDPE. Curve irregularities are due to measurement errors, as the losses presented approach the sensitivity limit of apparatus and are thus difficult to be measured accurately. At frequencies below ~100 Hz, negative values are obtained, and are thus absent from the log scale. The weak and broad loss peak of LDPE/IO5 in the high frequency region, starting from around 10^3 Hz, could be an interfacial loss peak resulted from a IoPOSS-LDPE conductivity mismatch, could be due to a conductive water layer loosely bounded at the IoPOSS-LDPE interface, or could arise from IoPOSS itself. The dielectric constant should also see an increase corresponding to this loss peak, but its variation is too small to be detected.

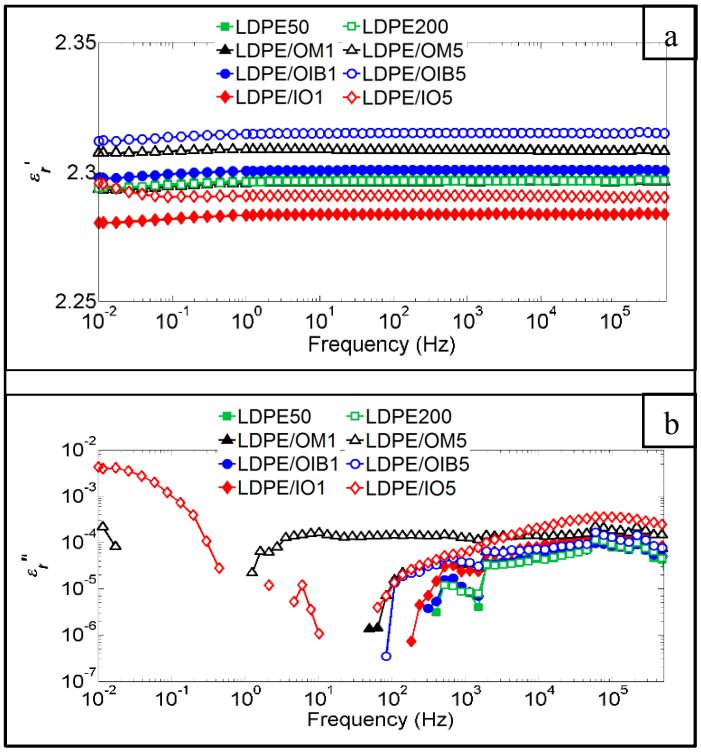

Figure 5.8 (a) Relative real dielectric permittivities ε_r' and (b) relative imaginary dielectric permittivities ε_r'' of LDPE and LDPE/POSS composites

5.3.6 Progressive-stress breakdown tests (PSB)

At ambient temperature, where breakdown tests were carried out, electron avalanche breakdown is the dominant failure mechanism (Ieda, Nagao et Hikita, 1994; Karlsson, 2014). Using Minitab software, the breakdown strengths obtained were fitted with the two-parameter Weibull distribution, as presented in Figure 5.9. Two useful parameters were extracted from the distribution: the shape parameter β and the scale parameter α, as shown in Table 5.3. β reflects the scattering of breakdown strengths, while α is the breakdown strength at which the cumulative probability of failure is 63.2%, and is used for breakdown strength comparison among various samples. As a general rule, the greater the values of β and α, the greater a material's resistance to dielectric breakdown.

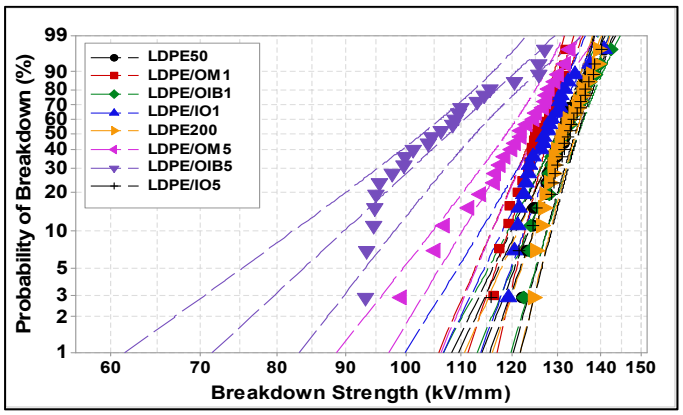

Figure 5.9 The two-parameter Weibull distribution of LDPE and LDPE/POSS composites (95% confidence interval)

Table 5.3 Scale (α) and shape (β) parameters of the two-parameter Weibull distribution

Sample	Shape parameter β	Scale parameter α (kV/mm)
LDPE50	29.3	133.5
LDPE/OM1	33.4	127.6
LDPE/OIB1	26.8	134.2
LDPE/IO1	23.0	130.2
LDPE200	32.5	133.7
LDPE/OM5	18.5	124.5
LDPE/OIB5	10.4	111.5
LDPE/IO5	30.7	134.2

As can be seen, POSS hardly increases the breakdown strength of LDPE. This is due to the competition between the benefits and drawbacks of POSS addition. On the one hand, POSS could contribute to increase the polymer breakdown strength by acting as electron-scattering sites, which reduces the energy of free electrons (Tian et al., 2012); by acting as electron scavengers, which reduces the density of free electrons (Takala et al., 2008), and by homogenizing PE morphology, which smooths breakdown-susceptible spherulite boundaries (Huang et al., 2009). On the other hand, however, POSS could also contribute to reduce the polymer breakdown strength by causing local field enhancements due to their greater dielectric constants, by introducing interfacial void defects that are susceptible to partial discharges, as well as by creating free volume (due to their plasticizing effect) where electrons are easily accelerated (Sabuni et Nelson, 1979). The negative effects offset or dominate the positive ones, resulting in all composites having breakdown strengths similar to or lower than those of LDPE.

As POSS loading increases, breakdown strengths of LDPE/OmPOSS and LDPE/OibPOSS decrease, due to the increase in the number and size of interfacial defects. LDPE/IO5, however, exceptionally increases its α and β values as compared to its 1 wt% counterpart. This, besides being attributable to favorable IoPOSS dispersion, could also be associated with enhanced thermal conductivity of LDPE/IO5, which helps reduce heat accumulation and damages from overheating (Xiao et Du, 2016). It is interesting to note that LDPE/OIB5 follows a three-parameter Weibull distribution with a threshold of 92 kV/mm. This is laudable from an application perspective as the dielectric strength of insulating materials is often determined by their weakest spots.

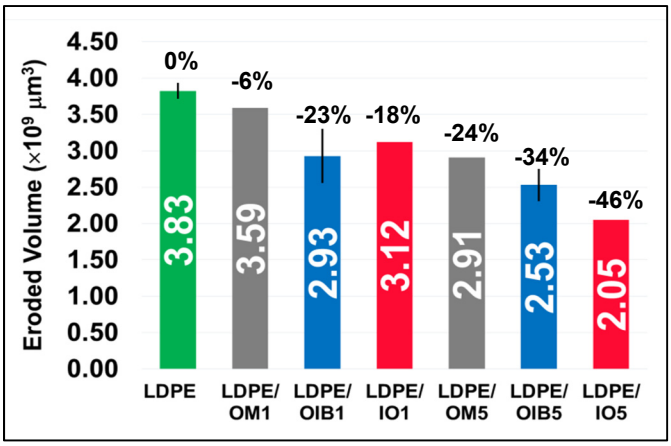

Figure 5.10 Eroded volumes of LDPE and LDPE/POSS composites
(error bars stand for standard deviations)

5.3.7 Surface partial discharge tests

Eroded volumes of LDPE and LDPE/POSS composites are shown in Figure 5.10. A reduced eroded volume, and thus an enhanced resistance to corona discharges, is always observed for POSS-loaded samples as compared to neat LDPE. This is attributable to erosion-resistant inorganic Si-O core of POSS, superior erosion resistance to atomic oxygen radicals of POSS, and formation of Si-O rich passivating layer at the sample surface near high electric field region (Horwath et Schweickart, 2002; Phillips et al., 2000).

Erosion resistance increases with POSS loading, thanks to the increase in the volume occupation and quantity of POSS, which multiplies the size and number of erosion-resistant sites. Erosion resistance tends to increase with the length of POSS alkyl group, possibly owing to the enhancement in POSS-LDPE compatibility and the improvement in POSS dispersion, which limit the size and number of erosion-susceptible interfacial defects. LDPE/OIB1 and LDPE/IO5 see the greatest improvements among the 1 wt% and the 5 wt% composites, respectively, in interesting accordance with their thermal conductivity results. It would not be surprising that thermal conductivity increase (even only 6%) contributes to erosion resistance enhancement by facilitating heat dissipation and reducing thermally-assisted damages.

5.4 Conclusion

LDPE-based composites containing various alkyl substituted POSS were studied in terms of their microscopic characteristics, melting and crystallization behaviors, thermal conductivities, rheological characteristics and electrical properties in order to evaluate the potential of these materials as electrical insulation for HV power cables.

Microscopic observations showed that good dispersions were achieved mainly at lower concentration of POSS functionalized with longer alkyl substituents. POSS caused little changes in the melting temperature or the degree of crystallinity of LDPE, indicating its insignificance in hindering the movements or disrupting the orderly packings of PE chains. POSS only had a small influence on the thermal conductivity of LDPE; the greatest improvements were found in LDPE/OIB1 and LDPE/IO5, both of whose thermal conductivities saw a 6% increase. Viscoelastic characteristics showed that POSS was rheologically compatible with LDPE, and that it largely retained or even reduced the viscosity of LDPE, causing little losses in processability. LDPE/POSS composites had low dielectric constants and dielectric losses at utility frequencies (50–60 Hz), which made it beneficial to use these materials as power cable insulation. All LDPE/POSS composites saw enhanced resistances to corona discharges as compared to neat LDPE, with LDPE/OIB1 and LDPE/IO5 seeing the greatest improvements among the 1 wt% and the 5 wt% composites, respectively. Moreover, only LDPE/OIB1 and LDPE/IO5 were capable of maintaining their breakdown strengths comparable to that of LDPE, whereas the rest of the composites suffered from reduced breakdown strengths of different degrees. The finer properties of LDPE/OIB1 and LDPE/IO5, besides being ascribed to their higher POSS-LDPE compatibilities and better POSS dispersions, which helped limit the size and number of interfacial defects, could also be associated with their higher thermal conductivities, which helped dissipate heat and reduce thermally-assisted damages.

Among the composites studied, LDPE/OIB1 and LDPE/IO5 have thus far been found to be the best in terms of property and manufacturing. However, elevated temperatures are often experienced by insulating materials in service conditions, whereas in this chapter, electrical

properties were only tested at ambient temperature. Therefore, measurements at elevated temperatures are needed to garner further information regarding the potential of these materials as electrical insulation for HV power cables.

5.5 Acknowledgements

The authors highly appreciate the financial support from Hydro-Québec and the Natural Sciences and Engineering Research Council of Canada (NSERC). Moreover, the authors are much indebted to Prof. L.A. Dissado and Dr. Yanhui Huang, for their timely and generous helps and insightful and valuable suggestions in dielectric response analysis.

CHAPTER 6

DIELECTRIC RESPONSES OF LDPE/POSS COMPOSITES AT ELEVATED TEMPERATURES

As a completion to Chapter 5, dielectric responses of LDPE/POSS composites (obtained by extrusion) at elevated temperatures are studied in this chapter, to garner further information regarding the potential of these materials as electrical insulation for HV power cables.

6.1 Dielectric responses of LDPE/POSS composites

Figure 6.1 presents the dielectric responses of LDPE/POSS composites at various temperatures.

As shown in the left column, dielectric constants of LDPE/POSS composites are similar to those of LDPE, i.e. ~2.30 at ambient temperature, and decrease slightly as temperature increases. This is ascribed to electronic polarization, which is relatively independent of temperature and decreases slightly with increasing temperature due to the decrease in material density.

As can be seen in the right column, dielectric losses of LDPE/POSS composites (except for LDPE/IO5) are similar to those of LDPE, which are generally in the vicinity of 10^{-4} in a wide frequency range. Loss variation in low frequency region at temperatures above 60 °C arises from charge transports (diffusion or conduction). The dielectric response of LDPE/IO5 is pretty different from that of LDPE and is explored further in the following sections.

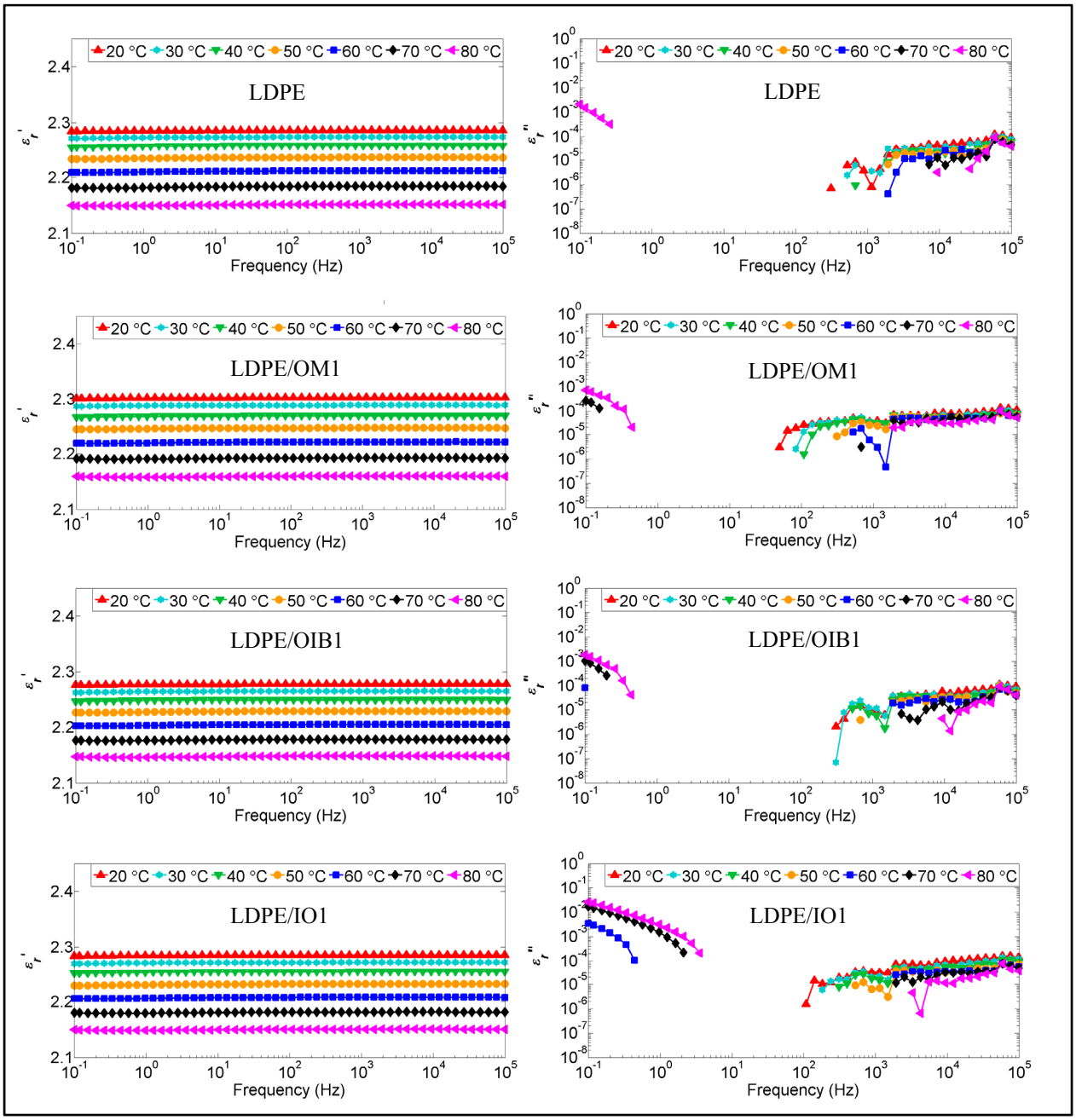

Figure 6.1 Dielectric responses of LDPE/POSS composites at various temperatures. Dielectric constants and dielectric losses are shown in the left and the right column, respectively

Figure 6.1 (Continued)

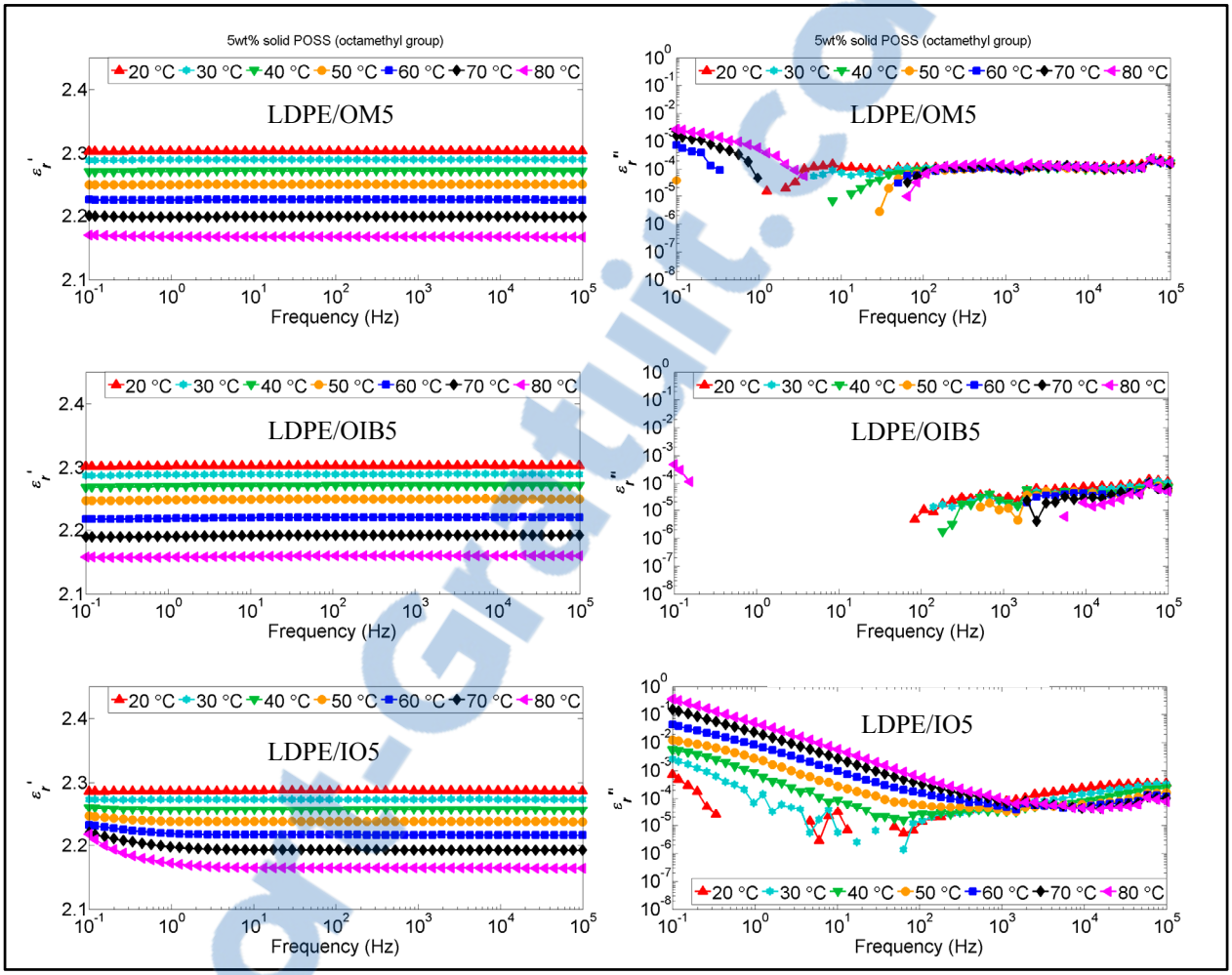

6.2 Charge transports in LDPE/IO5

A magnified view of the dielectric loss of LDPE/IO5 is presented in Figure 6.2. As can be seen, conduction brings loss proportional to f^{-n} with n close to 1, i.e., $\varepsilon_r'' \propto f^{-n}$ ($n \approx 1$). It extends to higher frequencies as temperature increases: 20 Hz at 40 °C, 50 Hz at 50 °C, 100 Hz at 60 °C, 400 Hz at 70 °C and 1000 Hz at 80 °C. This is resulted from the increase in ionic conductivity, thanks to (i) increased ion mobility, brought about by decreased material viscosity, and (ii) increased ion concentration, brought about by increased ion dissociation.

Pure DC conduction with ε_r'' proportional to f^{-1} is most dominant at 80 °C. The corresponding conductivity is estimated as $\sigma_0 = 3\times10^{-12}$ S/m, by taking $\varepsilon_r'' = 5.5\times10^{-4}$ at 100 Hz into equation (6.1).

$$\varepsilon_r'' = \frac{\sigma_0}{\varepsilon_0 \omega} \longrightarrow \log \varepsilon_r'' = \log \sigma_0 - \log(\varepsilon_0 \omega) \tag{6.1}$$

Below 1 Hz, the frequency dependence of ε_r'' is less, with the exponent n reducing to around 0.5. This behavior, corresponding to that observed for ε_r' in the same frequency region, results from charge diffusion in the region of electrode. As temperature increases, this diffusive response extends to higher frequencies, as can be clearly seen at 40 °C, 50 °C and 60 °C. However, it is hard to be discerned at 70 °C and 80 °C due to the domination of DC conduction.

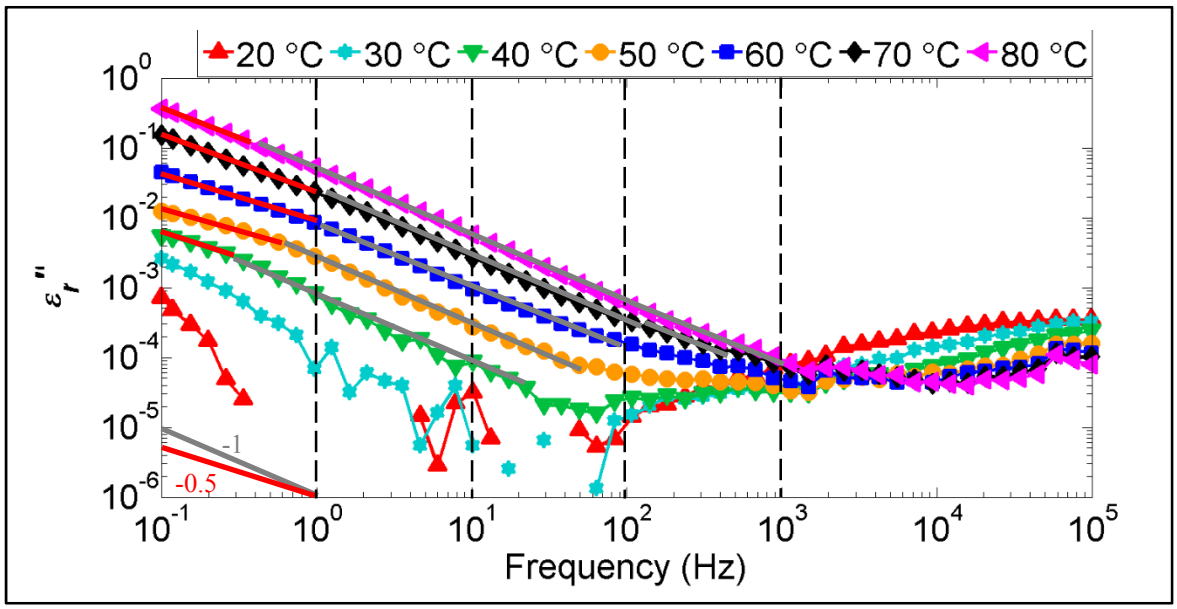

Figure 6.2 Dielectric losses of LDPE/IO5 at various temperatures. Curves' gradients are marked by straight grey and red lines. The grey and red lines in the lower-left corner signify gradients of -1 and -0.5, respectively

6.3 Activation energies of charge transports

As a further investigation of charge transports (i.e., diffusion and conduction), ε_r'' values at 0.1 Hz, 1 Hz, 10 Hz and 100 Hz were plotted against $1/T$, i.e., the inverse of temperature in the Kelvin unit, as shown in Figure 6.3. Only data at temperatures above 40 °C were used, as those below 40 °C were inevitably disrupted by noise, due to the sensitivity limit of the apparatus.

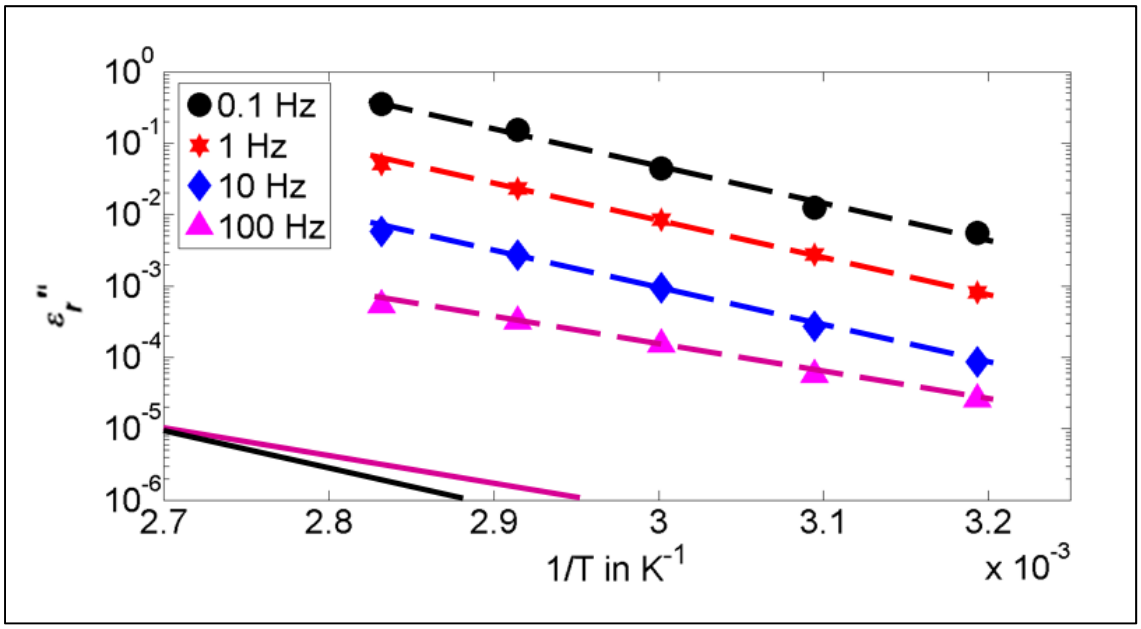

Figure 6.3 Dielectric losses of LDPE/IO5 at 0.1 Hz, 1 Hz, 10 Hz and100 Hz, plotted against the inverse of temperature in the Kelvin unit. The black and magenta lines in the lower-left corner have the same gradients with the black and magenta plots, respectively. Their x and y intercept values are used to calculate plot gradients in equation 6.4

As can be seen, all plots have a linear characteristic, following the Arrhenius equation:

$$\varepsilon_r'' = A\exp(-\frac{E_a}{k_B T}) \tag{6.2}$$

$$\rightarrow \log_{10}\left(\varepsilon_r''\right) = \log_{10} A + \left[-\frac{E_a}{k_B}\log_{10}(\mathrm{e})\right]\frac{1}{T}$$

where E_a is the activation energy of charge transports (in this case, diffusion process and conduction process), k_B is the Boltzmann constant and equal to 1.38×10^{-23} ($J\cdot K^{-1}$).

As shown in equation 6.2, the gradient (m) of the plot is related to E_a, by:

$$m = -\frac{E_a}{k_B}\log_{10}(e) \tag{6.3}$$

Taking the gradient of each plot, i.e.,

$$m_{0.1,1,10\,\mathrm{Hz}} = \frac{\Delta \log_{10} y}{\Delta x} = \frac{\log_{10}\left(10^{-5}\right) - \log_{10}\left(10^{-6}\right)}{\left(2.7-2.875\right)\times10^{-3}} = -5.71\times10^{3}\ (\mathrm{K}) \tag{6.4}$$

$$m_{100\,\mathrm{Hz}} = \frac{\Delta \log_{10} y}{\Delta x} = \frac{\log_{10}\left(10^{-5}\right) - \log_{10}\left(10^{-6}\right)}{\left(2.7-2.95\right)\times10^{-3}} = -4\times10^{3}\ (\mathrm{K})$$

into equation (6.3), activation energies at 0.1–10 Hz and 100 Hz are obtained, as 1.13 eV and 0.79 eV, respectively. The relatively high activation energy for diffusion and conduction up to 10 Hz is likely referred to charge transports through bulk LDPE. The relatively low activation energy for conduction process at 100 Hz is likely referred to charge transport along IoPOSS, where is less viscous and thus requires less energy for charge transport to occur.

6.4 Fitting the dielectric loss of LDPE/IO5 with MWS equation

The dielectric loss of LDPE/IO5 at 80 °C was fitted with MWS equation (equation (2.24)), by assuming (i) IoPOSS were randomly oriented fillers bearing a spherical shape, and (ii) dielectric responses of both LDPE (denoted by m) and IoPOSS (denoted by f) were described by Jonscher's Universal Law (equation. (2.20)). Following the earlier estimation, the conductivity of IoPOSS was taken as $\sigma_f = 3\times10^{-12}$ S/m. Several σ_m values, ranging from 10^{-14} S/m to 10^{-11} S/m, were taken for LDPE, as an attempt to find the value that best fit the

measurement result. As can be seen in Figure 6.4, the best theoretical fit is obtained with $\sigma_m = 3\times10^{-12}$ S/m. Although this value is relatively high for LDPE, it corresponds to the afore-discussed charge transport through bulk LDPE.

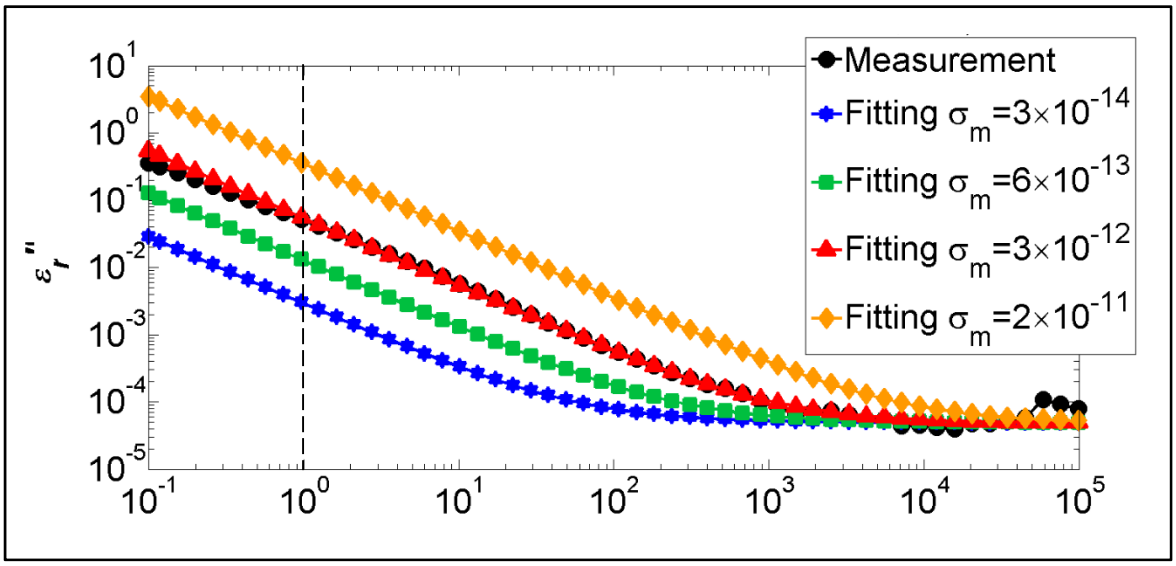

Figure 6.4 Dielectric losses of LDPE/IO5 at 80 °C, measured and fitted

CONCLUSION

Improvements in the dielectric and thermal performances of polyethylene (PE) insulation materials are needed to meet the increasing operating voltage and thermal load of underground power cables. This thesis aimed at developing performances-enhanced PE-based nanodielectrics as HV power cable insulating materials.

Instead of conventional inorganic nano-fillers, polyhedral oligomeric silsesquioxanes (POSS) were used, in an attempt to facilitate a homogeneous nanoscaled filler dispersion, prevent water absorption, and avoid troubles related to filler surface modifications. Besides conventional extrusion (E), ball milling (BM) and xylene solution blending (XSB) were attempted for producing nanodielectrics. The composites obtained were examined regarding their dielectric and thermal properties. Additional characterizations such as scanning electron microscopy (SEM) and differential scanning calorimetry (DSC) were also performed to obtain information for possible performance explanations. As a thorough investigation, three types of POSS with different alkyl substituents were studied—solid octamethyl-POSS (OmPOSS, OM), solid octaisobutyl-POSS (OibPOSS, OIB) and viscous-liquid isooctyl-POSS (IoPOSS, IO). By quantitative calculation of the Hildebrand solubility parameters of POSS, and qualitative evaluation of the length and shape of POSS' alkyl groups based on a "like dissolves like" rule, OmPOSS was estimated to have the lowest compatibility with PE; OibPOSS, a medium, and IoPOSS, the highest. To study the effect of POSS' concentration on composites' properties, POSS loadings of 1 wt% and 5 wt% were investigated.

The following conclusions are drawn from the works carried out in this research:

The influence of POSS and fabrication on the performance of PE/POSS composites

POSS dispersion within PE matrix was found to be influenced by the chain length of POSS' alkyl group: the longer the alkyl-group length, the higher the POSS-PE compatibility, the better the POSS dispersion within PE matrix. Solid OmPOSS and OibPOSS were hardly dispersed

at nanoscale by any of the used methods, possibly due to the strong intermolecular forces among POSS molecules. As for viscous-liquid IoPOSS, it might be dispersed in nanometric sizes by extrusion at the 1 wt% loading. Among the three methods used, ball milling was more effective in dispersing 5 wt% OibPOSS, extrusion and xylene solution blending were more effective in dispersing 1 wt% OibPOSS, and extrusion was more effective in dispersing IoPOSS.

POSS had only a small influence on PE's thermal conductivity, probably attributable to POSS' intrinsic low thermal conductivity. Fabrication methods had little effect on thermal conductivity, except when they induced critical POSS distributions, as in the cases of PE/IoPOSS composites. More specifically, thermal conductivities of PE/OmPOSS composites obtained by both extrusion (E) and xylene solution blending (XSB) were lower than that of PE and increased with OmPOSS loading; thermal conductivities of PE/OibPOSS composites obtained by both E and XSB had the greatest improvements (6%–8%) at 1 wt% OibPOSS content and decreased with filler loading. In contrast, E and XSB had different effects on the thermal conductivity of PE/IoPOSS composites: the thermal conductivity of PE/IO1 (XSB) saw an increase of 5% whereas that of PE/IO1 (E) had a decrease of 3%; on the other hand, the thermal conductivity of PE/IO5 (XSB) had a decrease of 3% whereas that of PE/IO5 (E) saw an increase of 6%. This difference may be ascribed to POSS distribution: possible filler alignment in PE/IO1 (XSB) may be the main reason for PE/IO1 (XSB)'s enhanced thermal conductivity over its extruded counterpart; similarly, possible filler quasi-connection in PE/IO5 (E) may be the main reason for PE/IO5 (E)'s enhanced thermal conductivity over its xylene-precipitated counterpart.

POSS had only a weak effect on PE's dielectric response at ambient temperature. The dielectric constants and the dielectric losses of the composites being, respectively, 2.25–2.35 and generally 10^{-5}–10^{-4}, were similar to that of PE. Fabrication methods had insignificant impact on dielectric response, except when they caused possible filler quasi-connection, as in the case of PE/IO5 (E) composite. At elevated temperatures, the influence of POSS on PE's dielectric response remained small, except for some loss increase in PE/IO1 (E) and PE/OM5 (E) at

frequencies below 10 Hz, and for enhanced charge transports (diffusion and conduction) in PE/IO5 (E).

All PE/POSS composites had enhanced resistances to corona discharges, from a minimum of 6% to a maximum of 61%, thanks to the erosion-resistant inorganic Si-O core of POSS. Erosion resistance is positively correlated to the size and number of erosion-resistant sites and negatively correlated to the size and number of erosion-susceptible interfacial defects. Consequently, as a general trend, erosion resistance increased with (1) POSS loading, thanks to the increase in POSS' quantity and volume occupation, and with (2) the length of POSS' alkyl group, owing to the enhancement in POSS-PE compatibility and the improvement in POSS dispersion. The method of material fabrication had an influence on erosion resistance: composites obtained by xylene solution blending generally had higher erosion resistances than those obtained by extrusion. This may be related to material precipitation and xylene evaporation processes, which somehow brought POSS to the surface of samples, forming an erosion-resistant layer that hindered erosion from further progression.

POSS was barely able to improve PE's dielectric breakdown strength; in the best-case scenario, dielectric breakdown strengths of PE/POSS composites were similar to that of PE. Fabrication method influenced dielectric breakdown strength through filler dispersion. Good filler dispersions with relatively small POSS sizes contributed to balance the benefits (e.g., electron-scattering sites) and the drawbacks (e.g., interfacial void defects) of POSS addition, and thus resulted in roughly maintained breakdown strengths, as in the cases of all 1 wt%-POSS composites, all 5 wt%-IoPOSS composites, and the 5 wt%-OibPOSS composite obtained by ball milling. On the other hand, compromised filler dispersions with relatively large POSS sizes rendered the domination of negative effects over positive ones, and thus resulted in reduced breakdown strengths, as in the case of all 5 wt%-solid-POSS composites produced by extrusion and xylene solution blending.

POSS caused little changes in PE's melting behavior, crystallization behavior, and degree of crystallinity, due to its ineffectiveness in hindering PE chains' movements and disrupting PE

chains' orderly arrangements necessary for crystallization. Moreover, POSS did not have any significant effect on PE's thermal stability in a nitrogen atmosphere, as they simply evaporated at temperatures lower than PE's degradation temperature.

The potential of PE/POSS composites as HV power cable insulation materials

Among all the composites studied, PE/OIB1 (E) is found to be the best material for HV power cable insulation. First of all, its erosion resistance has an enhancement of 23%, which strengthens the insulation against cumulative damages brought about by electrical degradation under service conditions. Moreover, it has low dielectric constants and dielectric losses under utility frequencies (50–60 Hz) at both ambient and elevated temperatures. In addition, it has an unreduced breakdown strength, which poses no threat to the reliability of power transmission/distribution systems. Furthermore, its thermal conductivity has an improvement of 6%, which not only helps reduce thermally-assisted aging and the chance of thermal breakdown, but also facilitates a faster and more uniform curing during XLPE manufacturing.

PE/IO5 (E) has good performances at ambient temperature, which, as a matter of fact, even outrun those of PE/OIB1 (E). However, due to possible filler quasi-connection, its dielectric properties at elevated temperatures are much less appealing: its dielectric loss increases through utility frequencies at above 50 °C; its breakdown strength may also be undermined due to intensified charge transports. Consequently, PE/IO5 (E) is not suitable for applications in HV power cables where elevated temperatures are often experienced by insulating materials in service conditions.

PE/IO5 (XSB) has good dielectric performances, especially its 61% improvement in erosion resistance. Moreover, different from PE/IO5 (E), it does not appear to have any quasi-connected filler distribution. However, compared to PE/OIB1 (E), it has a reduced thermal conductivity; it requires five times more filler content; and its fabrication method (i.e., xylene solution blending) is more demanding than traditional extrusion (e.g., xylene is relatively expensive and environmentally unfriendly).

PE/OIB1 (BM) and PE/OIB5 (BM) have low dielectric permittivities and well-maintained breakdown strengths. However, more characterizations are needed to evaluate their potentials to serve as the insulating materials for HV power cables.

Both PE/OM1 (XSB) and PE/IO1 (XSB) have a 40%-enhanced erosion resistance. However, PE/OM1 (XSB) suffers from a decreased thermal conductivity and a reduced breakdown strength, and PE/IO1 (XSB) has a diminished shape parameter and thus a greater breakdown-strength scattering. PE/OIB1 (XSB) has an 8%-increased thermal conductivity. However, its shape parameter is much lowered. Moreover, its erosion resistance has an improvement of only 17%, exceptionally smaller than other XSB-produced 1 wt% composites. As for PE/OM5 (XSB), PE/OIB5 (XSB), PE/OM5 (E) and PE/OIB5 (E), their breakdown strengths are largely reduced. Consequently, all of these materials are not competent insulation materials candidates for HV power cables.

RECOMMENDATIONS

Based on the works conducted and the results obtained on PE/POSS composites, the following research recommendations are proposed, in the aim of developing high-performance insulating materials that contribute to HV power cables' economic design and reliable operation over long time periods.

In the aspect of *property characterization*, HV broadband dielectric spectroscopy (BDS) will be worth conducting, to investigate the materials' dielectric response at HV levels. Moreover, electrical treeing tests will be worth performing, to further evaluate the materials' withstanding to long-term accumulative damages under service conditions. In addition, mechanical properties such as tensile strength and impact strength will be worth testing, for they not only provide information on the materials' resistance to mechanical damages, but also reflect their susceptibility to harmful structural defects (e.g., micro-voids and micro-cracks) that accelerate electrical degradation.

In the aspect of *material*, since XLPE is currently widely used for MV and HV power cables, it will be of practical value to study cross-linked systems by cross-linking our obtained thermoplastic PE/POSS composites. Moreover, the use of reactive POSS, i.e., POSS whose functional groups chemically react with PE, is worth considering. Potentially, molecular-leveled bonding will facilitate a nanoscaled POSS dispersion and contribute to greater property enhancements. Furthermore, it may be interesting to incorporate another well-reputed filler, such as zinc oxide (ZnO) nano-filler, into PE/POSS, to explore possible synergetic effects of two fillers and achieve more enhanced performances.

In the aspect of *material fabrication*, it will be of interest to use LDPE resin (instead of UHMWPE resin) in ball-milling related studies, as UHMWPE is seldom used in cable insulation industry. Moreover, in order to achieve better POSS dispersion, fabrication methods will be worth improving, possibly by (1) inducing faster precipitation process, to reduce the feasibility of POSS crystallization (2) extruding the materials several times (3) using high-

energy extensional-flow mixer, alone or in combination with extruder (4) combining different types of fabrication methods, such as having POSS ball milled first and then subjected to melt blending or xylene solution blending, etc.

APPENDIX I

PERSONAL PUBLICATION LIST

JOURNAL PUBLICATIONS

J1 Guo, Meng, Michel Fréchette, Éric David et Nicole R. Demarquette. 2015. « Polyethylene-Based Dielectric Composites Containing Polyhedral Oligomeric SilSesquioxanes Obtained by Ball Milling ». *Transactions on Electrical and Electronic Materials* vol. 16, no 2, p. 53-61.

J2 Guo, Meng, Michel Fréchette, Éric David, Nicole R. Demarquette et Jean-Christophe Daigle. 2016. « Polyethylene/Polyhedral Oligomeric Silsesquioxanes Composites: Electrical Insulation for High Voltage Power Cables ». *IEEE Transactions on Dielectrics and Electrical Insulation*, in press.

J3 Guo, Meng, Éric David, Michel Fréchette et Nicole R. Demarquette. 2017. « Polyethylene/Polyhedral Oligomeric Silsesquioxanes Composites: Dielectric, Thermal and Rheological Properties ». *Polymer*, submitted.

CONFERENCE PROCEEDINGS

C1 Guo, Meng, Michel Fréchette, Éric David, Hugues Couderc, Sylvio Savoie, Christèle Vanga-Bouanga et Nicole R. Demarquette. 2013. « Characterization of UHMWPE/POSS Composite Prepared by Ball Milling ». In *IEEE Electrical Insulation Conference (EIC)*. (2-5 June 2013), p. 444-448.

C2 Guo, Meng, Michel Fréchette, Éric David, Hugues Couderc et Nicole R. Demarquette. 2013. « Effects of stearic acid and thermal treatment on morphology and dielectric properties of UHMWPE/POSS composites prepared by ball milling ». In *IEEE Conference on Electrical Insulation and Dielectric Phenomena (CEIDP)*. (20-23 October 2013), p. 760-763.

C3 Guo, Meng, Michel Fréchette, Nicole R. Demarquette, Éric David, Hugues Couderc et Jean-Christophe Daigle. 2014. « Polyethylene-Based Nanodielectric Containing Octaisobutyl Polyhedral Oligomeric Silsesquioxanes Obtained by Hexane Slurry Blending ». In *International Symposium on Electrical Insulating Materials (ISEIM)*. (1-5 June 2014), p. 61-64.

C4 Guo, Meng, Michel Fréchette, Éric David, Nicole R Demarquette et Jean-Christophe Daigle. 2014. « Polyethylene-based nanodielectrics containing octaisobutyl polyhedral oligomeric silsesquioxanes obtained by solution blending in xylene ». In *IEEE Conference on Electrical Insulation and Dielectric Phenomena (CEIDP)*. (19-22 October 2014), p. 731-734.

C5 Guo, Meng, Nicole R. Demarquette, Éric David et Michel Fréchette. 2015. « Polyethylene-based composites containing octaisobutyl polyhedral oligomeric silsesquioxanes obtained by extrusion ». In *IEEE Conference on Electrical Insulation and Dielectric Phenomena (CEIDP)*. (18-21 October 2015), p. 527-530.

C6 Guo, Meng, Éric David, Michel Fréchette et Nicole R. Demarquette. 2016. « Low-density polyethylene/polyhedral oligomeric silsesquioxanes composites obtained by extrusion ». In *IEEE Conference on Electrical Insulation and Dielectric Phenomena (CEIDP)*. (16-19 October 2016), p. 647-650.

LIST OF BIBLIOGRAPHICAL REFERENCES

Applications of Polyhedral Oligomeric Silsesquioxanes. 2011. Coll. « Advances in Silicon Science ». Springer.

ASTM Standard D149. 2013. *Standard Test Method for Dielectric Breakdown Voltage and Dielectric Strength of Solid Electrical Insulating Materials at Commercial Power Frequencies*. West Conshohocken, PA: ASTM International.

ASTM Standard D150. 2011. *Standard Test Methods for AC Loss Characteristics and Permittivity (Dielectric Constant) of Solid Electrical Insulation*. West Conshohocken, PA: ASTM International.

ASTM Standard E1530. 2011. *Standard Test Method for Evaluating the Resistance to Thermal Transmission of Materials by the Guarded Heat Flow Meter Technique*. West Conshohocken, PA: ASTM International.

Bánhegyi, G. 1986. « Comparison of electrical mixture rules for composites ». *Colloid and Polymer Science,* vol. 264, nº 12, p. 1030-1050.

Bellucci, F., D. Fabiani, G. C. Montanari et L. Testa. 2010. « The Processing of Nanocomposites ». In *Dielectric Polymer Nanocomposites*, sous la dir. de Nelson, J. Keith. p. 31-64. Springer US. < http://dx.doi.org/10.1007/978-1-4419-1591-7_2 >.

Bernstein, Bruce S. 2011. « Fundamentals of Electrical Insulation Materials ». In *Electrical Power Cable Engineering*, third edition. p. 75-142. Coll. « Power Engineering (Willis) »: CRC Press. < http://dx.doi.org/10.1201/b11507-6 >.

Bernstein, Bruce S., et William A. Thue. 2011. « Historical Perspective of Electrical Cables ». In *Electrical Power Cable Engineering*, third edition. p. 1-12. Coll. « Power Engineering (Willis) »: CRC Press. < http://dx.doi.org/10.1201/b11507-2 >.

Cho, Kyucheol, Byung H. Lee, Kyu-Myun Hwang, Hoseok Lee et Soonja Choe. 1998. « Rheological and mechanical properties in polyethylene blends ». *Polymer Engineering & Science,* vol. 38, nº 12, p. 1969-1975.

Claude, Jason, Yingying Lu, Kun Li et Qing Wang. 2008. « Electrical Storage in Poly(vinylidene fluoride) based Ferroelectric Polymers: Correlating Polymer Structure to Electrical Breakdown Strength ». *Chemistry of Materials,* vol. 20, nº 6, p. 2078-2080.

Coates, John. 2006. « Interpretation of Infrared Spectra, A Practical Approach ». In *Encyclopedia of Analytical Chemistry*. John Wiley & Sons, Ltd. < http://dx.doi.org/10.1002/9780470027318.a5606 >.

Cordes, David B., Paul D. Lickiss et Franck Rataboul. 2010. « Recent Developments in the Chemistry of Cubic Polyhedral Oligosilsesquioxanes ». *Chemical Reviews,* vol. 110, nº 4, p. 2081-2173.

Dakin, T. W. 2006. « Conduction and polarization mechanisms and trends in dielectric ». *IEEE Electrical Insulation Magazine,* vol. 22, nº 5, p. 11-28.

David, Éric, et Michel Fréchette. 2013. « Polymer Nanocomposites—Major Conclusions and Achievements Reached So Far ». *IEEE Electrical Insulation Magazine,* vol. 29, nº 6, p. 29-36.

DeArmitt, Chris. 2010. « Polyhedral Oligomeric Silsesquioxane Handbook ». < http://phantomplastics.com/wp-content/uploads/2013/08/POSS-Handbook.pdf >.

Dielectric Polymer Nanocomposites. 2010. Springer US.

« Dispersants & Coupling Agents: New Chemistry for a Mature Industry ». 2013. < http://www.slideshare.net/Cray_Valley/dispersants-for-filled-polymers >.

Dissado, L. A. 2011. *Development of dielectric physics for electrical insulation*. Lectures.

Dissado, L. A., et J. C. Fothergill. 1992. *Electrical Degradation and Breakdown in Polymers*. Coll. « IEE Materials and devices series 9 ». London, United Kingdom: Peter Peregrinus Ltd. on behalf of the Institution of Electrical Engineers.

Ebadi-Dehaghani, Hassan, et Monireh Nazempour. 2012. « Thermal Conductivity of Nanoparticles Filled Polymers ». In *Smart Nanoparticles Technology*, sous la dir. de Hashim, Abbass. InTech. < http://www.intechopen.com/books/smart-nanoparticles-technology/thermal-conductivity-of-nanoparticles-filled-polymers- >.

El-Tonsy, MM, IM Fouda, AH Oraby, RM Felfel et MI El-Henawey. 2016. « Dependence of physical properties of linear low-density polyethylene on the silicon dioxide filler size ». *Journal of Thermoplastic Composite Materials,* vol. 29, nº 6, p. 754-767.

« Electronegativity ». 2017. < https://en.wikipedia.org/wiki/Electronegativity#Pauling_electronegativity >.

Fina, Alberto, Daniela Tabuani, Alberto Frache, Enrico Boccaleri et Giovanni Camino. 2005a. « Octaisobutyl POSS Thermal Degradation ». In *Fire Retardancy of Polymers: New Applications of Mineral Fillers*, sous la dir. de Bras, Michel Le, Charles A. Wilkie, Serge Bourbigot, Sophie Duquesne et Charafeddine Jama. p. 202-220. The Royal Society of Chemistry. < http://dx.doi.org/10.1039/9781847552396-00202 >.

Fina, Alberto, Daniela Tabuani, Alberto Frache et Giovanni Camino. 2005b. « Polypropylene–polyhedral oligomeric silsesquioxanes (POSS) nanocomposites ». *Polymer,* vol. 46, nº 19, p. 7855-7866.

Fothergill, J. C. 2013. *Nanodielectrics*. Bologna, Italy: IEEE Dielectric & Electrical Insulation Society. < http://www.ieeedeis.org/education/educational-video/2013-nanodielectrics-tutorial-john-fothergill/ >.

Fréchette, M., M. Trudeau, H. D. Alamdari et S. Boily. 2001. « Introductory remarks on nanodielectrics ». In *IEEE Conference on Electrical Insulation and Dielectric Phenomena (CEIDP), Annual Report*. p. 92-99.

Fréchette, Michel. 2013. « What Are Nanodielectrics? ». *IEEE Electrical Insulation Magazine,* vol. 29, nº 6, p. 8-11.

Fu, Bruce X., Ling Yang, Rajesh H. Somani, Steven X. Zong, Benjamin S. Hsiao, Shawn Phillips, Rusty Blanski et Patrick Ruth. 2001. « Crystallization studies of isotactic polypropylene containing nanostructured polyhedral oligomeric silsesquioxane molecules under quiescent and shear conditions ». *Journal of Polymer Science Part B: Polymer Physics,* vol. 39, nº 22, p. 2727-2739.

George, Soney C., et Sabu Thomas. 2011. « Manufacturing of Multiphase Polymeric Systems ». In *Handbook of Multiphase Polymer Systems*, sous la dir. de Boudenne, Abderrahim, Laurent Ibos, Yves Candau et Sabu Thomas. p. 123-160. John Wiley & Sons, Ltd. < http://dx.doi.org/10.1002/9781119972020.ch5 >.

Grulke, Eric A. 1999; 2005. « Solubility Parameter Values ». In *Polymer Handbook*, sous la dir. de Brandrup, J., Edmund H. Immergut et Eric A. Grulke, Fourth edition. John Wiley & Sons.

Guo, Meng, Michel Fréchette, Éric David, Nicole R. Demarquette et Jean-Christophe Daigle. 2016. « Polyethylene/Polyhedral Oligomeric Silsesquioxanes Composites: Electrical Insulation for High Voltage Power Cables ». *IEEE Transactions on Dielectrics and Electrical Insulation, in press*.

Han, Chang Dae, et Hsiao-Ken Chuang. 1985. « Criteria for rheological compatibility of polymer blends ». *Journal of Applied Polymer Science,* vol. 30, nº 11, p. 4431-4454.

Hanley, Tracey L., Robert P. Burford, Robert J. Fleming et Kenneth W. Barber. 2003. « A general review of polymeric insulation for use in HVDC cables ». *IEEE Electrical Insulation Magazine,* vol. 19, nº 1, p. 13-24.

Harrison, Philip G. 1997. « Silicate cages: precursors to new materials ». *Journal of Organometallic Chemistry,* vol. 542, nº 2, p. 141-183.

Horwath, J., et D. Schweickart. 2002. « Inorganic fillers for corona endurance enhancement of selected polymers ». In *IEEE International Power Modulator and High Voltage Conference (IPMHVC)*. (30 June-3 July 2002), p. 644-647.

Huang, Xingyi, Tomonori Iizuka, Pingkai Jiang, Yoshimichi Ohki et Toshikatsu Tanaka. 2012. « Role of Interface on the Thermal Conductivity of Highly Filled Dielectric Epoxy/AlN Composites ». *The Journal of Physical Chemistry C,* vol. 116, nº 25, p. 13629-13639.

Huang, Xingyi, Pingkai Jiang et Toshikatsu Tanaka. 2011. « A review of dielectric polymer composites with high thermal conductivity ». *IEEE Electrical Insulation Magazine,* vol. 27, nº 4, p. 8-16.

Huang, Xingyi, Liyuan Xie, Pingkai Jiang, Genlin Wang et Yi Yin. 2009. « Morphology studies and ac electrical property of low density polyethylene/octavinyl polyhedral oligomeric silsesquioxane composite dielectrics ». *European Polymer Journal,* vol. 45, nº 8, p. 2172-2183.

Hybrid. 2014. « The Catalog of POSS® ». < http://hybridplastics.com/?s=catalog >.

Ieda, M., M. Nagao et M. Hikita. 1994. « High-field conduction and breakdown in insulating polymers. Present situation and future prospects ». *IEEE Transactions on Dielectrics and Electrical Insulation,* vol. 1, nº 5, p. 934-945.

Ieda, Masayuki. 1980. « Dielectric Breakdown Process of Polymers ». *IEEE Transactions on Electrical Insulation,* vol. EI-15, nº 3, p. 206-224.

IEEE Standard 930. 2005. *IEEE Guide for the Statistical Analysis of Electrical Insulation Breakdown Data*. IEEE Dielectrics and Electrical Insulation Society.

Jonscher, A. K. 1981. « A new understanding of the dielectric relaxation of solids ». *Journal of Materials Science,* vol. 16, nº 8, p. 2037-2060.

Jonscher, A. K. 1983. *Dielectric Relaxation in Solids*, Reprinted by Xi'an Jiaotong University Press, Xi'an, China, 2008. Originally published by Chelsea Dielectrics Press, London, UK, 1983.

Jonscher, A. K. 1996. *Universal Relaxation Law*, Reprinted by Xi'an Jiaotong University Press, Xi'an, China, 2008. Originally published by Chelsea Dielectrics Press, London, UK, 1996.

Joshi, M., et B. S. Butola. 2004. « Studies on nonisothermal crystallization of HDPE/POSS nanocomposites ». *Polymer,* vol. 45, nº 14, p. 4953-4968.

Joshi, M., B. S. Butola, George Simon et Natalia Kukaleva. 2006. « Rheological and Viscoelastic Behavior of HDPE/Octamethyl-POSS Nanocomposites ». *Macromolecules,* vol. 39, nº 5, p. 1839-1849.

Karlsson, Mattias. 2014. « Investigation of the dielectric breakdown strength of polymer nanocomposites ». Uppsala University.

Krimm, S., C. Y. Liang et G. B. B. M. Sutherland. 1956. « Infrared Spectra of High Polymers. II. Polyethylene ». *The Journal of Chemical Physics,* vol. 25, nº 3, p. 549-562.

Landinger, Carl C. 2011. « Basic Dielectric Theory of Cable ». In *Electrical Power Cable Engineering*, third edition. p. 13-22. Coll. « Power Engineering (Willis) »: CRC Press. < http://dx.doi.org/10.1201/b11507-3 >.

Lau, K. Y., A. S. Vaughan, G. Chen, I. L. Hosier et A. F. Holt. 2013. « On the dielectric response of silica-based polyethylene nanocomposites ». *Journal of Physics D: Applied Physics,* vol. 46, nº 9, p. 095303.

Launer, Philip J. 2013. « Infrared analysis of organosilicon compounds: spectra-structure correlations ». In *Silicon Compounds: Silanes & Silicones*. Morrisville, PA: Gelest, Inc. < http://studylib.net/doc/8123238/infrared-analysis-of-organosilicon-compounds >.

Lewis, T. J. 2004. « Interfaces are the dominant feature of dielectrics at the nanometric level ». *IEEE Transactions on Dielectrics and Electrical Insulation,* vol. 11, nº 5, p. 739-753.

Loukus, J. E. , A. C. Halonen et M. Gupta. 2004. « Elongational Flow in Multiple Screw Extruders ». In *ANTEC*. Society of Plastics Engineers. < http://www.plasticflow.com/papers/ANTEC04_ringextruder.pdf >.

McCrum, N. G., C. P. Buckley et C. B. Bucknall. 1997. *Principles of Polymer Engineering*, Second. Oxford Science Publications.

Misra, Rahul, Bruce X. Fu, Andreas Plagge et Sarah E. Morgan. 2009. « POSS-nylon 6 nanocomposites: Influence of POSS structure on surface and bulk properties ». *Journal of Polymer Science Part B: Polymer Physics,* vol. 47, nº 11, p. 1088-1102.

Orton, Harry. 2013. « History of underground power cables ». *IEEE Electrical Insulation Magazine,* vol. 29, nº 4, p. 52-57.

Phillips, Shawn H., Rene I. Gonzalez, Kevin P. Chaffee, Timothy S. Haddad, Gar B. Hoflund, Benjamin S. Hsiao et Bruce X. Fu. 2000. « Remarkable AO Resistance of POSS Inorganic/Organic Polymers ». In *SAMPE Technical Conference*.

Pracella, Mariano, Donatella Chionna, Alberto Fina, Daniela Tabuani, Alberto Frache et Giovanni Camino. 2006. « Polypropylene-POSS Nanocomposites: Morphology and Crystallization Behaviour ». *Macromolecular Symposia,* vol. 234, nº 1, p. 59-67.

Raju, Gorur G . 2003a. « Dielectric Loss and Relaxation-I ». In *Dielectrics in Electric Fields*. Coll. « Power Engineering »: Marcel Dekker, Inc. .

Raju, Gorur G . 2003b. « Dielectric Loss and Relaxation-II ». In *Dielectrics in Electric Fields*. Coll. « Power Engineering »: Marcel Dekker, Inc. .

Raju, Gorur G . 2003c. « Polarization and Static Dielectric Constant ». In *Dielectrics in Electric Fields*. Coll. « Power Engineering »: Marcel Dekker, Inc. .

Reed, C. W. 2010. « The Chemistry and Physics of the Interface Region and Functionalization ». In *Dielectric Polymer Nanocomposites*, sous la dir. de Nelson, J. Keith. p. 95-131. Springer US. < http://dx.doi.org/10.1007/978-1-4419-1591-7_4 >.

Roy, M., J. K. Nelson, R. K. MacCrone et L. S. Schadler. 2007. « Candidate mechanisms controlling the electrical characteristics of silica/XLPE nanodielectrics ». *Journal of Materials Science,* vol. 42, nº 11, p. 3789-3799.

Roy, M., J. K. Nelson, R. K. MacCrone, L. S. Schadler, C. W. Reed, R. Keefe et W. Zenger. 2005. « Polymer nanocomposite dielectrics-the role of the interface ». *IEEE Transactions on Dielectrics and Electrical Insulation,* vol. 12, nº 4, p. 629-643.

Roy, Mihir. 2005. « An examination of the potential for nano-composites in the formulation of HV cable insulation ». PhD thesis. Troy, New York, Rensselaer Polytechnic Institute.

Sabuni, M. H., et J. K. Nelson. 1979. « The effects of plasticizer on the electric strength of polystyrene ». *Journal of Materials Science,* vol. 14, nº 12, p. 2791-2796.

Schwab, Joseph J., et Joseph D. Lichtenhan. 1998. « Polyhedral oligomeric silsesquioxane(POSS)-based polymers ». *Applied Organometallic Chemistry,* vol. 12, nº 10-11, p. 707-713.

Scott, Donald W. 1946. « Thermal Rearrangement of Branched-Chain Methylpolysiloxanes ». *Journal of the American Chemical Society,* vol. 68, nº 3, p. 356-358.

Shaffer, Milo S. P., et Alan H. Windle. 1999. « Fabrication and Characterization of Carbon Nanotube/Poly(vinyl alcohol) Composites ». *Advanced Materials,* vol. 11, nº 11, p. 937-941.

Sichina, W. J. . 2000. *DSC as Problem Solving Tool: Measurement of Percent Crystallinity of Thermoplastics*. PerkinElmer Instruments, USA.

Smith, R. C., C. Liang, M. Landry, J. K. Nelson et L. S. Schadler. 2008. « The mechanisms leading to the useful electrical properties of polymer nanodielectrics ». *IEEE Transactions on Dielectrics and Electrical Insulation,* vol. 15, nº 1, p. 187-196.

Steeman, P. A. M., et J. van Turnhout. 2003. « Dielectric Properties of Inhomogeneous Media ». In *Broadband Dielectric Spectroscopy*, sous la dir. de Kremer, Friedrich, et Andreas Schönhals. p. 495-522. Berlin, Heidelberg: Springer Berlin Heidelberg. < http://dx.doi.org/10.1007/978-3-642-56120-7_13 >.

Suryanarayana, C. 2001. « Mechanical alloying and milling ». *Progress in Materials Science,* vol. 46, p. 1-184.

Takala, M., M. Karttunen, P. Salovaara, S. Kortet, K. Kannus et T. Kalliohaka. 2008. « Dielectric properties of nanostructured polypropylene-polyhedral oligomeric silsesquioxane compounds ». *IEEE Transactions on Dielectrics and Electrical Insulation,* vol. 15, nº 1, p. 40-51.

Tanaka, Toshikatsu, Alexander Bulinski, Jérôme Castellon, Michel Fréchette, Stanislaw Gubanski, Josef Kindersberger, Gian Carlo Montanari, Masayuki Nagao, Peter Morshuis, Yasuhiro Tanaka, Serge Pélissou, Alun Vaughan, Yoshimichi Ohki, Clive W. Reed, Simon Sutton et Suh Joon Han. 2011. « Dielectric properties of XLPE/SiO_2 nanocomposites based on CIGRE WG D1.24 cooperative test results ». *IEEE Transactions on Dielectrics and Electrical Insulation,* vol. 18, nº 5, p. 1482-1517.

Tanaka, Toshikatsu, et Takahiro Imai. 2013. « Advances in nanodielectric materials over the past 50 years ». *IEEE Electrical Insulation Magazine,* vol. 29, nº 1, p. 10-23.

Tanaka, Toshikatsu, Masahiro Kozako, Norikazu Fuse et Yoshimichi Ohki. 2005. « Proposal of a multi-core model for polymer nanocomposite dielectrics ». *IEEE Transactions on Dielectrics and Electrical Insulation,* vol. 12, nº 4, p. 669-681.

Tanaka, Y., N. Ohnuma, K. Katsunami et Y. Ohki. 1991. « Effects of crystallinity and electron mean-free-path on dielectric strength of low-density polyethylene ». *IEEE Transactions on Electrical Insulation,* vol. 26, nº 2, p. 258-265.

Tian, Fuqiang, Qingquan Lei, Xuan Wang et Yi Wang. 2012. « Investigation of electrical properties of LDPE/ZnO nanocomposite dielectrics ». *IEEE Transactions on Dielectrics and Electrical Insulation,* vol. 19, nº 3, p. 763-769.

Tiemblo, Pilar, Mario Hoyos, Jose Manuel Gómez-Elvira, Julio Guzmán, Nuria García, Andrea Dardano et Francesco Guastavino. 2008. « The development of electrical treeing in LDPE and its nanocomposites with spherical silica and fibrous and laminar silicates ». *Journal of Physics D: Applied Physics,* vol. 41, nº 12, p. 125208.

Tsekmes, I. A., R. Kochetov, P. H. F. Morshuis et J. J. Smit. 2013. « Thermal conductivity of polymeric composites: A review ». In *IEEE International Conference on Solid Dielectrics (ICSD)*. (June 30-July 4 2013), p. 678-681.

Umeda, Shinji , Noboru Ishii, Noriaki Horiguchi, Makoto Maeda, Takumi Yamaguchi, Hideo Tanaka, Hiroshi Niinobe, Takehiko Mizuno, Satoru Maruyama, Kunio Iwasaki, Hiroyuki Majima, Shigekazu Amanuma, Hideki Kamiyama, Masaji Tokita, Shingo Oya, Hiromichi Shigeta et Hiroji Akasaka. 2007. *Underground Power Cable, Distribution Cable, Overhead Transmission Line, Industrial Cable and Their Accessories*. Furukawa Electric, VISCAS, Inoue Manufacturing, Asahi Electric Works, Furukawa Electric Industrial Cable.

« Underground Electric Transmission Lines ». 2011. < https://psc.wi.gov/thelibrary/publications/electric/electric11.pdf >.

Utracki, L. A. . 2008. « Polymeric nanocomposites: compounding and performance ». *Journal of nanoscience and nanotechnology,* vol. 8, nº 4, p. 1582-1596.

Van Krevelen, D. W. , et K. Te Nijenhuis. 2009. « Cohesive Properties and Solubility ». In *Properties of Polymers. Their Correlation with Chemical Structure; their Numerical Estimation and Prediction from Additive Group Contributions*, Fourth, completely revised edition. Elsevier. < http://www.sciencedirect.com/science/book/9780080548197 >.

Wen, Dongsheng, et Yulong Ding. 2004. « Effective Thermal Conductivity of Aqueous Suspensions of Carbon Nanotubes (Carbon Nanotube Nanofluids) ». *Journal of Thermophysics and Heat Transfer,* vol. 18, nº 4, p. 481-485.

Xiao, Meng, et Bo Xue Du. 2016. « Review of high thermal conductivity polymer dielectrics for electrical insulation ». *High Voltage,* vol. 1, nº 1, p. 34-42.

Zhang, D. L. 2004. « Processing of advanced materials using high-energy mechanical milling ». *Progress in Materials Science,* vol. 49, p. 537-560.

Zhang, S., X. Y. Cao, Y. M. Ma, Y. C. Ke, J. K. Zhang et F. S. Wang. 2011. « The effects of particle size and content on the thermal conductivity and mechanical properties of Al2O3/high density polyethylene (HDPE) composites ». *Express Polymer Letters,* vol. 5, nº 7, p. 581-590.

Zhou, Wenying, Shuhua Qi, Qunli An, Hongzhen Zhao et Nailiang Liu. 2007. « Thermal conductivity of boron nitride reinforced polyethylene composites ». *Materials Research Bulletin,* vol. 42, nº 10, p. 1863-1873.

Zhou, Zhiyong, Yong Zhang, Yinxi Zhang et Nianwei Yin. 2008. « Rheological behavior of polypropylene/octavinyl polyhedral oligomeric silsesquioxane composites ». *Journal of Polymer Science Part B: Polymer Physics,* vol. 46, n^{o} 5, p. 526-533.